Assessment of Uncertainty in Decay Heat for the Integral Inherently Safe Light Water Reactor

A Thesis
Presented to
The Academic Faculty

By

Matthew E. Lynch

In Partial Fulfillment
of the Requirements for the Degree of
Master of Science in Nuclear Engineering

Georgia Institute of Technology

August 2015

Assessment of Uncertainty in Decay Heat for the Integral Inherently Safe Light Water Reactor

Approved:

Dr. Bojan Petrovic, Advisor
Nuclear & Radiological Engineering Program
School of Mechanical Engineering
Georgia Institute of Technology

Dr. Nolan Hertel
Nuclear & Radiological Engineering Program
School of Mechanical Engineering
Georgia Institute of Technology

Dr. Dingkang Zhang
Nuclear & Radiological Engineering Program
School of Mechanical Engineering
Georgia Institute of Technology

Date Approved: 24 July 2015

Acknowledgements

First and foremost, I would like to thank my advisor, Dr. Bojan Petrovic, for his tireless and insightful assistance in completing this thesis, and for his leadership on the entire I^2S-LWR project. I didn't know what to expect when I started this project, but Dr. Petrovic has made it a wonderful and enlightening experience. Further, I would like to thank my committee members, Dr. Nolan Hertel for providing me with updated ANS decay heat standards, and to him and Dr. Dingkang Zhang for volunteering their time and expertise as members of my committee.

I would like to thank my labmates: Tim Flaspoehler for his assistance with SCALE modeling and UNIX programming, Michael Huang for help with SCALE depletion modeling and ORIGEN formatting, Kyle Ramey, Chris Kinsgbury, Joey Burns, and Mike Chin for their help with SCALE and general I^2S-LWR questions.

On a personal note, I would like to thank my best friend Greg Hock for helping to keep me sane and deal with the stress of grad school over these past 2 years. It's really impossible to overstate how much he's done for me or give him enough credit, let alone in this one paragraph, and there's a good chance this thesis would not have been completed if not for him.

The NRC, the NRE Department, and the Department of Energy all deserve recognition for providing me with funding. In particular, Drs. Farzad Rahnema and Dingkang Zhang deserve recognition for offering me an NRC fellowship during my first year at Tech.

One final acknowledgement is due to Dr. Tom Haley of RPI-he first got me interested in used nuclear fuel and criticality safety, both as an instructor and Senior Design advisor, and it is largely thanks to him that I chose this field of research.

Bettis Atomic Power Laboratory and Mr. Kyle Loschke were also instrumental to this thesis, as their confidence in me gave me the motivation and courage to see this thesis to completion and make it the best possible so as to justify their faith in me.

This research was performed using funding received from the DOE Office of Nuclear Energy's Nuclear Energy University Program, to which thanks is also due.

Table of Contents

Acknowledgements ..... **iii**

List of Tables ..... **vi**

List of Figures ..... **vii**

Summary ..... **x**

1 Overview **1**

2 The Integral Inherently Safe Light Water Reactor **2**

2.1 I^2S-LWR Core Design 2

2.2 Comparison of I^2S-LWR with Traditional PWR 5

2.3 I^2S-LWR Fuel Cycle 8

3 Decay Heat **11**

3.1 Fission products 11

3.2 Scope 12

3.3 Literature Search 12

3.3.1 Existing decay heat models 12

3.3.2 Limitations of Existing Models 19

4 The SCALE Code System **21**

4.1 Boltzmann Transport Equation & the S_N Method 21

4.2 NEWT & the Characteristic S_N method 22

4.3 Depletion module TRITON 25

4.4 ORIGEN 26

5 Computational Model **28**

5.1 SCALE Model 28

5.1.1 Quarter Assembly Model, I^2S-LWR 29

5.1.2 Geometry, I^2S-LWR 31

5.1.3 Quarter assembly model, traditional PWR 33

5.1.4 Geometry, traditional PWR 34

5.1.5 Transition from a traditional PWR to I^2S-LWR 36

5.2 Cases Considered 36

5.2.1 Baseline Cases 36
5.2.2 Uses of ORIGEN 36
5.2.3 Sensitivity/Perturbation Analyses 37
5.2.4 Covariance Studies and Independence of Perturbations 39
5.3 Forms of Decay Heat 40
5.4 Critical Boron Concentration 40
6 Results 42
6.1 General results 42
6.1.1 Critical Boron Concentration 42
6.1.2 Spectral Index 42
6.1.3 Depletion of Uranium-235 46
6.1.4 Actinide production and depletion 48
6.1.5 Changes in Reactivity 56
6.2 Decay Heat Results 58
6.2.1 Transition to I^2S-LWR 58
6.2.2 Sensitivity to Enrichment 63
6.2.3 Sensitivity to Discharge Burnup & Operating Time 70
6.2.4 Sensitivity to Operating Power 73
6.2.5 Sensitivity to Specific Power Oscillations 83
6.2.6 Sensitivity to Fuel Management Strategy 91
6.2.7 Single-pin analysis and isotopic decay heat 96
6.3 Comparison to ANS 5.1-2005 97
6.3.1 Generation of power data 97
6.3.2 Analysis of 2-batch case 100
6.3.3 Analysis of 3-batch case 102
6.3.4 Sensitivity to power data 104
6.4 Covariance Studies 109
7 Conclusions and Future Work 111
Appendix A: Sample Depletion File for I^2S-LWR 114
Appendix B: Sample ORIGEN File 148
Bibliography 161

List of Tables

Table 1: Composition of APMT Stainless Steel Clad [9] 3
Table 2: Composition of Ag-In-Cd control rod [2] 4
Table 3: Possible I^2S-LWR fuel cycle scenarios [1] 9
Table 4: Uranium composition within fuel 10
Table 5: Densities & Temperatures in NEWT model [2] 30
Table 6: Densities & Temperatures in NEWT model, traditional PWR 34
Table 7:Matrix of cases to be modelled 39
Table 8: Power histories for sensitivity studies 54
Table 9: Listing of cases for burnup sensitivity studies 70
Table 10: Operating power histories for burnup sensitivity study 74
Table 11: Contribution to operating power by isotope, 2-batch case 98
Table 12: Contribution to operating power by isotope, 3-batch case 99
Table 13: Power histories for I^2S-LWR fuel assembly 99
Table 14: End-of-cycle contribution by isotope to operating power, 2-batch I^2S-LWR fuel 105
Table 15: End-of-cycle contribution by isotope to operating power, 3-batch I^2S-LWR fuel 105

List of Figures

Figure 1: I²S-LWR fuel pin without IFBA (L), with IFBA (R) 3
Figure 2: I²S-LWR Control Rod [3] 4
Figure 3: I²S-LWR fuel assembly, 156 IFBA design [11] 5
Figure 4: I²S-LWR Fuel layout [2] 5
Figure 5: AP-1000 Assembly, 112 IFBA Design [14] 7
Figure 6: AP1000 fuel pin without IFBA (L) and with IFBA (R) [12] 8
Figure 7: Sample computational cell [25] 24
Figure 8: T-DEPL Methodology [26] 26
Figure 9: Quarter assembly layout in I²S-LWR 30
Figure 10: I²S-LWR Fuel rod unit cell with IFBA (L) and equivalent cylindrical cell (R) 31
Figure 11 (L-R): Whole Fuel pin without IFBA, whole fuel pin with IFBA, half fuel pin (horizontal) without IFBA, half fuel (horizontal) pin with IFBA, half fuel pin (vertical) without IFBA, half fuel pin (vertical) with IFBA 32
Figure 12 (L-R): Whole guide tube, partial (horizontal) guide tube, partial (vertical) guide tube, water cell 32
Figure 13:I²S-LWR Assembly mesh 32
Figure 14: Quarter assembly layout in traditional PWR 33
Figure 15 (L-R): Fuel unit cell without IFBA, fuel unit cell with IFBA, equivalent unit cell with IFBA for traditional PWR 34
Figure 16: Mesh used for PWR depletion 35
Figure 17(L-R): Meshes for fuel pin without IFBA, fuel pin with IFBA, horizontal half pin without IFBA, horizontal half pin with IFBA, vertical half pin without IFBA, vertical half pin with IFBA 35
Figure 18 (L-R): Meshes for guide tube, horizontal half tube, vertical half tube, instrumentation tube 36
Figure 19: Critical boron concentration for 2-batch I²S-LWR 42
Figure 20: Burnup-dependent spectral index for fuel irradiated to 44 GWD/MTHM 44
Figure 21: Burnup-dependent spectral index, 54 GWD/MTHM case 45
Figure 22: Burnup-dependent spectral index in I²S-LWR 46
Figure 23: Uranium-235 number density as a function of burnup in I²S-LWR and traditional PWR 47
Figure 24: Burnup dependent fissile plutonium concentrations in I²S-LWR and traditional PWR 50
Figure 25: Burnup-dependent fertile plutonium concentration in I²S-LWR and traditional PWR 51
Figure 26: Burnup-dependent fissile plutonium percentage in I²S-LWR and PWR 52
Figure 27: Burnup-dependent concentration of Americium-241 in I²S LWR and PWR 53
Figure 28: Burnup-dependent fissile plutonium density in 2-batch I²S-LWR 54
Figure 29: Burnup-dependent fertile plutonium density in 2-batch I²S-LWR 55
Figure 30: Burnup dependent Americium-241 density in 2-batch I²S-LWR 55
Figure 31: Burnup-dependent K-effective in 44 GWD/MTHM fuel 56
Figure 32: Difference in reactivity between b1 and k-effective methods of solution for I²S-LWR fuel irradiated to 44 GWD/MTHM 57
Figure 33: Absolute (blue) and percent (gray) decay heat from PWR oxide fuel irradiated to 44 GWD/MTHM 58
Figure 34: Absolute (blue) and percent (orange) difference in decay heat from UO2- and U3Si2- fuelled traditional PWRs 59

Figure 35: Absolute (blue) and percent (orange) difference in decay heat between traditional PWR and I2S-LWR 60
Figure 36: Gamma ray decay heat for AP1000 fuel irradiated to 44 GWD/MTHM 61
Figure 37: Absolute (blue) and percent (orange) difference in gamma heating between oxide-fueled traditional PWR and I^2S-LWR 62
Figure 38: Fraction of decay heat from gamma rays in 44 GWD/MTHM fuel 63
Figure 39: Decay heat from 4.95 w/o, 44 GWD/MTHM fuel from I^2S-LWR 63
Figure 40: Difference between decay heat from 4.95 & 4.45 w/o I^2S-LWR fuel in watts(orange) & percentage (gray) 64
Figure 41: Percent (orange) and absolute (blue) difference in gamma ray emissions 65
Figure 42: Gamma ray decay heat from 4.95 w/o, 44 GWD/MTHM I^2S-LWR fuel 66
Figure 43: Decay heat from 6.50 w/o I^2S-LWR fuel irradiated to 70 GWD/MTHM 67
Figure 44: Percent (orange) and absolute (blue) difference in decay heat between 6.50 and 4.95 w/o fuel 68
Figure 45: Absolute (blue) and percent (orange) difference in gamma ray decay heat between 4.95 and 6.50 w/o I^2S-LWR fuel irradiated to 70 GWD/MTHM 69
Figure 46: Fraction of decay heat coming from gamma rays, enrichment study 69
Figure 47: Decay heat from discharged I^2S-LWR, constant power 71
Figure 48: Absolute difference in decay heat, constant specific power, varying burnup 72
Figure 49: Percent difference in decay heat 73
Figure 50:Decay heat curves for 40 GWD/MTHM I^2S-LWR fuel at varying specific powers 74
Figure 51: Decay heat as percentage of operating power for 40 GWD/MTHM I^2S-LWR fuel 75
Figure 52: Percent (blue, orange) and absolute (yellow, gray) differences in decay heat in 40 GWD/MTHM I^2S-LWR fuel 76
Figure 53: Gamma-ray decay heat in discharged I^2S-LWR fuel irradiated to 40 GWD/MTHM 77
Figure 54: Comparison of percent difference in gamma ray decay heat from 40 GWD/MTHM I^2S-LWR fuel 78
Figure 55: Fraction of decay heat due to gamma rays in 40 GWD/MTHM I^2S-LWR fuel 79
Figure 56: Decay heat as a function of time for 60 GWD/MTHM I^2S-LWR fuel 79
Figure 57: Decay heat as a percent of operating power for 60 GWD/MTHM I^2S-LWR fuel 80
Figure 58: Percent (orange, blue) and absolute (yellow, gray) difference in baseline and 20 MW/MT and 60 MW/MT operating power in 60 GWD/MTHM fuel 81
Figure 59: Gamma ray decay heat from I^2S-LWR fuel irradiated to 60 GWD/MTHM 81
Figure 60: Percent difference in gamma ray heat compared with 40 MW/MT case 82
Figure 61: Fraction of decay heat coming from gamma rays, 60 GWD/MTHM burnup 83
Figure 62: Decay heat curves for I^2S-LWR at constant 44 GWD/MT burnup, varying specific power 84
Figure 63: Decay heat for I^2S-LWR fuel irradiated to 44 GWD/MTHM 85
Figure 64: Percent difference in normalized decay heat 86
Figure 65: Difference from baseline fuel management strategy for 44 GWD/MTHM I^2S-LWR fuel 87
Figure 66: Gamma ray decay heat from 44 GWD/MTHM I^2S-LWR fuel at varying specific powers 88
Figure 67: Gamma ray decay heat per unit operating power at discharge for 44 GWD/MTHM I^2S-LWR Fuel 89
Figure 68: Percent difference in gamma ray decay heats for 44 GWD/MTHM I^2S-LWR fuel 90
Figure 69: Percent difference from case 1 in unnormalized gamma ray heat, specific power study 91

Figure 70: Comparison of decay heat for 2- and 3- batch I^{2}S-LWR fuel 92
Figure 71: Absolute difference in decay heat, 3- vs 2- batch cases 93
Figure 72: Normalized decay heat, I^{2}S-LWR multibatch 93
Figure 73: Percent difference in normalized decay heat 94
Figure 74: Decay heat as a function of operating power, 2- and 3- batch I^{2}S-LWR fuel 95
Figure 75: Percent difference in gamma ray decay heat for 54 and 44 GWD/MTHM I^{2}S-LWR fuel 95
Figure 76: Total Decay heat by isotope from I^{2}S-LWR fuel pin irradiated to 44 GWD/MTHM 96
Figure 77: Gamma ray Decay heat by isotope from I^{2}S-LWR fuel pin irradiated to 44 GWD/MTHM 97
Figure 78: SCALE results vs ANS 2014 Standard, 44 GWD/MTHM decay heat 101
Figure 79: Difference in decay heat for SCALE and ANS standard, 2-batch I^{2}S-LWR core 102
Figure 80: Decay heat for 3-batch I^{2}S-LWR fuel, SCALE results vs ANS standard 103
Figure 81: Difference between SCALE and ANS Standard for decay heat of 54 GW/MTHM I^{2}S-LWR fuel 104
Figure 82: Decay heat for 44 GWD/MTHM I^{2}S-LWR fuel, ANS-5.1 using end of cycle compositions vs SCALE results 106
Figure 83: Comparison of differences from SCALE decay heat results, I^{2}S-LWR 2-batch fuel 107
Figure 84: Decay heat for 54 GWD/MTHM I^{2}S-LWR fuel, ANS-5.1 using end of cycle compositions vs SCALE results 107
Figure 85:Comparison of differences from SCALE decay heat results, I^{2}S-LWR 3-batch fuel 108
Figure 86: Comparison of percent difference (blue, orange) and the ratio of percent differences (gray) for covariance study 110

Summary

Depletion studies were performed on an I2S-LWR quarter assembly lattice, and decay heat curves were generated considering sensitivity to enrichment, burnup, power, power oscillations, and fuel management strategy. Overall, I2S-LWR fuel has greater decay heat than a standard PWR, both in absolute and relative terms. Covariance of burnup and power is found to be nonzero.

1 Overview

The Integral Inherently Safe Light Water Reactor (I^2S-LWR) is a new, passively safe light water reactor (LWR) concept [1] incorporating, among other things, novel silicide fuel and advanced steel clad for enhanced safety. Owing to the new geometry and fuel composition present in the I^2S-LWR, decay heat generation and used fuel composition must be re-assessed to determine used fuel storage and safety aspects. This thesis will calculate decay heat in used I^2S-LWR fuel as a function of burnup, operating power, and enrichment using SCALE 6.1, analyze the resulting uncertainties, and benchmark the results against the existing ANS-5.1 standard for LWR decay heat. As a further precaution & to determine differences in decay heat due to the different spectrum and new fuel in the I^2S-LWR, a traditional pressurized water reactor (PWR) assembly will also be subjected to the same depletion analysis as an I^2S-LWR assembly. For ease of computing time, all depletion calculations were run with the NEWT/TRITON modules in scale on a reflected quarter assembly. This has an additional benefit, in that any error or uncertainties inherent in the SCALE code package are consistent throughout and present in all models.

This thesis contains 7 chapters, including this one and not including appendices. Chapter 2 provides a detailed overview of the I^2S-LWR design and fuel cycle, chapter 3 covers the causes of and practical concerns presented by decay heat, chapter 4 discusses the SCALE code system and associated underlying theory, chapter 5 details the cases to be studied and perturbation/sensitivity studies, chapter 6 contains all results and discussion, while chapter 7 contains conclusions and recommendations for future work.

2 The Integral Inherently Safe Light Water Reactor

The I^2S-LWR is a "Generation III++" PWR designed to incorporate small modular reactor (SMR) safety features with the power output and economic viability of existing commercial large LWR power plants. The I^2S-LWR incorporates an integral design, where the pressurizer and heat exchangers are within the reactor pressure vessel, and aims to be able to achieve indefinite passive cooling in the event of an accident [2]. The I^2S-LWR power output has been fixed at 2850 MW_t, with an electric output of approximately 1000 MW_e [3].

2.1 I^2S-LWR Core Design

Unlike existing uranium dioxide (UO_2)-fueled LWRs, the I^2S-LWR uses uranium silicide (U_3Si_2) fuel [2]. Uranium silicide's higher density and thermal conductivity allow for a high power density core with passive safety benefits [2]. While steel introduces a reactivity penalty compared with zircaloy due to its higher neutron absorption, mainly in iron and chromium [4] [5], it was ultimately chosen as the clad due to its reduced oxidation rate at high temperatures [6] [7]. More specifically, owing to its superior thermal characteristics, advanced FeCrAl-type steel, such as Kanthal APMT, is used as clad over stainless steel-304 in the fuel [3]. Additionally, to control excess reactivity during the first part of cycle, select fuel rods are coated with integral fuel burnable absorber (IFBA) comprised of zirconium diboride (ZrB_2), containing boron enriched to 60 w/o boron-10 (^{10}B) with a density of 2.5 mg ^{10}B/inch [3]. Since ^{10}B is a thermal neutron absorber with a 2200 m/s absorption cross section of 3840 b [8], the IFBA will result in a harder (faster) neutron spectrum, resulting in increased reactivity of discharged fuel [9] [6]. I^2S-LWR fuel pins with and without IFBA are shown below in figure 1, with clad composition given in table 1.

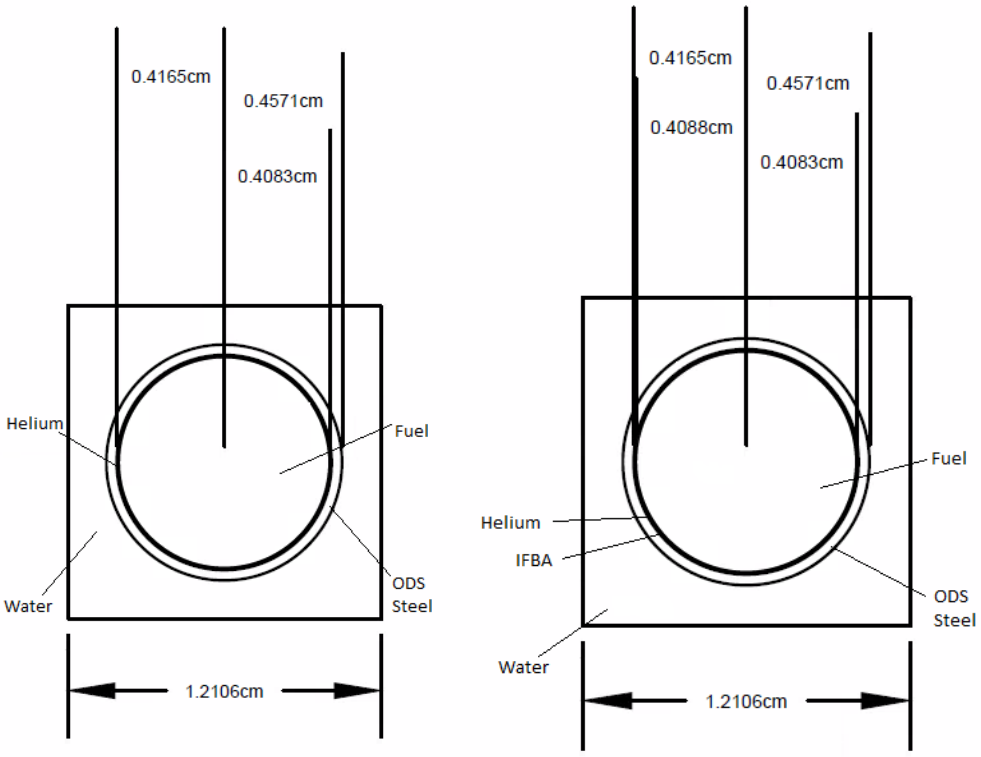

Figure 1: I²S-LWR fuel pin without IFBA (L), with IFBA (R)

Table 1: Composition of APMT Stainless Steel Clad [9]

Material	Weight fraction [w/o]
Iron	69.82
Chromium	21
Aluminum	5
Molybdenum	3
Silicon	0.7
Manganese	0.4
Carbon	0.08

Ag-In-Cd control rods are used in reactor startup and shutdown, and for supplemental reactivity control in addition to boric acid. As is the case with the fuel pins, a helium gap is present; the control rod is diagrammed in Figure 2 and the composition is documented in Table 2.

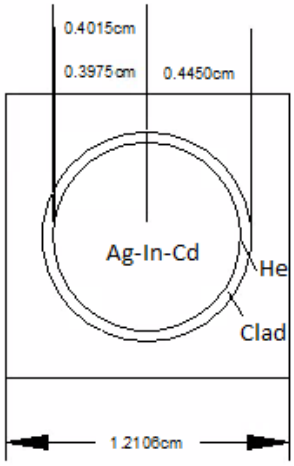

Figure 2: I²S-LWR Control Rod *[3]*

Table 2: Composition of Ag-In-Cd control rod [2]

Material	Weight fraction [w/o]
Silver	80
Indium	15
Cadmium	5

As is the case with most PWRs, control rods are used only for start-up and shut down, rather than reactivity control during operations, and boric acid (H_3BO_3) is the primary method of reactivity control over core lifetime [10] with control rods fully withdrawn or in the "biting" position.

A 19 rod by 19 rod assembly containing 336 fuel pins, 24 guide tubes, and 1 instrumentation tube has been proposed for the I^2S-LWR, and a 121-assembly core has been proposed; both are shown below in figures 3 and 4, respectively.

Fuel IFBA	Fuel	Fuel	Fuel	Fuel IFBA	Fuel	Fuel	Fuel IFBA	Fuel IFBA	Fuel	Fuel IFBA	Fuel IFBA	Fuel	Fuel	Fuel IFBA	Fuel	Fuel	Fuel	Fuel IFBA
Fuel	Fuel	Fuel IFBA	Fuel	Fuel	Fuel IFBA	Fuel	Fuel	Fuel	Fuel IFBA	Fuel	Fuel	Fuel	Fuel IFBA	Fuel	Fuel	Fuel IFBA	Fuel	Fuel
Fuel	Fuel IFBA	Fuel	Fuel IFBA	Fuel IFBA	Control Rod	Fuel IFBA	Fuel IFBA	Fuel IFBA	Control Rod	Fuel IFBA	Fuel IFBA	Fuel IFBA	Control Rod	Fuel IFBA	Fuel IFBA	Fuel	Fuel IFBA	Fuel
Fuel	Fuel	Fuel IFBA	Control Rod	Fuel IFBA	Fuel IFBA	Fuel	Fuel	Fuel	Fuel IFBA	Fuel	Fuel	Fuel	Fuel IFBA	Fuel IFBA	Control Rod	Fuel IFBA	Fuel	Fuel
Fuel IFBA	Fuel	Fuel IFBA	Fuel IFBA	Fuel IFBA	Fuel IFBA	Fuel	Fuel	Fuel	Fuel IFBA	Fuel	Fuel	Fuel	Fuel IFBA	Fuel IFBA	Fuel IFBA	Fuel IFBA	Fuel	Fuel IFBA
Fuel	Fuel IFBA	Control Rod	Fuel IFBA	Fuel IFBA	Control Rod	Fuel IFBA	Fuel IFBA	Fuel IFBA	Control Rod	Fuel IFBA	Fuel IFBA	Fuel IFBA	Control Rod	Fuel IFBA	Fuel IFBA	Control Rod	Fuel IFBA	Fuel
Fuel	Fuel	Fuel IFBA	Fuel	Fuel	Fuel IFBA	Fuel	Fuel	Fuel	Fuel IFBA	Fuel	Fuel	Fuel	Fuel IFBA	Fuel	Fuel	Fuel IFBA	Fuel	Fuel
Fuel IFBA	Fuel	Fuel IFBA	Fuel	Fuel	Fuel IFBA	Fuel	Fuel	Fuel	Fuel IFBA	Fuel	Fuel	Fuel	Fuel IFBA	Fuel	Fuel	Fuel IFBA	Fuel	Fuel IFBA
Fuel IFBA	Fuel	Fuel IFBA	Fuel	Fuel	Fuel IFBA	Fuel	Fuel	Fuel	Fuel IFBA	Fuel	Fuel	Fuel	Fuel IFBA	Fuel	Fuel	Fuel IFBA	Fuel	Fuel IFBA
Fuel	Fuel IFBA	Control Rod	Fuel IFBA	Fuel IFBA	Control Rod	Fuel IFBA	Fuel IFBA	Fuel IFBA	Instrumentation	Fuel IFBA	Fuel IFBA	Fuel IFBA	Control Rod	Fuel IFBA	Fuel IFBA	Control Rod	Fuel IFBA	Fuel
Fuel IFBA	Fuel	Fuel IFBA	Fuel	Fuel	Fuel IFBA	Fuel	Fuel	Fuel	Fuel IFBA	Fuel	Fuel	Fuel	Fuel IFBA	Fuel	Fuel	Fuel IFBA	Fuel	Fuel IFBA
Fuel IFBA	Fuel	Fuel IFBA	Fuel	Fuel	Fuel IFBA	Fuel	Fuel	Fuel	Fuel IFBA	Fuel	Fuel	Fuel	Fuel IFBA	Fuel	Fuel	Fuel IFBA	Fuel	Fuel IFBA
Fuel	Fuel	Fuel IFBA	Fuel	Fuel	Fuel IFBA	Fuel	Fuel	Fuel	Fuel IFBA	Fuel	Fuel	Fuel	Fuel IFBA	Fuel	Fuel	Fuel IFBA	Fuel	Fuel
Fuel	Fuel IFBA	Control Rod	Fuel IFBA	Fuel IFBA	Control Rod	Fuel IFBA	Fuel IFBA	Fuel IFBA	Control Rod	Fuel IFBA	Fuel IFBA	Fuel IFBA	Control Rod	Fuel IFBA	Fuel IFBA	Control Rod	Fuel IFBA	Fuel
Fuel IFBA	Fuel	Fuel IFBA	Fuel IFBA	Fuel IFBA	Fuel IFBA	Fuel	Fuel	Fuel	Fuel IFBA	Fuel	Fuel	Fuel	Fuel IFBA	Fuel IFBA	Fuel IFBA	Fuel IFBA	Fuel	Fuel IFBA
Fuel	Fuel	Fuel IFBA	Control Rod	Fuel IFBA	Fuel IFBA	Fuel	Fuel	Fuel	Fuel IFBA	Fuel	Fuel	Fuel	Fuel IFBA	Fuel IFBA	Control Rod	Fuel IFBA	Fuel	Fuel
Fuel	Fuel IFBA	Fuel	Fuel IFBA	Fuel IFBA	Control Rod	Fuel IFBA	Fuel IFBA	Fuel IFBA	Control Rod	Fuel IFBA	Fuel IFBA	Fuel IFBA	Control Rod	Fuel IFBA	Fuel IFBA	Fuel	Fuel IFBA	Fuel
Fuel	Fuel	Fuel IFBA	Fuel	Fuel	Fuel IFBA	Fuel	Fuel	Fuel	Fuel IFBA	Fuel	Fuel	Fuel	Fuel IFBA	Fuel	Fuel	Fuel IFBA	Fuel	Fuel
Fuel IFBA	Fuel	Fuel	Fuel	Fuel IFBA	Fuel	Fuel	Fuel IFBA	Fuel IFBA	Fuel	Fuel IFBA	Fuel IFBA	Fuel	Fuel	Fuel IFBA	Fuel	Fuel	Fuel	Fuel IFBA

Figure 3: I²S-LWR fuel assembly, 156 IFBA design *[11]*

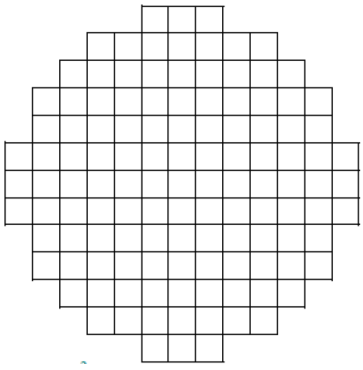

Figure 4: I²S-LWR Fuel layout *[2]*

2.2 Comparison of I²S-LWR with Traditional PWR

One of the goals of this thesis is to compare decay heat from used I^2S-LWR fuel to that of used fuel from an existing PWR, and determine the impact that each stage of the transition to the I^2S-LWR design has on decay heat. The traditional PWR used to benchmark results against will be the Westinghouse AP1000, a GW-electric class PWR using oxide fuel and zircaloy cladding. Comparing with the AP-1000, the I^2S-LWR has several notable differences from a core design perspective in addition to the integral design and novel fuel chemistry described above. Compared to the AP1000, which uses 17x17 assemblies with higher specific power, I^2S-LWR uses 19x19 assemblies [12] [13]; this decreases the number of fuel assemblies present from 157 [13]in AP1000 design to 121 [3]in the I^2S-LWR. Further, this change in design has increased the number of fuel rods per assembly from 264 to 336. An AP1000 assembly is shown below in Figure 5, with the same notation as used above for the I^2S-LWR assembly in Figure 3.

-

Fuel IFBA	Fuel IFBA	Fuel	Fuel	Fuel	Fuel	Fuel	Fuel	Fuel	Fuel	Fuel	Fuel	Fuel	Fuel	Fuel	Fuel IFBA	Fuel IFBA
Fuel IFBA	Fuel	Fuel	Fuel	Fuel	Fuel IFBA	Fuel	Fuel	Fuel IFBA	Fuel	Fuel	Fuel IFBA	Fuel	Fuel	Fuel	Fuel	Fuel IFBA
Fuel	Fuel	Fuel	Fuel IFBA	Fuel IFBA	Control Rod	Fuel IFBA	Fuel IFBA	Control Rod	Fuel IFBA	Fuel IFBA	Control Rod	Fuel IFBA	Fuel IFBA	Fuel	Fuel	Fuel
Fuel	Fuel	Fuel IFBA	Control Rod	Fuel IFBA	Fuel IFBA	Fuel	Fuel	Fuel IFBA	Fuel	Fuel	Fuel IFBA	Fuel IFBA	Control Rod	Fuel IFBA	Fuel	Fuel
Fuel	Fuel	Fuel IFBA	Fuel IFBA	Fuel	Fuel IFBA	Fuel	Fuel	Fuel IFBA	Fuel	Fuel	Fuel IFBA	Fuel	Fuel IFBA	Fuel IFBA	Fuel	Fuel
Fuel	Fuel IFBA	Control Rod	Fuel IFBA	Fuel IFBA	Control Rod	Fuel IFBA	Fuel IFBA	Control Rod	Fuel IFBA	Fuel IFBA	Control Rod	Fuel IFBA	Fuel IFBA	Control Rod	Fuel IFBA	Fuel
Fuel	Fuel	Fuel IFBA	Fuel	Fuel	Fuel IFBA	Fuel	Fuel	Fuel IFBA	Fuel	Fuel	Fuel IFBA	Fuel	Fuel	Fuel IFBA	Fuel	Fuel
Fuel	Fuel	Fuel IFBA	Fuel	Fuel	Fuel IFBA	Fuel	Fuel	Fuel IFBA	Fuel	Fuel	Fuel IFBA	Fuel	Fuel	Fuel IFBA	Fuel	Fuel
Fuel	Fuel IFBA	Control Rod	Fuel IFBA	Fuel IFBA	Control Rod	Fuel IFBA	Fuel IFBA	Control Rod	Fuel IFBA	Fuel IFBA	Control Rod	Fuel IFBA	Fuel IFBA	Control Rod	Fuel IFBA	Fuel
Fuel	Fuel	Fuel IFBA	Fuel	Fuel	Fuel IFBA	Fuel	Fuel	Fuel IFBA	Fuel	Fuel	Fuel IFBA	Fuel	Fuel	Fuel IFBA	Fuel	Fuel
Fuel	Fuel	Fuel IFBA	Fuel	Fuel	Fuel IFBA	Fuel	Fuel	Fuel IFBA	Fuel	Fuel	Fuel IFBA	Fuel	Fuel	Fuel IFBA	Fuel	Fuel
Fuel	Fuel IFBA	Control Rod	Fuel IFBA	Fuel IFBA	Control Rod	Fuel IFBA	Fuel IFBA	Control Rod	Fuel IFBA	Fuel IFBA	Control Rod	Fuel IFBA	Fuel IFBA	Control Rod	Fuel IFBA	Fuel
Fuel	Fuel	Fuel IFBA	Fuel IFBA	Fuel	Fuel IFBA	Fuel	Fuel	Fuel IFBA	Fuel	Fuel	Fuel IFBA	Fuel	Fuel IFBA	Fuel IFBA	Fuel	Fuel
Fuel	Fuel	Fuel IFBA	Control Rod	Fuel IFBA	Fuel IFBA	Fuel	Fuel	Fuel IFBA	Fuel	Fuel	Fuel IFBA	Fuel IFBA	Control Rod	Fuel IFBA	Fuel	Fuel
Fuel	Fuel	Fuel	Fuel IFBA	Fuel IFBA	Control Rod	Fuel IFBA	Fuel IFBA	Control Rod	Fuel IFBA	Fuel IFBA	Control Rod	Fuel IFBA	Fuel IFBA	Fuel	Fuel	Fuel
Fuel IFBA	Fuel	Fuel	Fuel	Fuel	Fuel IFBA	Fuel	Fuel	Fuel IFBA	Fuel	Fuel	Fuel IFBA	Fuel	Fuel	Fuel	Fuel	Fuel IFBA
Fuel IFBA	Fuel IFBA	Fuel	Fuel	Fuel	Fuel	Fuel	Fuel	Fuel	Fuel	Fuel	Fuel	Fuel	Fuel	Fuel	Fuel IFBA	Fuel IFBA

Figure 5: AP-1000 Assembly, 112 IFBA Design *[14]*

Comparing fuel unit cell layouts with the I^2S-LWR fuel cells above in Figure 1, the smaller fuel assembly in the AP1000 is accompanied by larger individual fuel pins and cells, i.e. larger fuel diameter and pitch between rods, as seen in Figure 6.

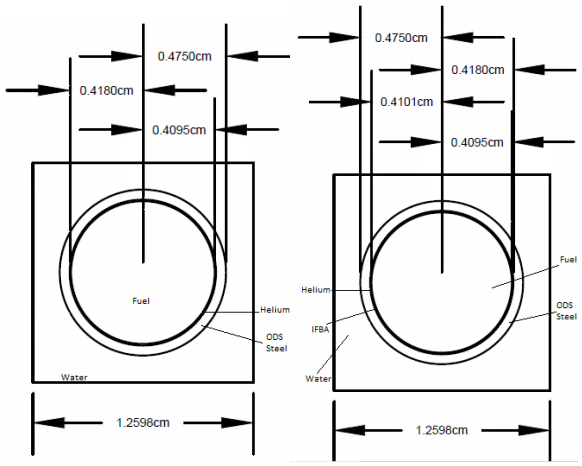

Figure 6: AP1000 fuel pin without IFBA (L) and with IFBA (R) *[12]*

2.3 I^{2}S-LWR Fuel Cycle

A number of fuel management strategies have been proposed for the I^{2}S-LWR, and the four representative reloading strategies are considered in this work and described below in Table 3: A 3 batch, 4.45 w/o core on a 12 month cycle, a 2 batch, 4.95 w/o core on an 18 month cycle, a 3 batch 6.50 w/o core on an 18 month cycle, and a 2 batch, 6.50 w/o core on a 24 month cycle. Since the isotopic composition and volume of used fuel depends on burnup and initial enrichment, the used fuel composition and activity will vary for each case. An I^{2}S-LWR quarter assembly is known to contain 150.7 kilograms or 0.1507 metric tons [3] of uranium, regardless of enrichment.

Table 3: Possible I²S-LWR fuel cycle scenarios [1]

Case	Fuel enrichment [w/o]	Cycle length [months]	Number of batches	# Assemblies per reload	Assembly mean burnup [GWd/MTU]
1	4.45	12	3	40	41.2
2	4.95	18	2	60	42.0
3	6.50	18	3	40	62.9
4	6.50	24	2	60	56.6

In the 3-batch cores, a typical fuel assembly is in the reactor for 3 cycles; due to the 121-assembly layout, however, one assembly will remain in the core for a fourth cycle. Similarly, most assemblies will be in the reactor for 2 cycles in a 2-batch core, with one assembly remaining for a third [2].

Turning now to composition of the fuel itself, ^{234}U constitutes a minor, but non-negligible, component of uranium in reactor fuel. Since gaseous diffusion is the standard enrichment technique in the United States [15], Graham's Law applies and can be used to derive an expression for ^{234}U content in enriched fuel. It should be noted that ^{236}U will not be considered here, or anywhere else in this thesis.

If UF_6 is used in the enrichment process, as is standard practice in the United States, the atomic masses for $^{234}UF_6$, $^{235}UF_6$ and $^{238}UF_6$ are 348, 349, and 352 g/mol, respectively [15]; using these masses and the natural abundances of 0.005 w/o for ^{234}U and 0.7 w/o for ^{235}U [10], Graham's Law can be used to find fuel compositions for 4.45, 4.95, and 6.50 w/o fuel which are summarized in Table 4 below.

Table 4: Uranium composition within fuel

Case	^{234}U content [w/o]	^{235}U content [w/o]	^{238}U content [w/o]
1	0.03183	4.45	95.51817
2	0.03541	4.95	95.01459
3,4	0.04649	6.50	93.45351

3 Decay Heat

3.1 Fission products

In a typical fission reaction, some 200 MeV are released in the form of kinetic energy of neutrons, gamma rays, antineutrinos, and two daughter nuclei; this 200 MeV figure includes energy released in decay of short-lived products [10]. Of this energy, approximately 10 MeV, in the form of kinetic energy of neutrinos, is lost from the reactor, while the other 190 MeV is deposited within the reactor. In a significant portion of these fissions [10], the daughter nuclei will be radioactive and will continue to produce heat even after the fission reaction ceases. As a result, determining the activity and, by extension, the decay heat of irradiated fuel is necessary to determine cooling and shielding concerns in used nuclear fuel, shielding concerns from operating reactors, and passive cooling requirements during reactor shutdown.

Broadly speaking, the products of decay heat can be practically divided into two categories: Charged and uncharged (neutral) particles. Charged particles, mostly alpha and beta particles but also daughter nuclei from spontaneous fission, deposit their energy in the fuel and as such are a concern from a reactor safety perspective, but not a shielding one. Conversely, neutral particles, specifically gamma rays, deposit their energy primarily in the coolant and have the potential to even leak from the reactor [10], requiring reactor shielding and creating a separate heat source from charged particles.

Production of neutral particles and the associated decay heat in this thesis will focus on gamma rays, as their production in decay of used fuel [10] has been found to be much greater than neutron production in spontaneous fission or neutron decay in burnt or even fresh fuel [10]. However, since neutron production in spontaneous fission increases with burnup, the heat source due to neutron

production will also be modelled as a precautionary measure. Antineutrinos needn't be considered since, as mentioned above, their energy is not deposited in the reactor [10].

3.2 Scope

This thesis will aim to benchmark the decay heat generated from depletion models against the American Nuclear Society (ANS) 2005 standard, using the same time intervals as the ANS standard. As such, it will examine decay heat going from 1 second after discharge out to 10^{10} seconds (approximately 317 years), with an emphasis on shorter-term (< 100 year, or ~$3.2 * 10^9$ seconds) decay heat models for used-fuel storage applications.

3.3 Literature Search

3.3.1 Existing decay heat models

Using a formula originally developed by Way and Wigner, Ragheb (2011) offers a simple model for decay heat which provides a correlation for LWR decay heat based on operating power and time since discharge; this model is designed to be valid over a wide range of operating times and powers, and for both BWR and PWR plants [16]. Using the same model for BWR and PWR plants is valid, as the plot of decay heat vs. time since discharge is the same for both. Ragheb estimates beta & gamma production rates, which must be calculated separately as they deposit their energy in different regions of the assembly, and then multiplies by a mean energy of 0.4 MeV and 0.7 MeV for betas & gammas, respectively, to obtain energy production from fission products at some time *t* [16]. Notably, rather than sum over all nuclides and use radioactive decay laws, a correlation is used, finding that decay heat/fission-second is approximately given by $T^{-1.2}$. Integrating these equations from shutdown to some arbitrary time *t* and assuming a constant 200 MeV/fission, Way and Wigner find that decay heat at time *t* after shutdown at time T_0 is given by

$$P_{decay}(t) = 6.48 * 10^{-2} * P_0(t^{-0.2} - (t + T_0)^{-0.2}),$$

Equation 1: Decay Heat, Way-Wigner Model as cited by Ragheb

where decay heat generation rate P_{decay} and P_0, the reactor operating power are in the same, arbitrarily chosen units, and *t* and T_0 are in seconds. This equation can be integrated again to obtain total energy released over some time interval, which is a useful metric in reactor accidents. Ragheb's model unfortunately has limitations as well, neglecting neutron capture in fission products and plutonium production/uranium depletion; the former changes decay product concentrations while the latter determines fission product production, as each nuclide has different fission product spectra and energy release per fission [16].

The other model proposed in Ragheb's analysis expands on the one described above and attempts to correct some of its limitations. Rather than fuel depletion or breeding, a ratio of Pu^{239} production to U^{235} consumption of 1 is assumed, while Pu^{240} and U^{238} fission are ignored on the grounds that their contributions to reactor power are only 2% in a thermal reactor. While this may be valid for short operating times, such as the 0-5000 hour, this may not be appropriate for an LWR running on a 1-2 year (~8700-17000 hour) fuel cycle, as these reactors are obtaining a non-trivial portion of their operating power from plutonium by the time they are shut down for refueling. Additionally, as was the case in his other model, neutron capture in fission products and changes in fission product yields over fuel cycle are ignored, However, unlike the above model, this revised model includes decay heat due to decay of U^{239} and Np^{239} [16].

Ragheb finally compares his models to those of Way and Wigner, who derived an expression for decay heat combining beta and gamma energy into a single term; this correlation's estimate for decay heat also finds that decay heat generation is proportional to $T^{-1.2}$ MeV/sec-fission, but that the amount is roughly double that generated in Ragheb's model. Correcting for

U^{239} and Np^{239}, Wigner & Way develop a 4-term formula for short cooling times where minor actinides are still present; this model is significantly more accurate than that of Ragheb or their previous, more general, model [16].

Using Way and Wigner's revised decay heat equation, Garland (1999) found that it became inaccurate after roughly 10^6 seconds (about 12 days) when modeling the data from his university's reactor [17]. As a result, he instead used ANS 5.1-N18.6, which would later become part of ANS 5.1-1973, with a piecewise curve generated by Glasstone to fit the data, which is said to match the ANS data to within 6%. Garland concludes that Ragheb's original model is valid between 10 seconds to 100 days, while Glasstone's curve was found to be valid to within 20% except for times less than 1000 seconds, or greater than 10^7 seconds (115 days).

ANS 5.1-2005 takes a fundamentally different approach to decay heat modeling: Rather than measure or model decay heat given off by a continuously irradiated fuel element or assembly, the decay heat generated from either a single fission pulse or quasi-infinite (10^{13} second) irradiation is exactly determined; this response is then generalized to a range of operating powers, operating times, and time since discharge [18]. In particular, functions $f(t)$, a function measuring decay heat after the fission pulse, and F(t,T), a function measuring decay heat t seconds after discharge from a reactor running for T seconds. F(t,T) is only evaluated at $T=\infty$, i.e. for an infinite irradiation time, with a correction term to measure decay heat provided later in the standard: To obtain decay heat in MeV/fission for a finite operating time, one simply computes $F(t,\infty)-F(t+T,\infty)$. This can easily be generalized to an arbitrary power history or composition by calculating $F(t,\infty)-F(t+T,\infty)$ for each isotope and operating power and summing over all of them. Since ANS 5.1-2005 is a revision to previous ANS/ANSI standards, several improvements were made from its predecessors, but it also retains some of their errors: The standard is designed for LWRs, decay

heat from Np^{239} and U^{239} is modelled and treated separately from fission product decay heat, and neutron capture in fission products is now included in the model. However, the fission energy release *Q* is held to be constant when in reality it varies between nuclides and by extension over core life, empirical verification is not used for cooling times exceeding 10^5 seconds (about 27.78 hours), and does not separate beta & heavy nuclide production, where energy deposition is local within the fuel from gamma production, where energy is deposited in the coolant, in determining the decay heat. Unique to ANS-5.1 2005 is that it generates separate source terms for each fissile nuclide, improving accuracy over Ragheb & Way & Wigner's models.

The 2014 revision to the ANS standard also introduced a function *F(t,T)* for finite operating times: While tracking production and decay of every nuclide in used fuel would be impractical, the authors found that it could be well approximated by a sum of 23 exponentials. In this model, summing over all 23 indices gives one the decay heat power, in MeV/Fission, for nuclide *i*:

$$DH = \sum_{j=1}^{23} \frac{\alpha_{ij}}{\lambda_{ij}} e^{-\lambda_{ij} t} (1 - e^{-\lambda_{ij} T})$$

Equation 2: Alternative decay heat, ANS 2014 standard [19]

Where α_{ij} is the j^{th} coefficient for nuclide *i*, and λ_{ij} is the decay constant for that group and nuclide. As was the case with the $F(t,\infty)$ function, one must also sum over all nuclides to obtain total decay heat. The $F(t,\infty)$ function from ANS-5.1-2005 is included in the 2014 edition of the standard as well, but with modifications only to uncertainties and not tabulated values of $F(t,\infty)$. One final addition to the 2014 revision is the presence of a correlation for decay heat from longer-lived fuel elements.

The JEF working group wrote its report specifically to address then-current deficiencies in decay heat data [20], and many of the problems with the other models discussed above were

corrected: Summation calculations were not used for short-lived fission products and neutron capture in fission products was also taken into account, which has a pronounced effect of up to 10 percent in the time range of 115 days to 30 years after fuel discharge, i.e. for spent fuel pool & dry storage cask design, while the model is more accurate for times outside this range [20]. Since this report was meant as a correction to discrepancies between the various existing models of decay heat, improved statistical analysis of Tobias' data was used, while measurement technique discrepancies were also discussed. Ultimately, data from Oak Ridge was used primarily used, since their trendline generally fit the data but with an incorrect prediction of initial decay heat. Further, the group accounts for energy dependence of fission product mass distributions, with a discussion of delayed neutron spectra and resulting post-shutdown fission power [20]. However, like most of the other papers, continuous irradiation is instead represented as a series of fission bursts, which neglects capture and could potentially underestimate decay heat from short lived isotopes, and the decay heat curves from each burst, which are added to get the total decay heat, are known to underestimate decay heat. Several of the problems from Ragheb are also present here: Constant mean beta & gamma energies are assumed, which probably are over- and under- estimates, respectively [20]. This model also tracks fewer nuclides than the Ragheb and ANS standards, but these omissions were not found to impact accuracy [20].

The authors comment that one of the major differences between thermal and fast reactors from a reactor physics perspective is that $\frac{\sigma_{\gamma,fission\ product}}{\sigma_f}$, where σ is the macroscopic cross section, is much greater for LWRs than for fast reactors, meaning that neutron capture in an LWR is much more relevant in LWRs than in fast reactors. While fast reactor analysis is outside of the scope of this thesis, the authors conclude that current fast reactor decay heat standards may not be accurate, as they are based on a neutron spectrum which is much harder than that in a typical fast reactor

[20]. Tobias' data, which is widely accepted as the a decay heat model for times under 10^5 seconds, is used for this standard, while computational models were used for times greater than 10^5 seconds; finally, these results were benchmarked against previous JEF standards, and it was found that the previous JEF-1 standards had underestimated decay heat by approximately 2% for times exceeding 800 seconds and overestimated it by as much as 5% for shorter times; as was the case with the other models, JEF-1 struggled with appropriate modeling of short-lived fission products [20]. Additionally, over- and under- estimation of beta & gamma energies, respectively, is corrected for using summation.

The JEF report also compares Japanese, European, and American standards: The Japanese standards consistently underestimate decay heat, especially at short times after discharge, due to a higher assumed fission energy, an assumption which accounts for the majority of the discrepancy between these and the ANS/ANSI standards [20]. While the American standards are closer to the observed decay heat values than their Japanese counterparts, they are invalid beyond 10^9 seconds (31.7 years) and need revisions to uncertainty in decay heat from fission of Pu^{239} and U^{235}, and values for U^{238} should be re-calculated based on observation, as the model in ANS/ANSI 5.1-1993 was derived from first principles rather than observations [20]. While these concerns were valid at the time, they have all been addressed in ANS/ANSI 5.1-2005 since then.

10 CFR 50.46, which is based on the then-current 1994 ANS decay heat standard, provides a detailed model for decay heat [21]. Neutron capture effects are tracked using a set of piecewise equations, with separate equations for shutdown times above & below 10^4 seconds, while an "infinite" operating time, which is assumed in generating decay heat for shutdown times below 10^4 second, is approximated as 10^8 seconds [21] (3.17 years), which is reasonably accurate for a typical LWR in the United States [21]. The variable ψ, the number of fissions per initial fissile

atoms, was chosen to be 1, corresponding to high Pu^{239} production, as a measure of conservatism; additionally, Pu^{241} fission is introduced and tracked separately from other fissile nuclides, decay of the short-lived U^{239} and Np^{239} is accounted for, and the difference in fission energy between actinides is even accounted for in determining initial reactor power [21]. Uncertainties in decay heat are averaged over all nuclides by the fraction of fissions produced in that nuclide [21]. These results were then benchmarked against ORIGEN and the ANS-1994 standard, and found to be in good agreement, with the exception of the ratio of fissions/fissile material loading, which ranged from 0.508 in a BWR to 0.514 in a PWR; however, calculations based on both ANS 1973 and 1994, which used the same input data as the test cases with the revised decay heat standards, assumed this ratio to be equal to 0.7, which could have resulted in inaccurate results based on those standards [21].

The authors of 10 CFR 50 also performed a sensitivity analysis to validate their results: Performing an ORIGEN simulation of a PWR, the authors confirmed that ANS/ANSI 5.1-1994 was more conservative than their model or the reactor modeled in ORIGEN, and that the decay heat due to actinides other than U^{239} and Pu^{239} was non-negligible and needed to be considered in decay heat analyses [21].

Cho et al (2012) discuss the need for decay heat curves with an emphasis on South Korea's growing UNF problem and planned construction of a sodium-cooled fast reactor [22]: Since pyroprocessing and waste from the fast reactor will be disposed in permanent storage alongside LWR fuel, it is vital to know the decay heat of the whole system, which requires that separate decay heat models be generated for fast & thermal reactors due to their different fission product yields [22]. Using a spatially independent model, the source term is generated as {rate of change of nuclide j} = {decay of other isotopes to nuclide j} + {production in fission} – {decay} –

{neutron capture}, an expression that can easily be obtained from reactor physics. To generate a more general decay heat model, specific power or neutron flux & operating time are taken as arguments, with separate inputs for each operating cycle, typically using a code package such as ORIGEN; this approach allows for consideration of fuel shuffling and time-dependent flux with multiple specific power & operating time arguments. Since the source term equation is a spatially independent "zero-dimensional" model, this model would use a volume average flux for axial subdivisions of the fuel to get an axial distribution of decay heat; axial power histories would also have to be known in this case. Source term generation is complicated by the fact that the reprocessing process proposed in South Korea could produce new fuel or waste for permanent storage where the constituent pellets have non-uniform power history, time since discharge, etc., and none of the existing codes can concurrently model multiple irradiation histories [22]. Further, since waste is separated into three categories in pyroprocessing, decay heat from each category must be tracked, meaning that it is inadequate to only measure decay heat from the entire assembly or fuel pin. To address this, Cho writes a series of scripts to automate ORIGEN-S: A mean flux is generated from specific power and scaled to determine clad activation, the restart file allows for depletion modeling of already irradiated fuel, and fission product inventories are scaled using the ReproRun code to account for removal of fission products in reprocessing. Finally, a batch-average homogenized number density is calculated to account for the presence of assemblies with nonuniform operating power history in the UNF.

3.3.2 Limitations of Existing Models

As discussed above in Cho et al, the fuel chemistry and neutron spectrum also contribute to decay heat: Decay heat for fast reactors is different from that for LWRs [10]; as will be discussed below, the spectrum in the I^2S-LWR is harder than in traditional LWRs. As such, the

possibility that the novel design of I^2S-LWR could result in different decay heat results is entirely possible and should be examined, though ANS-5.1-2005 should be close to the calculated results.

4 The SCALE Code System

4.1 Boltzmann Transport Equation & the S_N Method

The Boltzmann transport equation is an eigenvalue equation and neutron conservation statement that exactly models neutron behavior in a reactor in terms of the angular flux ψ, defined as the number of neutrons passing through a surface per unit time per unit area per unit solid angle (steradian).

$$\hat{\Omega} * \nabla\psi(E,\hat{\Omega},\vec{r}) + \sigma_{tot}(E)\psi(E,\hat{\Omega},\vec{r}) = \int_{4\pi}\int_{0}^{\infty}\sigma_s(E'\to E,\hat{\Omega}'\to\hat{\Omega},\vec{r})\psi(E',\hat{\Omega}',\vec{r})dE'd\hat{\Omega}' + \frac{\chi(E)}{k}\int_{4\pi}\int_{0}^{\infty}\upsilon\sigma_f(E',\hat{\Omega}'\to\hat{\Omega},\vec{r})\psi(E',\hat{\Omega}',\vec{r})dE'd\hat{\Omega}'$$

Equation 3: Boltzmann transport equation, eigenvalue form [23]

In the above equation, Ω is the solid angle, ψ the angular flux, σ_{tot} the total macroscopic cross section, σ_s (E' → E, Ω'→ Ω) and σ_f (E' → E, Ω'→ Ω) the macroscopic scattering and fission cross sections, respectively, from E' and Ω' into E and Ω, υ(E') the number of neutrons per fission from a fission event at energy E', χ(E) the fission energy spectrum, and k the criticality eigenvalue. Equation 3 assumes that neutron spectrum is independent of incident neutron energy.

To simplify the generation and treatment of cross sections, it is common to discretize the energy variable into a set of *G* energy groups, with group 1 containing the fastest neutrons and group *G* containing the slowest. Using flux averaging for cross sections, the multigroup transport equation can be written as:

$$\hat{\Omega} * \nabla\psi_g(\hat{\Omega},,\vec{r}) + \sigma_{tot,g}\psi_g(\hat{\Omega},,\vec{r}) = \sum_{g'=1}^{G}\int_{4\pi}\sigma_{s,g'\to g}(\vec{r},\hat{\Omega}'\to\hat{\Omega})\psi_{g'}(\hat{\Omega}',\vec{r})d\hat{\Omega}' + \frac{\chi_g}{4\pi k}\sum_{g'=1}^{G}\int_{4\pi}\upsilon\sigma_{f,g'}(r)\psi_{g'}(\hat{\Omega}',\vec{r})d\hat{\Omega}'$$

Equation 4: Multigroup neutron transport equation, adapted from [23]

Where ψ_g is the angular flux in group *g*, $\sigma_{s,g'\to g}(\hat{\Omega}'\to\hat{\Omega})$ is the scattering cross section from solid angle Ω' and group *g*' into solid angle Ω and group g, $\sigma_{tot,g}$ is the total cross section in group g, $\sigma_{f,g}$ is the fission cross section in group g and χ_g is the fission spectrum in group *g*,

i.e. the fraction of fission neutrons born into group g. Since fission is an isotropic process, the solid angle dependence of the fission cross section has been removed.

The discrete ordinates (S_N) method was used to solve the transport equation in this thesis, as exact analytic solutions do not exist for the geometry modelled. In the S_N approach, it is assumed that the transport equation given in equation X is valid for a discrete set of directions using a collocation method. This allows one to convert the integrals $\int_{4\pi}\sigma_{s,g'\to g}(\vec{r},\hat{\Omega}'\to\hat{\Omega})\psi_{g'}(\hat{\Omega}',\vec{\boldsymbol{r}})d\hat{\Omega}'$ and $\frac{\chi_g}{4\pi k}\int_{4\pi}\upsilon\sigma_{f,g'}(r)\psi_{g'}(\hat{\Omega}',\vec{\boldsymbol{r}})d\hat{\Omega}'$ into a summation over a discrete number N of possible solid-angle trajectories, yielding the following simplified equations:

$$\hat{\Omega}_n * \nabla\psi_{g,n}(\vec{\boldsymbol{r}}) + \sigma_{tot,g}\psi_{g,n}(\vec{\boldsymbol{r}}) = \sum_{m=1}^{N}\sum_{g'=1}^{G} w_m\sigma_{s,g'\to g}(\vec{r},\hat{\Omega}_m{}'\to\hat{\Omega}_n)\psi_{g'}(\hat{\Omega}'_n,\vec{\boldsymbol{r}}) + \frac{\chi_g}{4\pi k}\sum_{m=1}^{N}\sum_{g'=1}^{G} w_m\upsilon\sigma_{f,g'}(r)\psi_{g'}(\hat{\Omega}'_m,\vec{\boldsymbol{r}})$$

Equation 5: Multigroup S_N transport equation, arbitrary geometry, adapted from [23]

Where $\psi_{n,g}$ is the angular flux in the nth angular direction, w_m is the weight in the nth angular direction, and the gth group and $\sigma_{s,g'\to g}(\vec{r},\hat{\Omega}_m{}'\to\widehat{\Omega_n})$ is the scattering cross section from group g' and direction $\hat{\Omega}'_m$ to group g and solid angle $\widehat{\Omega}_n$. It should be noted from equation 5 that, since solid angle has now been discretized, each allowed solid angle has a corresponding angular flux.

The notable restriction of this approach is the so-called "ray effect", where neutron sources or absorbers that do not fall along one of the solid angles are not considered in flux calculations; however, due to the uniform geometry & low streaming in an LWR, this should not be a significant concern here.

4.2 NEWT & the Characteristic S_N method

Introducing a new spatial variable *s* in the direction of Ω, such that $\widehat{\Omega} * \nabla\psi = \frac{\partial\psi}{\partial s}$, and picking a computational cell small enough that σ_{tot} and all sources on the right hand side of equation X are constant [24], it is trivial to show that the flux is given by:

$$\psi(s) = \psi(0)e^{-\sigma_{tot}s} + \frac{Q}{\sigma_t}(1 - e^{-\sigma_{tot}s})$$

Equation 6: Characteristic solution to Boltzmann equation [24]

Where *Q* is the scatter plus fission sources, and all other terms are as defined above. Group indices have been omitted for conciseness. Additionally, since the $\widehat{\Omega}$ term has been incorporated into $\frac{\partial\psi}{\partial s}$, it follows that, in characteristic S_N, there are a finite number of directions *s* that need be considered, with weights and directional cosines determined by the quadrature set [24].

One limitation of characteristic S_N, however, is its inability to compute angular or scalar flux along cell boundaries. To maintain neutron balance and find cell-boundary flux for calculations in adjacent cells, the boundary-average flux is used instead. From the diagram below in Figure X, *A* and *B* are two arbitrary line segments, with distances s_1 and s_2 between their respective end points and parallel to the unit vector Ω_k.

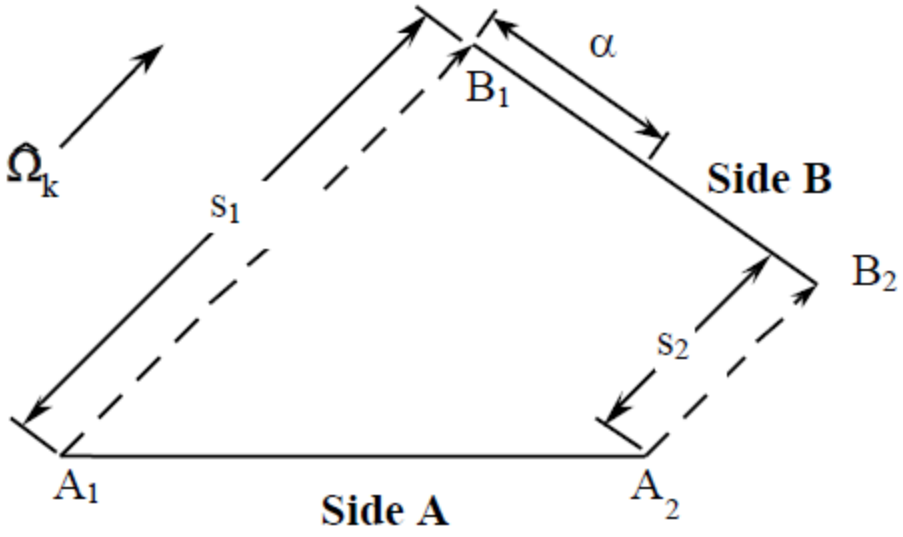

Figure 7: Sample computational cell *[25]*

Using these definitions, the distance *s* in the direction of Ω_k is given by:

$$s = \frac{s_2 - s_1}{L}\alpha + s_1$$

Equation 7: direction parallel to solid angle [24]

Where *L* is the length of side *B*. With these newly defined coordinates, the average flux on side *B* is given by:

$$\bar{\psi}_B = \frac{1}{L}\int_0^L \psi(\alpha)d\alpha$$

Equation 8: Side-average flux [24]

This expression can be evaluated using equation 6, with the initial condition $\psi(0) = \bar{\psi}_A$.

For a cell-averaged flux, it is insufficient to average the surface average fluxes; instead, one must use the surface-average fluxes as inputs to the Boltzmann's transport equation to ensure neutron balances are preserved. Applying this gives the final characteristic equation:

$$\bar{\psi}_{cell,j} = \frac{Q}{\sigma_{tot}} - \sum_{i=1}^{N} \bar{\psi}_i \hat{\Omega}_j * \hat{n}_i L_i$$

Equation 9: Cell-average flux [24]

Where the summation is over all *N* sides of the cell, L_i is the length of the i^{th} side of the cell, and $\bar{\psi}_{cell,j}$ is the cell-average angular flux in the j^{th} direction. Notice that, since the summation is now over an arbitrary number of sides, one can apply this to an arbitrary or mixed geometry, which enables a more accurate of fuel pins as many-sided polygons, rather than representing them as cuboids.

One further correction that needs to be made is neutron streaming in the z-direction: While NEWT is a 2-D (x-y) code, the constraint $|\Omega| = 1$ requires that $\mu^2 + \eta^2 + \xi^2 = 1$, where μ, η and ξ are the directional cosines in the x-, y-, and z- directions, respectively [24]. Thus, the total distance *s* travelled by a neutron must be adjusted to account for movement in the z direction, as given by

$$s = \frac{S_{2D}}{\sqrt{\mu^2 + \eta^2}} = \frac{S_{2D}}{\sqrt{1 - \xi^2}}$$

Equation 10: Relation of distance traveled to its 2D projection [24]

Where S_{2D} is the distance travelled in the x-y plane, and all other variables are as defined above.

4.3 Depletion module TRITON

Figure 8 depicts how depletion is performed in TRITON: Using user-defined unit cells, multigroup material and homogenized cell cross sections are generated from continuous energy data; flux calculations are then performed using equations 5 and 9 in NEWT. Taking specific power and time interval as arguments, fuel is then depleted at constant power for the specified

time interval until the desired specific power is achieved; additionally, this scaled flux can be used to deplete other materials without considering power using the flux depletion option; since nearly all power in a reactor comes from fission, it is typical to flux deplete all materials except for fuel. Fission products are tabulated and, for depletion after the first time interval, inventories are updated to account for production, depletion, and decay over the interval. This entire process, including microscopic cross section generation, is then repeated for each depletion step in the input file. Fission product inventories are tabulated separately for each material in the problem, so that fuel depletion, fission product production and depletion, and burnup, can be tracked separately for each fuel pin rather than uniformly depleting all fuel present in the system.

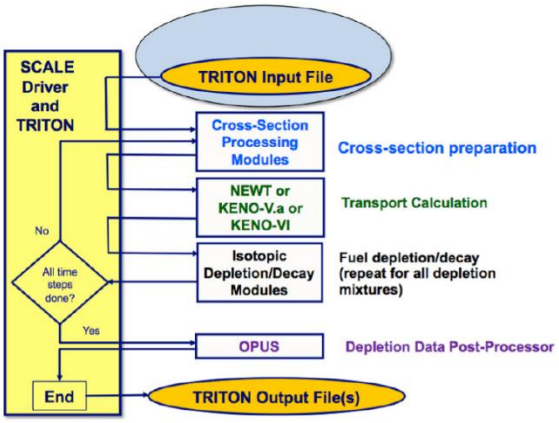

Figure 8: T-DEPL Methodology *[26]*

4.4 ORIGEN

Oak Ridge Isotope GENeration Automatic Rapid Processing (ORIGEN-ARP) is another module of SCALE used for determining used-fuel composition. For the purposes of this thesis, only the decay capabilities were used, as ORIGEN's depletion options were limited to more traditional assembly designs. Taking an output file with fuel isotopics from NEWT as its argument, ORIGEN then did simple decay-chain calculations to determine used fuel composition, total decay heat, decay heat from gamma rays, and gamma & neutron spectra at user specified times after

discharge. Notably, this enables one to find decay heat at multiple distinct times after discharge without having to repeat the entire depletion calculation.

5 Computational Model

5.1 SCALE Model

Since a full core 3-D model was not viable from a computing time standpoint, a reflected 2D quarter assembly was instead used: Using a specular reflection (mirror) boundary condition, which sets the net current equal to 0 on the sides of the quarter assembly, the flux in the quarter assembly would be a reasonably accurate representation of flux in a typical assembly in the reactor. P_1S_4 quadrature was chosen, as there is minimal streaming or anisotropic scattering; however, as a precaution, select cases were modelled in P_2S_6 and P_3S_8 to verify that higher quadrature sets and cross section expansions would not change the results. Further, to reduce the number of materials tracked, 1/8 assembly symmetry was used.

In a typical PWR, excess reactivity is controlled not with control rods, but with a soluble poison, e.g. boric acid, with control rods used only for startup and shutdown [10]. To introduce such an absorber and maintain assembly criticality, the b1 approximation is introduced; this correction adjusts the spectrum and cross sections based on the B_1 transport equations [10] to maintain criticality when the assembly would otherwise be subcritical or supercritical.

Due to its low density and cross section [10], Helium was represented with a void so that SCALE would not have to calculate cross sections for the gap regions. To further reduce computing time, an assign statement was used: Rather than compute cross sections for each fuel pin and IFBA material, two unit fuel cells were defined, one for a unit cell without IFBA, and one for a unit cell with IFBA; the group-dependent cross sections generated for these cells were then assigned to all other unit cells with the same composition, that is, the

cross sections for the unit cell without IFBA were assigned to all pins without IFBA, and the cross sections for the unit cell with IFBA were assigned to all pins with IFBA. Since there is no option for a pin with IFBA in a square pitch in SCALE's unit cell data, it was necessary to find an equivalent cylindrical cell. Assuming that equivalent cells have equal volumes [10] equation X was used to relate the radius of the equivalent cell and the pitch in the I^2S-LWR unit cell:

$$p^2 = \pi R_{eq}^2$$

Equation 10: Relation between pitch and equivalent cell radius [10]

Where p is the pitch between adjacent fuel pins, and R is the radius of the equivalent cylindrical cell, giving a radius of 0.683 cm. The radii of the fuel pin, gap, IFBA, and clad, were not changed. The actual and equivalent cylindrical fuel pin unit cells are shown in Figure 10.

5.1.1 Quarter Assembly Model, I^2S-LWR

If the flux is assumed to have 1/8 assembly symmetry, the quarter assembly can be modelled using 49 fuel materials and 22 IFBA materials for depletion, as shown in figure 9. Fuel was power-depleted, i.e. flux was calculated and then scaled so that the specific power in the fuel reached the desired value, and this scaled flux was then used to determine IFBA depletion. To account for variations in burnup between assemblies, the specific power for each model was varied between that case's expected minimum and maximum burnup.

Half Fuel 7	Fuel 20 IFBA	Fuel 25 IFBA	Fuel 28	Fuel 31	Fuel 34 IFBA	Fuel 37	Fuel 39	Fuel 41	Fuel 42 IFBA
Half Fuel 6	Fuel 16	Fuel 21	Fuel 26	Fuel 29 IFBA	Fuel 32	Fuel 35	Fuel 38 IFBA	Fuel 40	Fuel 41
CR5	Fuel 13 IFBA	Fuel 17 IFBA	Fuel 22 IFBA	CR 2	Fuel 30 IFBA	Fuel 33 IFBA	Fuel 36	Fuel 38 IFBA	Fuel 39
Half Fuel 5	Fuel 10	Fuel 14	Fuel 18	Fuel 23	Fuel 27 IFBA	CR 3	Fuel 33 IFBA	Fuel 35	Fuel 37
Half Fuel 4	Fuel 7	Fuel 11	Fuel 15	Fuel 19 IFBA	Fuel 24	Fuel 27 IFBA	Fuel 30 IFBA	Fuel 32	Fuel 34 IFBA
CR4	Fuel 5 IFBA	Fuel 8 IFBA	Fuel 12 IFBA	CR 1	Fuel 19 IFBA	Fuel 23 IFBA	CR 2	Fuel 29 IFBA	Fuel 31
Half Fuel 3	Fuel 3	Fuel 6	Fuel 9	Fuel 12 IFBA	Fuel 15	Fuel 18	Fuel 22 IFBA	Fuel 26	Fuel 28
Half Fuel 2	Fuel 2	Fuel 4	Fuel 6	Fuel 8 IFBA	Fuel 11	Fuel 14	Fuel 17 IFBA	Fuel 21	Fuel 25 IFBA
Half Fuel 1	Fuel 1	Fuel 2	Fuel 3	Fuel 5 IFBA	Fuel 7	Fuel 10	Fuel 13 IFBA	Fuel 16	Fuel 20 IFBA
	Half Fuel 1 IFBA	Half Fuel 2 IFBA	Half Fuel 3 IFBA	CR4	Half Fuel 4 IFBA	Half Fuel 5 IFBA	CR5	Half Fuel 6 IFBA	Half Fuel 7

Figure 9: Quarter assembly layout in I²S-LWR

Axially averaged fuel and moderator temperatures and densities were used and are listed in Table 5, since a 2D model does not allow for axial dependence of temperature or density.

Table 5: Densities & Temperatures in NEWT model [2]

Material	Density [g/cm^3]	Temperature [K]
Uranium Silicide	11.773	900
Zirconium diboride	6.085	700
APMT Stainless Steel	7.25	650
Stainless Steel-304	7.25	579.25
Water	0.71347	579.25

As a final measure to improve runtime, only three steel materials were used: One for all fuel pins without IFBA, a second one for all fuel pins with IFBA, and a third for guide tubes. While this is inaccurate, since changes to steel composition are assumed to be

constant across all fuel rods without considering difference in flux between pins, steel has such a low [27] radioactivity when activated compared with fuel that clad depletion may be ignored in determining used fuel composition. By the same reasoning, only four water materials were used, rather than assign a unique material identifier to the water in each cell: One water material was declared for all fuel pins with IFBA, one for all pins without IFBA, and one each for the water cell & gap.

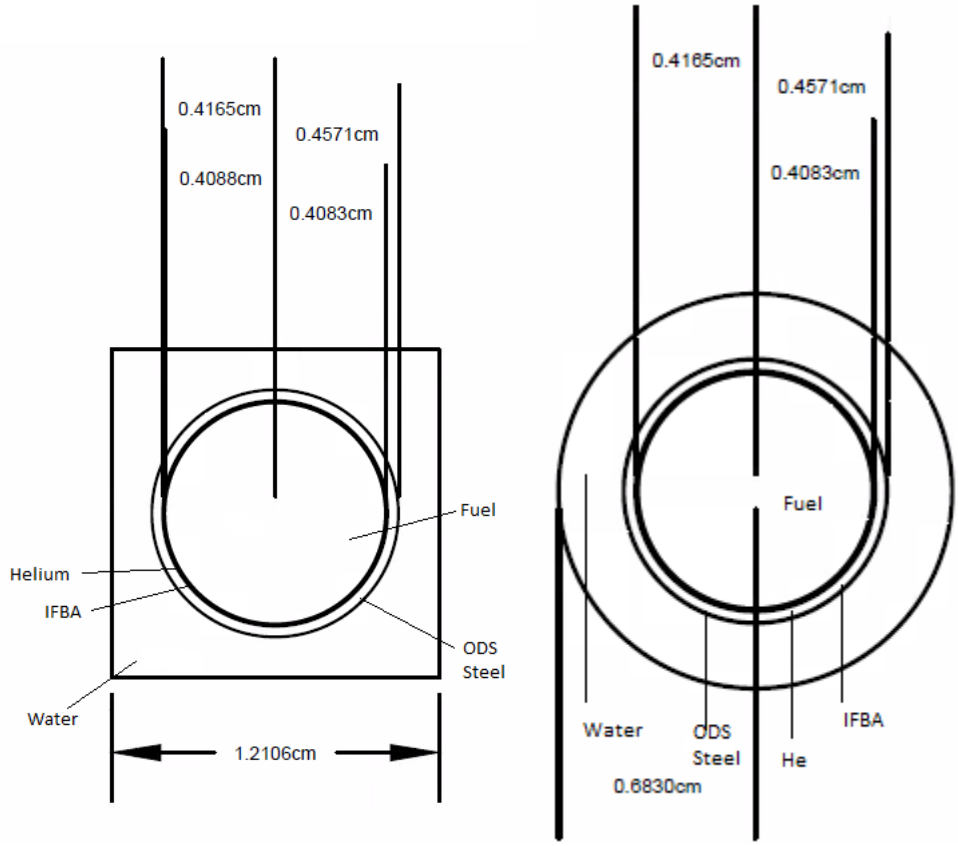

Figure 10: I²S-LWR Fuel rod unit cell with IFBA (L) and equivalent cylindrical cell (R)

5.1.2 Geometry, I²S-LWR

The quarter assembly is depicted in figure X: To account for the depression in thermal flux caused by the IFBA, 10x10 meshes were used in fuel cells containing IFBA, while 6x6 meshes were used in all other fuel pins, 4x4 mesh in the guide tubes, and a 2x2

mesh in the water cell. For unit cells on the bottom edge, a 10x5 mesh was used, since the cell is of half the height of other fuel unit cells; by the same reasoning, 6x3 meshes were used for the fuel cell without IFBA, and a 4x2 mesh in the guide tube cells. Similarly, 5x10 meshes, 3x6 meshes, and 2x4 meshes were used for fuel with IFBA, fuel without IFBA, and guide tubes, respectively, on the left edge of the assembly. These unit cells are shown in detail in figures 11 and 12, with the whole assembly shown in figure 13.

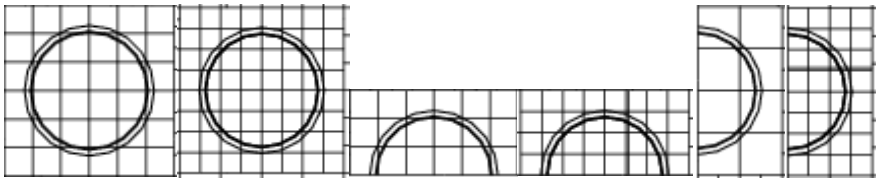

Figure 11 (L-R): Whole Fuel pin without IFBA, whole fuel pin with IFBA, half fuel pin (horizontal) without IFBA, half fuel (horizontal) pin with IFBA, half fuel pin (vertical) without IFBA, half fuel pin (vertical) with IFBA

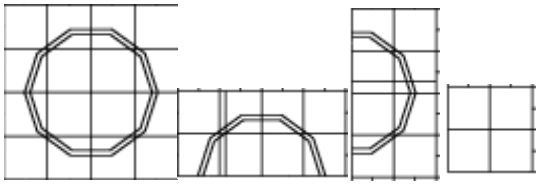

Figure 12 (L-R): Whole guide tube, partial (horizontal) guide tube, partial (vertical) guide tube, water cell

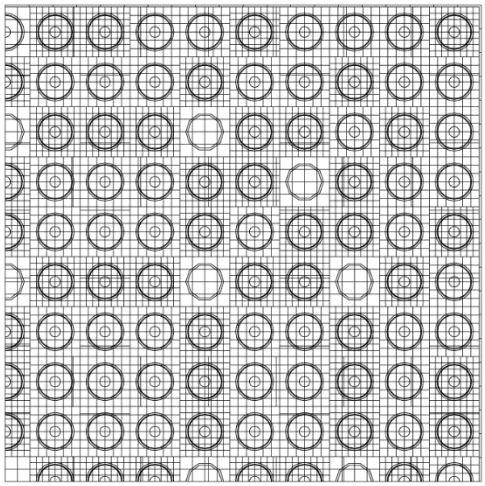

Figure 13:I^{2}S-LWR Assembly mesh

5.1.3 Quarter assembly model, traditional PWR

A quarter assembly has also been modelled for a traditional PWR, once again using a zero-current boundary condition. Owing to the smaller assembly in a traditional PWR, however, only 39 fuel materials and 17 IFBA materials are included, compared with 49 and 22, respectively, in the I^{2}S-LWR, as can be seen in Figure 14.

Half Fuel 6	Fuel 16	Fuel 19	Fuel 22	Fuel 25	Fuel 28	Fuel 30	Fuel 32 IFBA	Fuel 33 IFBA
Half Fuel 5 IFBA	Fuel 12	Fuel 17	Fuel 20 IFBA	Fuel 23	Fuel 26	Fuel 29	Fuel 31	Fuel 32 IFBA
Guide Tube	Fuel 9 IFBA	Fuel 13 IFBA	Guide Tube	Fuel 21 IFBA	Fuel 24 IFBA	Fuel 27	Fuel 29	Fuel 30
Half Fuel 4 IFBA	Fuel 7	Fuel 10	Fuel 14 IFBA	Fuel 18 IFBA	Guide Tube	Fuel 24 IFBA	Fuel 26	Fuel 28
Half Fuel 3 IFBA	Fuel 5	Fuel 8	Fuel 11 IFBA	Fuel 15	Fuel 18 IFBA	Fuel 21 IFBA	Fuel 23	Fuel 25
Guide Tube	Fuel 3 IFBA	Fuel 6 IFBA	Guide Tube	Fuel 11 IFBA	Fuel 14 IFBA	Guide Tube	Fuel 20 IFBA	Fuel 22
Half Fuel 2 IFBA	Fuel 2	Fuel 4	Fuel 6 IFBA	Fuel 8	Fuel 10	Fuel 13 IFBA	Fuel 17	Fuel 19
Half Fuel 1 IFBA	Fuel 1	Fuel 2	Fuel 3 IFBA	Fuel 5	Fuel 7	Fuel 9 IFBA	Fuel 12	Fuel 16
Guide Tube	Half Fuel 1 IFBA	Half Fuel 2 IFBA	Guide Tube	Half Fuel 3 IFBA	Half Fuel 4 IFBA	Guide Tube	Half Fuel 5 IFBA	Half Fuel 6

Figure 14: Quarter assembly layout in traditional PWR

Once again, axially averaged temperatures were used. To determine the sensitivity of decay heat to geometry and composition only, the same temperatures were used as in the I^{2}S-LWR depletion case; these temperatures are shown below in Table 6.

Table 6: Densities & Temperatures in NEWT model, traditional PWR

Material	Density [g/cm^3]	Temperature [K]
Uranium Oxide	10.4215	900
Zirconium diboride	6.085	700
Zircaloy	7.25	650
Stainless Steel-304	7.25	579.25
Water	0.71347	579.25

The geometry was also slightly changed from the I^{2}S-LWR design; notably, the rod pitch and diameter are greater than in the I^{2}S-LWR. As such, new unit cells had to be generated, including a new equivalent cylindrical cell for IFBA pins using equation 10; these are documented in figure 15, while the non-IFBA unit cell was generated using data from figure 6 above.

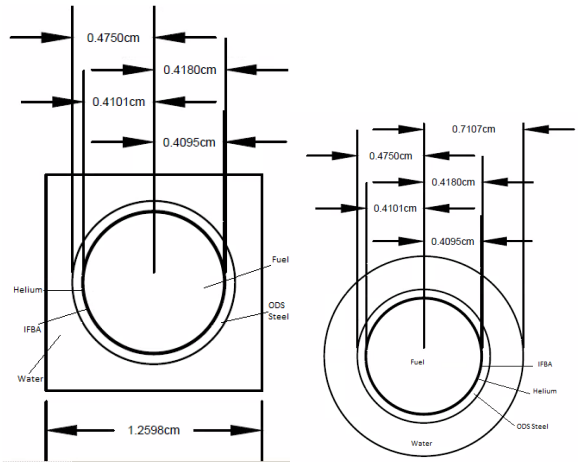

Figure 15 (L-R): Fuel unit cell without IFBA, fuel unit cell with IFBA, equivalent unit cell with IFBA for traditional PWR

5.1.4 Geometry, traditional PWR

Once again, the meshes from the I^{2}S-LWR depletion were also used here: 6x6 for non-IFBA whole fuel pins, 10x10 mesh for fuel pins with IFBA, 4x4 fuel pins for guide tubes, and a 2x2 mesh for the instrumentation tube. For the vertical (y-axis) half-cells, the meshes used were

3x6, 5x10, and 2x4 for non-IFBA fuel pins, IFBA fuel pins, and guide tubes, respectively; for horizontal, the meshes were 6x3, 10x5, and 4x2. These cells are depicted in Figures 17 and 18, while the quarter assembly is shown in Figure 16.

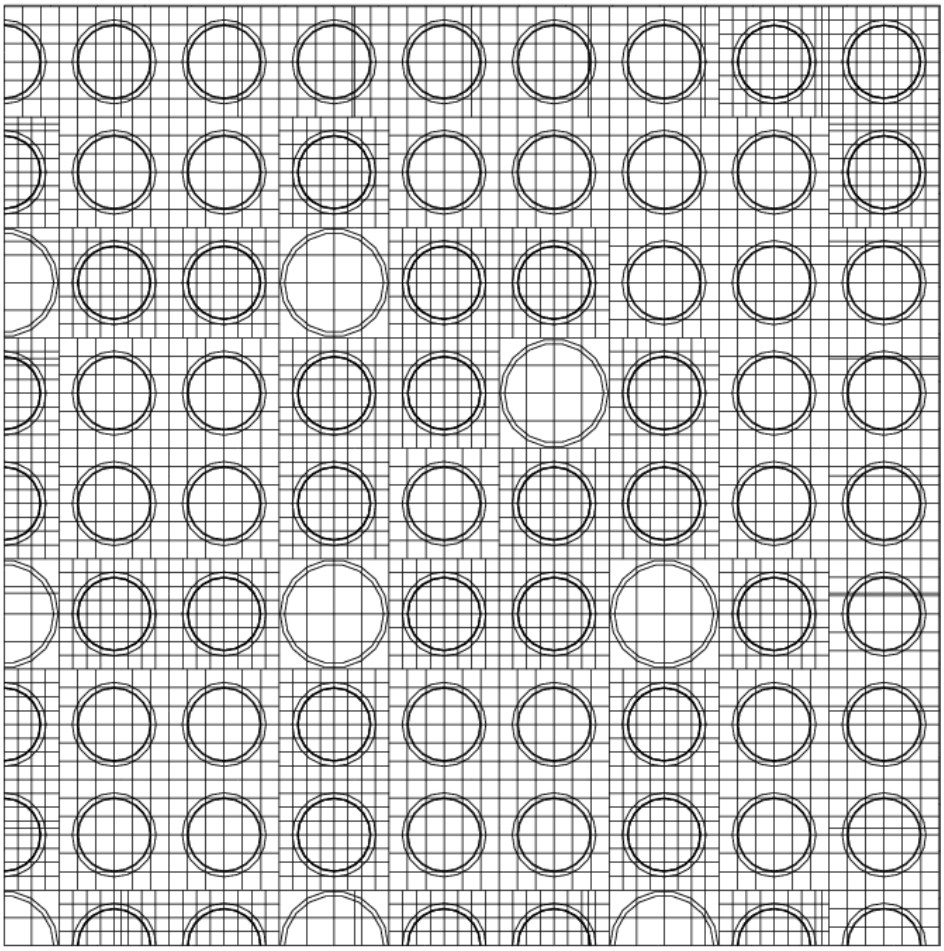

Figure 16: Mesh used for PWR depletion

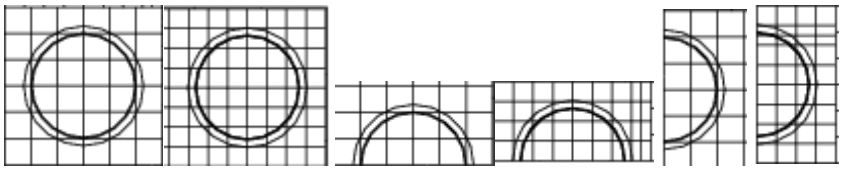

Figure 17(L-R): Meshes for fuel pin without IFBA, fuel pin with IFBA, horizontal half pin without IFBA, horizontal half pin with IFBA, vertical half pin without IFBA, vertical half pin with IFBA

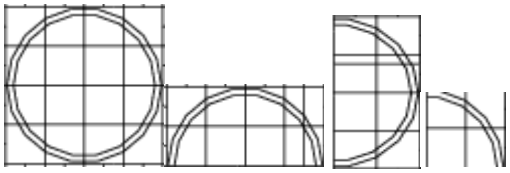

Figure 18 (L-R): Meshes for guide tube, horizontal half tube, vertical half tube, instrumentation tube

5.1.5 Transition from a traditional PWR to I²S-LWR

To specifically identify the causes of differing decay heat in I²S-LWR compared to a traditional PWR, it was decided to model the "transition" from a typical 17x17 UO_2-fuelled PWR assembly to the 19x19 U_3Si_2 design used in I²S-LWR. Starting with the 17x17 PWR assembly, the fuel was first changed from oxide to silicide. From there, the assembly was changed from 17x17 to 19x19 geometry, and as a final step the clad was changed from zircaloy to stainless steel.

5.2 Cases Considered

5.2.1 Baseline Cases

The I²S-LWR is tentatively expected to run on a "2.5-batch" core, a hybrid of the 2- and 3-batch cores discussed in Chapter 1, where roughly half of the fuel is discharged after 2 18-month cycles, and the remainder is discharged after 3 18-month cycles; while the uranium utilization in the 2-batch case is less than that in the 3-batch case, economics require that this fuel management approach be used. The baseline cases will use 4.95 w/o fuel on an 18-month cycle, with a 24 GW-day/MT and 20 GW-day/MT cycle burnup for the 2-batch case, and cycle burnups of 22 GW-day/MT, 18 GW-day/MT, and 14 GW-day/MT for the 3-batch case.

5.2.2 Uses of ORIGEN

As described above, ORIGEN can be used to determine decay heat and composition in used fuel post-discharge.

This use of ORIGEN has a significant limitation for reactor safety applications: Reactor power is non-zero for the first minute after shutdown, if not longer, due to delayed

neutrons from fission product decay [10] [28]. As such, additional reactor kinetics analyses which are outside the scope of this thesis should be performed for reactor safety assessments immediately following an accident or shutdown.

5.2.3 Sensitivity/Perturbation Analyses

In addition to the above cases, the baseline case of 44 GW-day/MTU was subjected to several variations, to determine the sensitivity of decay heat from I^2S-LWR fuel to changes in operating conditions.

As a significant simplifying assumption, all sensitivity analyses only changed one variable at a time, while all others were assumed to be those of the below-described baseline cases. For example, a sensitivity analysis considering power oscillations would not concurrently analyze a different fuel enrichment; the enrichment would be held constant at its original value of 4.95 w/o. This assumption is assumed to be valid without justification and will be discussed further in the following section, but for the time being the covariance of the variables being examined here is assumed to be small. In other words, the changes in decay heat from, e.g. a change in fuel enrichment and a change in discharge burnup are assumed to be expressed as a combination of the changes to decay heat from each of these changes separately.

With all this being said, table 7 documents the baseline case, included here as the first line, and all perturbations to be made. The k_{eff} solution type with no boron will assume a clean core with no soluble boron or adjustments to cross sections, while the k_{eff} with critical boron should, in theory, produce the same results as the B_1 approximation. The numbers in the "cycle burnup" column refer to the first and second cycle burnups, respectively; it should be noted that these all correspond to a discharge burnup of 44 GWD/MTHM. As for the "burnup" column, the 54 GWD/MTHM case is a 3-batch, 1.5-year cycle with cycle burnups of 22 GWD/MTHM, 18

GWD/MTHM and 14 GWD/MTHM, while the 40, 50, 60, and 70 GWD/MTHM burnup cases are at a constant specific power of 40 MW/MT and varying operating times.

Further, the 40 GWD/MTHM, 60 GWD/MTHM, and 70 GWD/MTHM were subjected to additional perturbations: the 40 GWD/MTHM and 60 GWD/MTHM cases were irradiated to these burnups at a higher and lower specific power of 62.5 MW/MTHM and 20 MW/MTHM, respectively, while the 70 GWD/MTHM was irradiated to this burnup at the same power as before, but at an enrichment of 6.50 w/o; this would provide a rough model of, or equivalency to, the high-burnup, high-enrichment fuel management strategy described in chapter 2.

Of these cases, only the first two, the 44 GWD/MTHM case with 4.95 w/o fuel, will be applied to a traditional PWR: The B_1 solution will be used to compare results with decay heat from I^2S-LWR, while B_1 and k_{eff} solutions will be compared to determine reactivity changes & sensitivity to method of solution.

Table 7:Matrix of cases to be modelled

Burnup	Power	Enrichment	Cycle burnup [GWD/MT]	Solution type
44 GWD/MTHM	45 MW/MT 38 MW/MT	4.95 w/o	24, 20	B_1
44 GWD/MTHM	45 MW/MT 38 MW/MT	4.95 w/o	24, 20	k-effective no boron
44 GWD/MTHM	45 MW/MT 38 MW/MT	4.45 w/o	24, 20	B_1
70 GWD/MTHM	40 MW/MT	4.95 w/o	70	B_1
70 GWD/MTHM	40 MW/MT	6.50 w/o	70	B_1
40 GWD/MTHM	40 MW/MT	4.95 w/o	40	B_1
50 GWD/MTHM	40 MW/MT	4.95 w/o	50	B_1
60 GWD/MTHM	40 MW/MT	4.95 w/o	60	B_1
40 GWD/MTHM	20 MW/MT	4.95 w/o	40	B_1
40 GWD/MTHM	62.5 MW/MT	4.95 w/o	40	B_1
60 GWD/MTHM	20 MW/MT	4.95 w/o	60	B_1
60 GWD/MTHM	62.5 MW/MT	4.95 w/o	60	B_1
44 GWD/MTHM	42 MW/MT 42 MW/MT	4.95 w/o	22, 22	B_1
44 GWD/MTHM	38 MW/MT 45 MW/MT	4.95 w/o	20, 24	B_1
44 GWD/MTHM	54 MW/MT 29 MW/MT	4.95 w/o	28.6-15.4	B_1
44 GWD/MTHM	29 MW/MT 54 MW/MT	4.95 w/o	15.4-28.6	B_1
54 GWD/MTHM	42 MW/MT 34 MW/MT 27 MW/MT	4.95 w/o	22, 18, 14	B_1

5.2.4 Covariance Studies and Independence of Perturbations

As mentioned above, covariance in decay heat, i.e. variance due to the combination of perturbations, rather than due to the perturbations separately, was ignored for most of the cases considered. However, to verify this assumption, the independence of burnup & specific power will be investigated since, as will be further discussed in Chapter 6, the primary determinants of decay heat were discharge burnup and operating power. If the covariance of burnup and operating power is zero, then it follows that, if the burnup *BU* is changed to some new burnup $BU + \Delta BU$, then, for decay heat given as some function of power & burnup $F(P,BU)$, equation 11 must hold.

$$\frac{F(P,BU+\Delta BU)-F(P,BU)}{F(P,BU)} = C * \frac{F(P\prime,BU+\Delta BU)-F(P\prime,BU)}{F(P\prime,BU)}$$

Equation 11: Non-covariant relation of decay heat

That is, the percent difference introduced by a change in burnup should be the same at any power, or the percent difference introduced should be the same at all times after discharge, times a time-independent constant. If this is not the case, then power and burnup are said to be covariant.

5.3 Forms of Decay Heat

As discussed in chapter 2, decay heat can broadly be broken into two categories: Charged and neutral particles. To this end, total decay heat and decay heat due to gamma rays will be tracked separately, and decay heat from charged particles will be defined simply as total decay heat minus decay heat produced by gamma rays.

5.4 Critical Boron Concentration

As mentioned above, PWRs, including the I^2S-LWR, use boric acid rather than control rods to achieve and maintain criticality. To determine the critical boron concentration, one uses the k_{eff} solution method in SCALE rather than the b1 approximation. Much like the b1 approximation, the k_{eff} solution method solves the transport equation as an eigenvalue problem. However, unlike b1, the k_{eff} solution does not adjust the cross sections to achieve criticality; as such, the spectrum is different from that of the actual reactor. This allows one to determine the critical boron concentration: By running SCALE depletion runs in the k_{eff} mode with borated water, one can interpolate to find critical boron concentration using equation 12:

$$k = \frac{k_2 - k_1}{SB_2 - SB_1} * SB + k_0$$

Equation 12: k as a function of soluble boron concentration

Where SB_2 and SB_1 are the concentrations of natural boron in ppm and k_2 and k_1 the corresponding k_{eff} eigenvalues, and k_0 is the k_{eff} corresponding to a system with no soluble boron. Since SCALE reports k_{eff} at each time interval, the critical boron concentration can also be found at each time step. This critical boron data was then used in a series of RESTART files in SCALE, using the calculated critical boron concentration in the k_{eff} solution rather than b1 to create a critical spectrum. While this approach is at least as accurate as the b1 approximation in determining the neutron spectrum and maintains criticality, unlike b1, it has one significant limitation: k_{eff} is less than 1.0 at end-of-cycle, as in a real reactor k_{eff} would be increased by the addition of fresh fuel, and there would be a net current into once- burned assemblies assemblies, such as the one modelled in this thesis, to maintain criticality. As such, critical boron concentration cannot be calculated for high-burnup fuel using this model.

6 Results

6.1 General results

6.1.1 Critical Boron Concentration

Using the method described in section 5.4, two cases were run in the k_{eff} mode, one with a natural boron concentration of 1800 ppm, the other with a concentration of 2100 ppm. Using the k_{eff} results from this and equation 11, critical boron concentration was found & plotted in Figure 19.

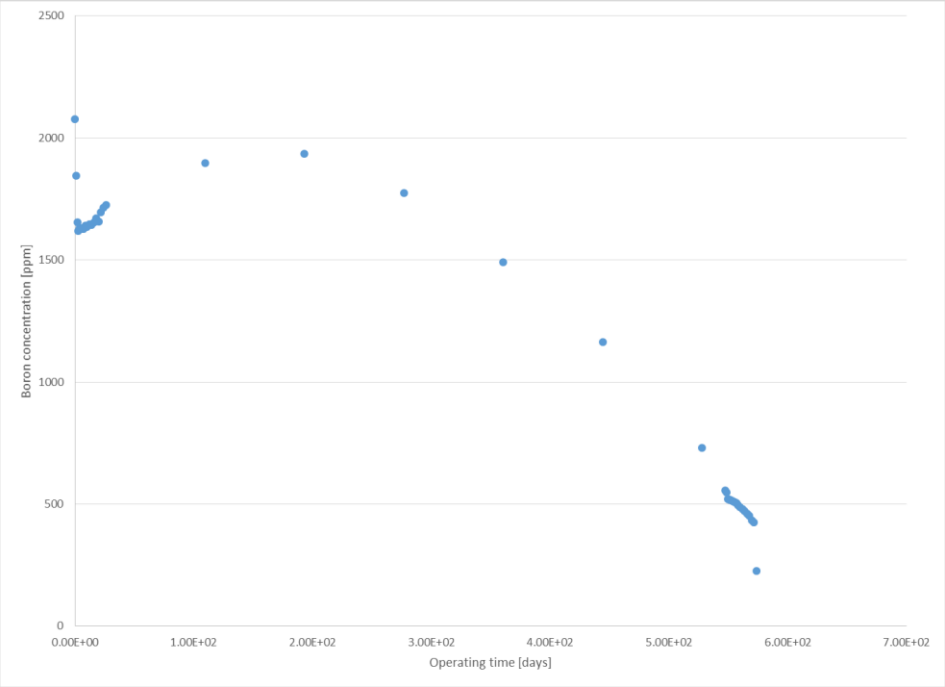

Figure 19: Critical boron concentration for 2-batch I²S-LWR

It should be noted that critical boron concentration is not defined beyond 574 days operating time due to the way in which the SCALE model was created. The k_{eff} found with the zero-current boundary condition is less than 1 at these times, as in the real reactor a net current into the assembly from other, lower-burnup assemblies would maintain criticality.

6.1.2 Spectral Index

To measure the changes in neutron energy, a new variable, the so-called spectral index *S*, is introduced. Defined as the ratio of quarter-assembly flux with energy < 0.625 eV to flux of all energies, as seen in equation 13, the spectral index provides a single number to measure the spectral hardening/softening in a system.

$$SI = \frac{\int_V \int_0^{0.625\ eV} \phi(\vec{r}, E) dE dV}{\int_V \int_0^{\infty} \phi(\vec{r}, E) dE dV}$$

Equation 13: Spectral Index

Another important way of characterizing a reactor's spectrum is its ratio of moderator to fuel [10]; in the case of any LWR, this is equivalent to the ratio of hydrogen to uranium (H:U ratio). For passive safety purposes, both the AP1000 and I^{2}S LWR have a "conservative" H:U ratio such that an increase in H:U will increase reactivity; this is also referred to as an "undermoderated" system [29]. Assuming a moderator density of 0.71347 gram/cubic centimeter [3], the H:U ratios for an oxide-fueled traditional PWR, a silicide-fueled traditional PWR and I^{2}S-LWR are found to be 3.429, 3.259, and 3.106, respectively. The lower H:U ratio in I^{2}S-LWR will result in a harder (faster) spectrum and consequently a lower spectral index compared to a traditional PWR, regardless of fuel composition in that traditional PWR.

Comparing a UO_2 fueled PWR to a silicide fueled PWR, one sees a constant decrease in the spectral index of approximately 0.4 x 10^{-2} at each depletion step. One would also expect a harder spectrum, i.e. a higher *S*, in I^{2}S-LWR compared with a traditional PWR because of the thermal neutron absorption in the I^{2}S-LWR cladding, and this is seen in figures 20 and 21: At beginning of cycle, the spectral index is approximately 0.5 * 10^{-2} lower in the I^{2}S-LWR than in a

silicide fuelled PWR, or 0.9 * 10 $^{-2}$ less than in an oxide fuelled PWR, for a total difference of 0.9 x 10^{-2}, or 9%.

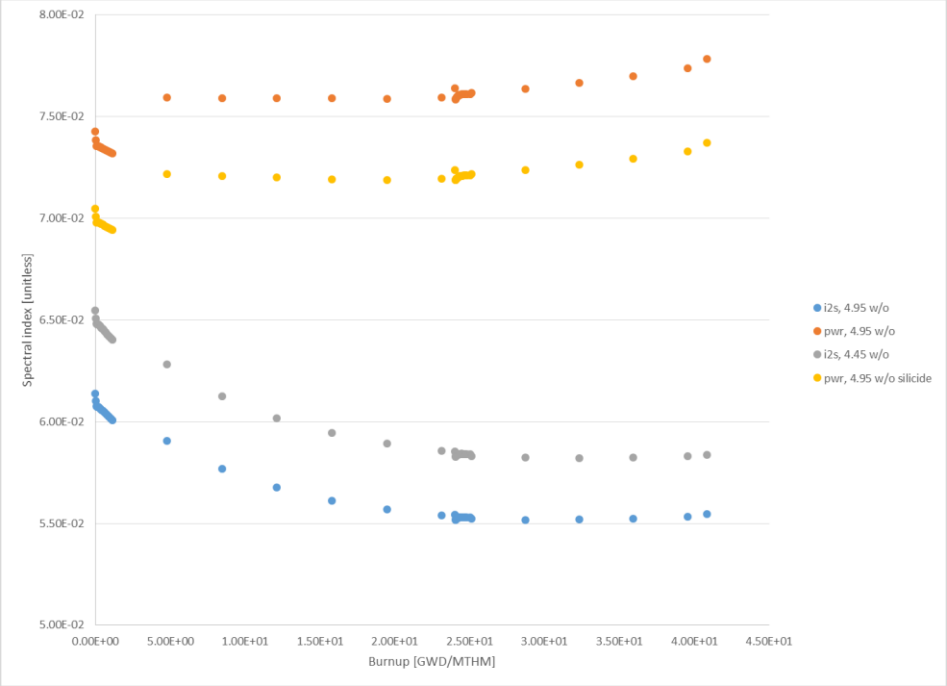

Figure 20: Burnup-dependent spectral index for fuel irradiated to 44 GWD/MTHM

Not only is the spectral index much higher in a PWR than in the I^{2}S-LWR, but the time behavior of the indices is also different: While the spectral index drops by 0.02 in both cases after startup, the index then returns to a value greater than its starting value in the PWR, and increases with burnup over the fuel's irradiation time. By contrast, in the I^{2}S-LWR, the initial decrease in spectral index is then followed by a continuous decrease until a burnup of 28.35 GWD/MTHM, at which point it increases, albeit at a slower rate than that of the index of a PWR. Since silicide fuel reduced the spectral index in a traditional PWR but did not change the trend it followed over time, at this preliminary stage it is likely that the change in time behavior of the spectral index is not due to the change in fuel chemistry, but rather the novel geometry and cladding present instead. Additionally, comparing the two I^{2}S-LWR cases to each other, the trend or time-dependent

behavior is the same for 4.45 and 4.95 w/o fuel, while the spectral index is ~0.05 (5%) higher in the 4.45 w/o case.

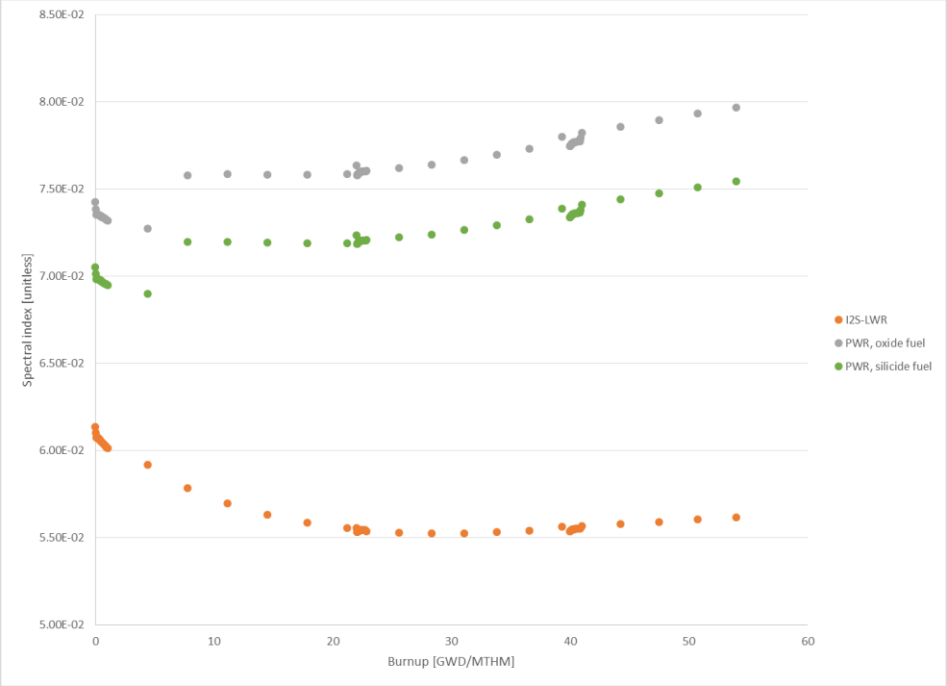

Figure 21: Burnup-dependent spectral index, 54 GWD/MTHM case

Once again, the same trends are on display in the 3-batch case. Spectral index drops immediately after startup in a traditional PWR, regardless of fuel chemistry, and then sharply increases at a burnup of 4.4 GWD/MTHM, then slowly increasing with burnup for the rest of the fuel's in-core residence time; also, just like the 2-batch case, the spectral index is consistently in the silicide fuelled case than the oxide fuelled ones, but follows the same trend. The I^2S-LWR also displays this sharp decrease and continues to decrease until a burnup of 28.35 GWD/MTHM, exactly the same burnup at which it begins to increase in the 2-batch case as well. Further, just as was the case with the 2-batch core, there is a difference of ~0.013 between the traditional oxide-fuelled PWR and I^2S-LWR, and ~0.95 between the silicide-fuelled PWR and I^2S-LWR.

One other consideration is the dependence of spectral index on fuel management strategy. As mentioned above, two of the proposed strategies are a 2-batch, 44 GWD/MTHM approach, and a 3-batch, 54 GWD/MTHM approach; the spectral indices are plotted below in Figure 22.

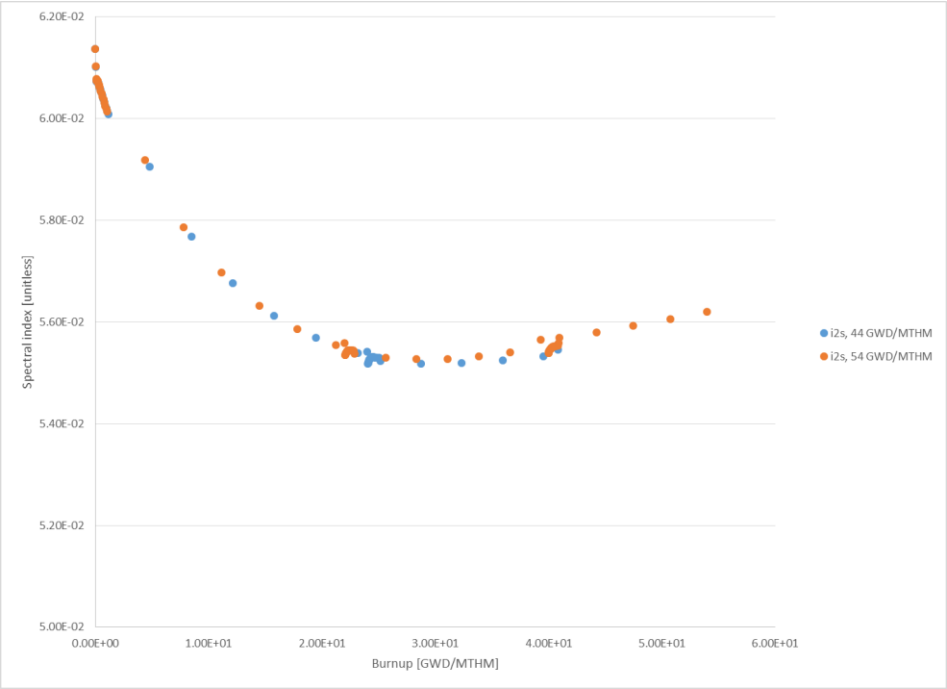

Figure 22: Burnup-dependent spectral index in I²S-LWR

Up to the 2-batch case's discharge burnup at 44 GWD/MTHM, the 2- and 3- batch cases have the exact same dependence on burnup. Therefore, it appears that specific power & fuel management strategy do not change the spectral index, which depends only on burnup for a given reactor type.

6.1.3 Depletion of Uranium-235

The number density of ^{235}U will, of course, deplete over the fuel cycle as it is consumed in fission. Since the I^{2}S-LWR has a different spectrum from a traditional PWR, this may impact its ability to burn ^{235}U.

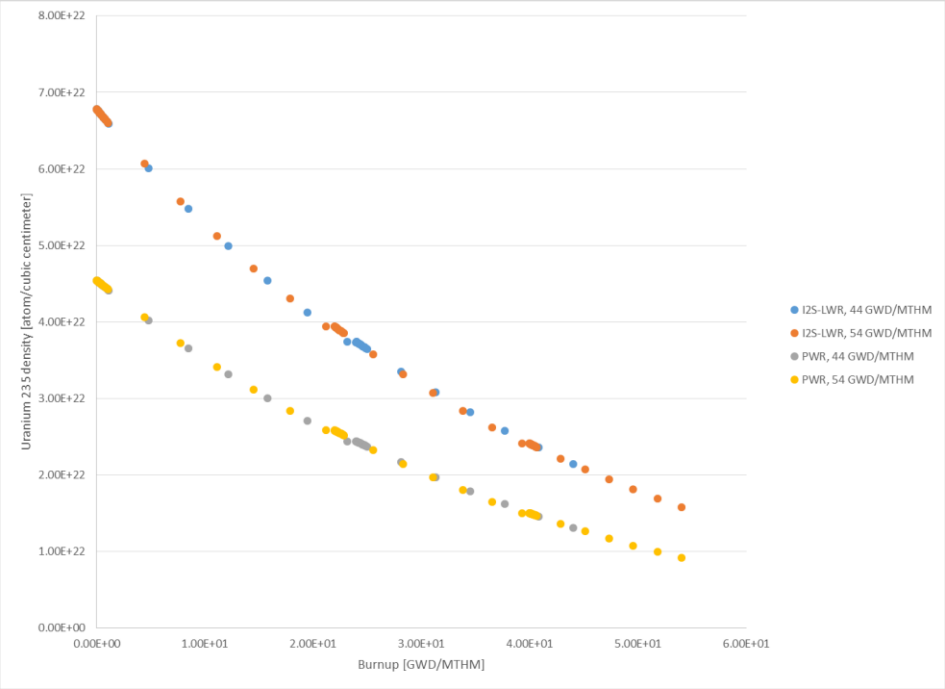

Figure 23: Uranium-235 number density as a function of burnup in I^{2}S-LWR and traditional PWR

Notice in Figure 23 that, when measuring ^{235}U number density as a function of burnup rather than time, the density is now highly similar for both the 44 and 54 GWD/MTHM fuel management approaches. Turning now to the question of how the transition to the I^{2}S-LWR design impacts ^{235}U consumption, calculating the percent of initial ^{235}U remaining lets one directly compare these I^{2}S-LWR and a traditional PWR while incorporating the difference in fuel chemistry. By this metric, the I^{2}S-LWR has slightly inferior ^{235}U consumption: Where 79.52% of ^{235}U is consumed in the 54 GWD/MTHM case for a traditional PWR, 76.84% of ^{235}U is consumed in I^{2}S-LWR, a difference of 2.67%. Examining the 44 GWD/MTHM case, 71.15% of ^{235}U is consumed in a traditional PWR, compared with 68.29% in the I^{2}S-LWR, a difference of 2.86%. Given the I^{2}S-LWR's lower excess reactivity and operating power, it is to be expected that its uranium consumption would be lower. Further, as discussed below in section 6.1.4, the I^{2}S-LWR has greater ^{239}Pu and ^{241}Pu production than a traditional PWR, meaning that the I^{2}S-

LWR could offset its lower ^{235}U consumption with the consumption of additional produced ^{239}Pu and ^{241}Pu.

6.1.4 Actinide production and depletion

As is the case with any LWR using ^{238}U- containing fuel, the I^{2}S-LWR produces Plutonium-239,240,241, and 242 (^{239}Pu, ^{240}Pu, ^{241}Pu, ^{242}Pu) and Americium 241 (^{241}Am) over its operating lifecycle, as given by the following reactions [10]:

$$^{238}U + n \rightarrow {}^{239}U \xrightarrow{\beta} {}^{239}Np \xrightarrow{\beta} {}^{239}Pu$$

$$^{239}Pu + n \rightarrow {}^{240}Pu$$

$$^{240}Pu + n \rightarrow {}^{241}Pu$$

$$^{241}Pu + n \rightarrow {}^{242}Pu$$

$$^{241}Pu \xrightarrow{\beta} {}^{241}Am$$

$$^{241}Am + n \rightarrow {}^{242}Am$$

Of these isotopes, ^{239}Pu, ^{241}Pu, ^{241}Am, and ^{242}Am are fissile, while ^{240}Pu and ^{242}Pu are fissionable nuclei and resonance absorbers [10] [27]. It is useful to examine plutonium and americium buildup & depletion in the I^{2}S-LWR compared with a traditional PWR, both because it could explain differences in decay heat between I^{2}S-LWR and a traditional PWR, and because it lets one see the impact from a fuel-cycle perspective of the transition from a traditional PWR to this novel design.

As mentioned above, not all of the transuranics produced are fissile. To account for this, a new variable FF, standing for "fissile fraction", is introduced and defined in equation 14 as the number density of ^{239}Pu plus the number density of ^{241}Pu, divided by the number density of all plutonium and multiplied by 100, to represent the atom percentage of fissile plutonium.

$$FF = 100 * \frac{N_{^{239}Pu} + N_{^{241}Pu}}{N_{^{239}Pu} + N_{^{240}Pu} + N_{^{241}Pu} + N_{^{242}Pu}}$$

Equation 14: Fraction of fissile plutonium

While this does not account for the atom density of ^{241}Am, subsequent analysis found that the atom density of ^{241}Am is much less than that of any of the Pu isotopes, meaning that its exclusion would have minimal impact on the "enrichment" of plutonium.

With these definitions in mind, the buildup of ^{239}Pu and ^{241}Pu will be plotted below, along with the FF parameter. Rather than plot plutonium atom density of a function of time, it will instead be plotted as a function of burnup to account for the multiple fuel-management strategies considered in this thesis.

The first set of comparisons will be for the 2- and 3- batch cores in both the I^{2}S-LWR and traditional PWR. The 3-batch core will have discharge burnup of 54 GWD/MTHM with cycle burnups of 22 GWD/MTHM, 18 GWD/MTHM and 14 GWD/MTHM, while the 2-batch core will have discharge burnup of 44 GWD/MTHM achieved with cycle burnups of 24 GWD/MTHM and 20 GWD/MTHM. Comparing both fuel cycles for a traditional PWR and I^{2}S-LWR, figure 24 documents the burnup-dependent concentration of fissile plutonium.

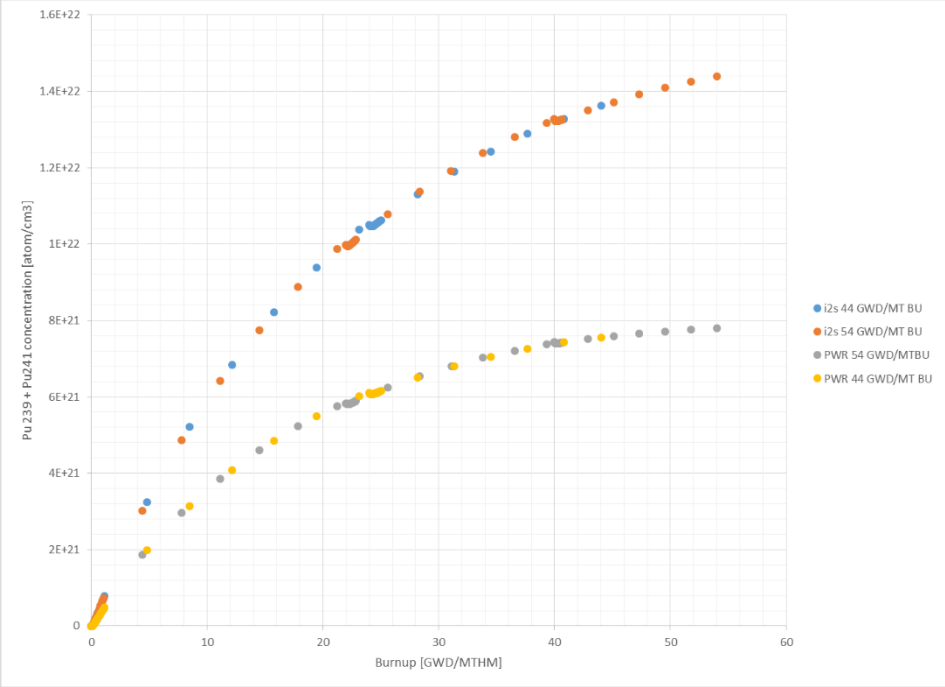

Figure 24: Burnup dependent fissile plutonium concentrations in I²S-LWR and traditional PWR

It is readily apparent from figure 24 that fissile plutonium production is greater in the I²S-LWR compared with a traditional PWR, and the concentration is determined by reactor geometry, composition and burnup, meaning that it is independent of specific power or fuel management strategy used.

This strong dependence on burnup and reactor design, and insensitivity to operating power or fuel management strategy is also present in the buildup and depletion of ^{240}Pu and ^{242}Pu. Once again, as seen in figure 25, one sees a consistent, burnup-dependent concentration, with little (>1%) difference between the two fuel management strategies, and a much greater (<5%) difference between reactor designs.

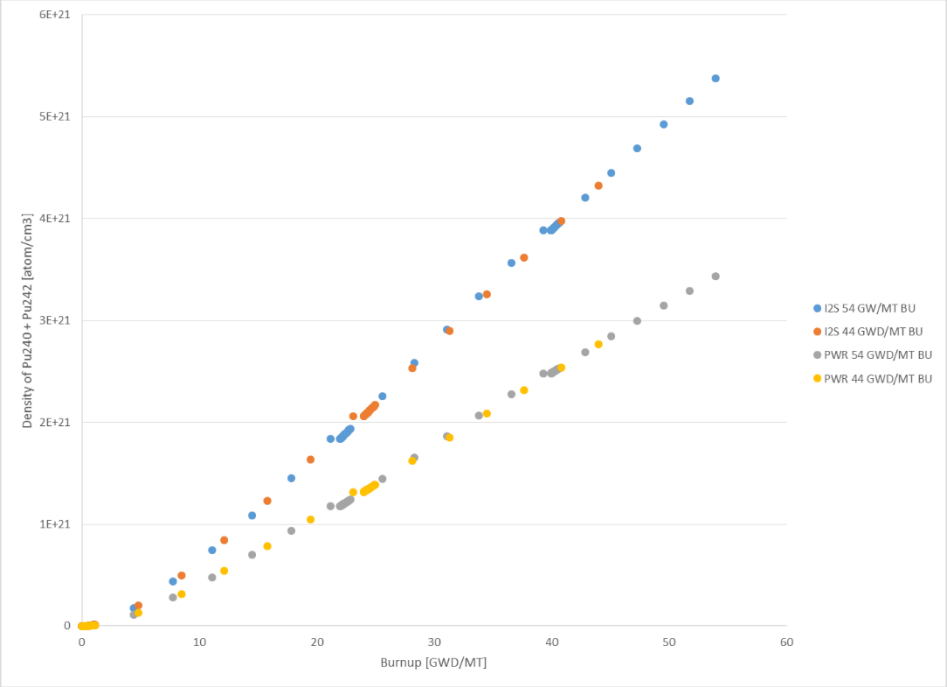

Figure 25: Burnup-dependent fertile plutonium concentration in I²S-LWR and traditional PWR

This trend also holds for the "fissile fraction" parameter defined above, as seen in figure 26: Reactor design and burnup, not fuel management strategy or specific power, determines plutonium composition. Additionally, one can also see that the fissile fraction of plutonium in I²S-LWR is greater than the fissile fraction in a traditional PWR, and that this difference increases with burnup, going from less than 0.1% at burnups below 1 GWD/MT to 3.3% difference at 54 GWD/MT: The fissile fraction of discharged I²S-LWR fuel is 72.785 a/o compared to 69.434 in the standard PWR.

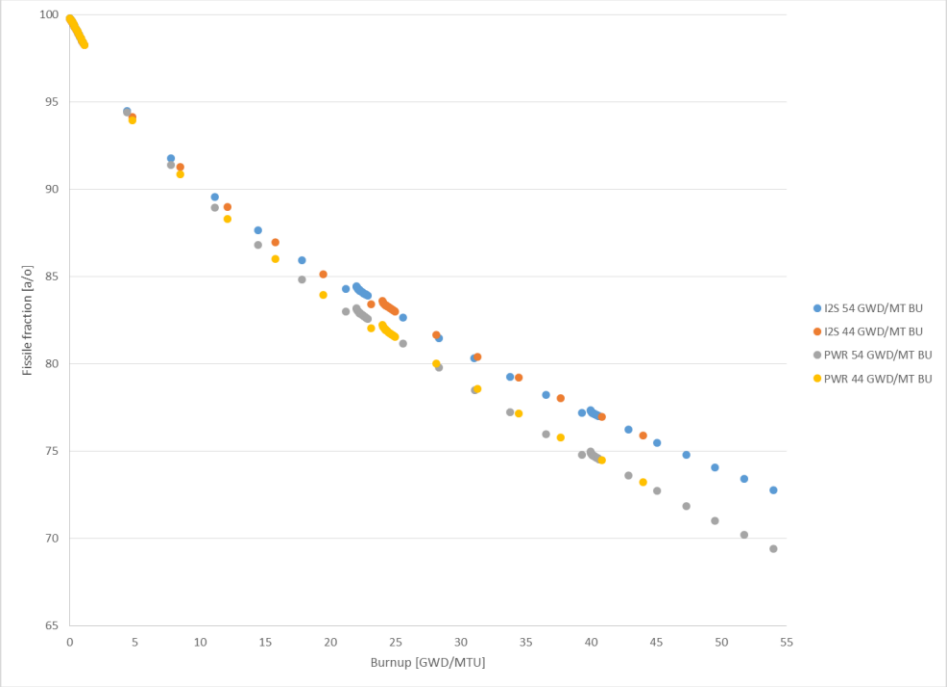

Figure 26: Burnup-dependent fissile plutonium percentage in I^{2}S-LWR and PWR

As mentioned above, fissile ^{241}Am is produced in conventional LWRs. Once again, in figure 27, one sees greater ^{241}Am content in the I^{2}S-LWR compared with a traditional PWR. This is to be expected, as ^{241}Am is formed from the β decay of ^{241}Pu, and ^{241}Pu content is greater in an I^{2}S-LWR than a traditional PWR. However, unlike any of the plutonium isotopes, ^{241}Am content is sensitive to fuel management strategy and specific power: 2-batch I2S-LWR fuel contains 8 * 10^{19} atom/cm^3 of ^{241}Am, compared with 1.04 * 10^{20} atom/cm^3 at a burnup of 43 GWD/MTHM in the 3-batch core, a difference of 23.08%, and 1.55 * 10^{20} atom/cm^3 at its discharge burnup of 54 GWD/MTHM, a difference of 43.38%. Clearly, reactor design & burnup alone are not enough to calculate ^{241}Am production, and specific power must also be considered.

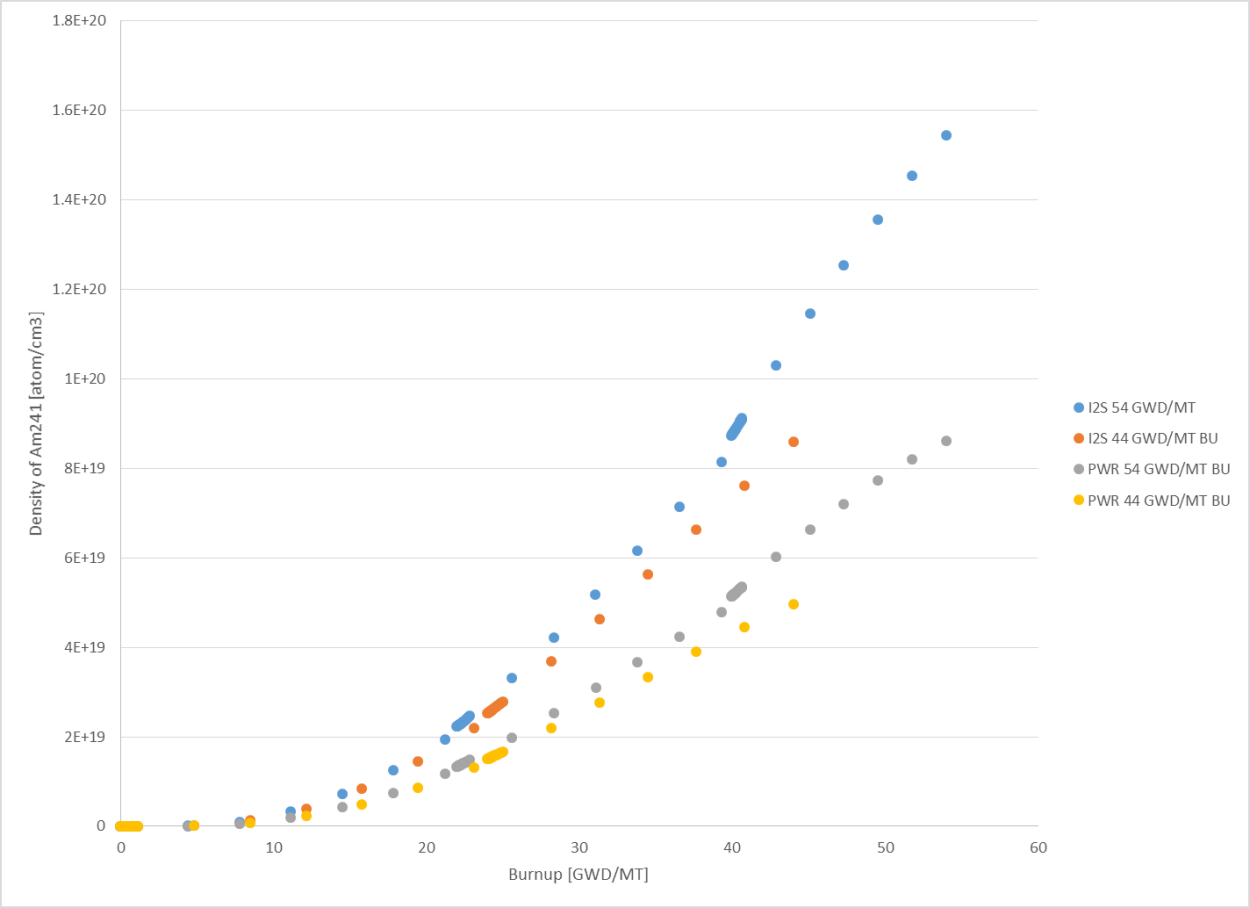

Figure 27: Burnup-dependent concentration of Americium-241 in I²S LWR and PWR

As a final sensitivity study, the 44 GWD/MTHM, 2-batch case was re-simulated subject to multiple variations documented in section 6.2.4, and reproduced below in Table 8. Case 1 is the baseline 2-batch core, and cases 2-5, while having the same discharge burnup and operating time, have different cycle burnups to study the effects of power oscillations. As can be seen in figures 28 and 29, the atom density of Plutonium-239, Plutonium-240, Plutonium-241 and Plutonium-242 is independent of power oscillations within a given fuel management strategy, confirming the original claim that burnup and reactor design are the primary determinants of plutonium concentration. The "clusters" of data points at certain burnups are an artifact from SCALE, rather than an indication of unusual data.

Table 8: Power histories for sensitivity studies

Case number	First cycle burnup [GWD/MTHM]	Second cycle burnup [GWD/MTHM]
1	24	20
2	22	22
3	20	24
4	28.6	15.4
5	15.4	28.6

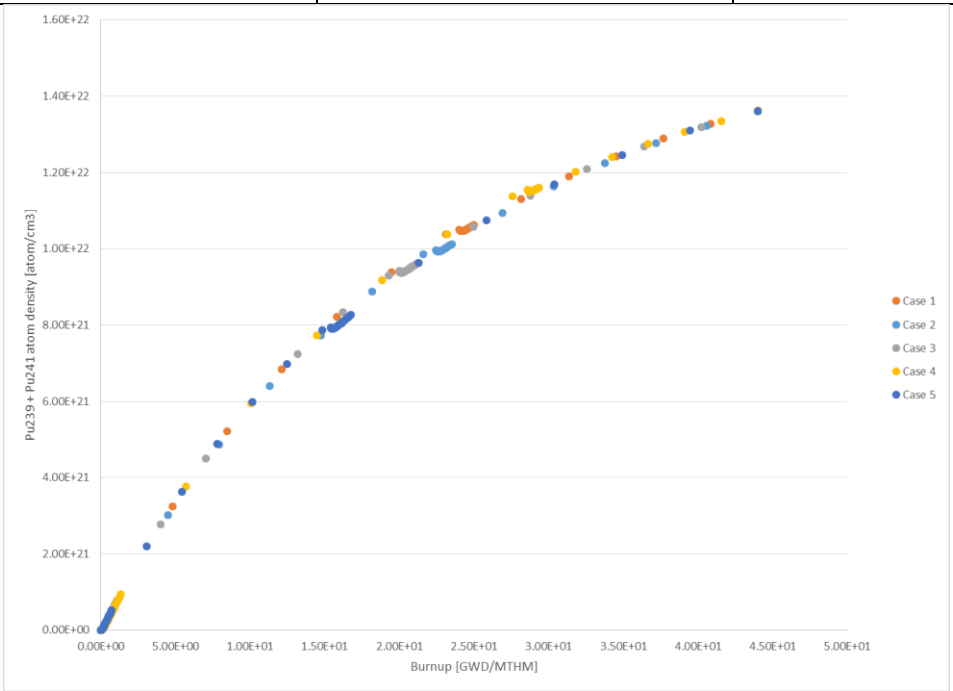

Figure 28: Burnup-dependent fissile plutonium density in 2-batch I²S-LWR

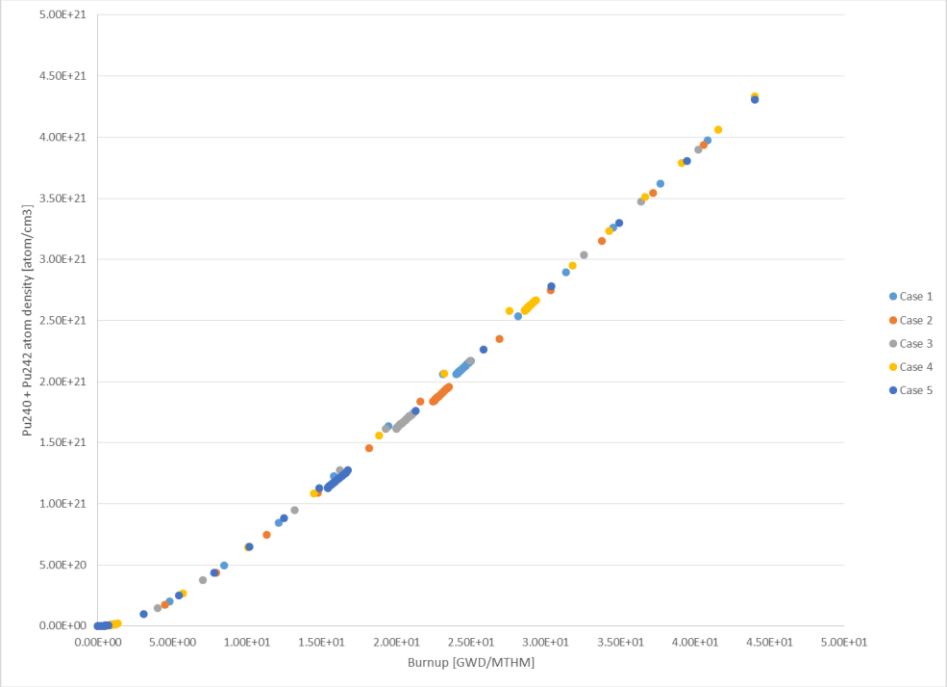

Figure 29: Burnup-dependent fertile plutonium density in 2-batch I²S-LWR

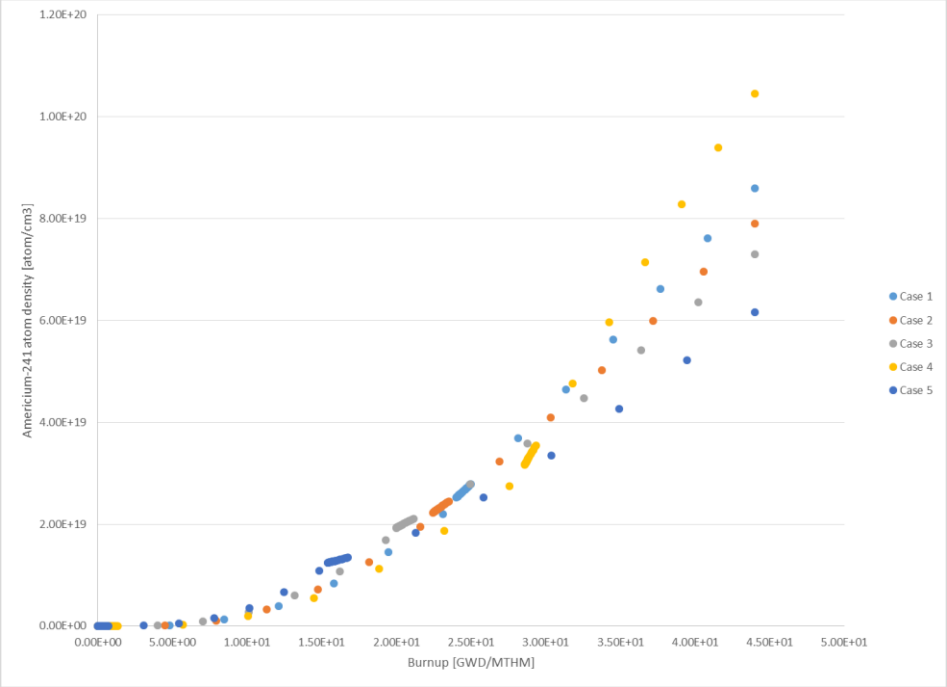

Figure 30: Burnup dependent Americium-241 density in 2-batch I²S-LWR

Once again, looking at Figure 30, Americium-241 production depends on specific power. Here, however, the oscillating power at fixed burnup provides new information: Looking at figure 18, one sees discharge ^{241}Am content decreases with second-cycle burnup, and that the

change in operating power after refueling changes the ^{241}Am production rate; specifically, an increasing in operating power results in a lower ^{241}Am production rate, and vice-versa.

6.1.5 Changes in Reactivity

The excess reactivity ρ_{ex} of the uncontrolled core will be greater than 0 throughout reactor operations, with boric acid and IFBA coating used to control it. Over reactor operations, this excess is reduced due to fuel burnup and fission product poisoning [10]. In this section, changes in reactivity due to SCALE will be examined: Whereas the b1 solution method adjusts cross sections to achieve a critical flux spectrum, the k_{eff} solution method does not, meaning the flux spectrum will not necessarily be that of a critical system. Comparing the k_{eff} and b1 solutions for I^{2}S-LWR, one gets:

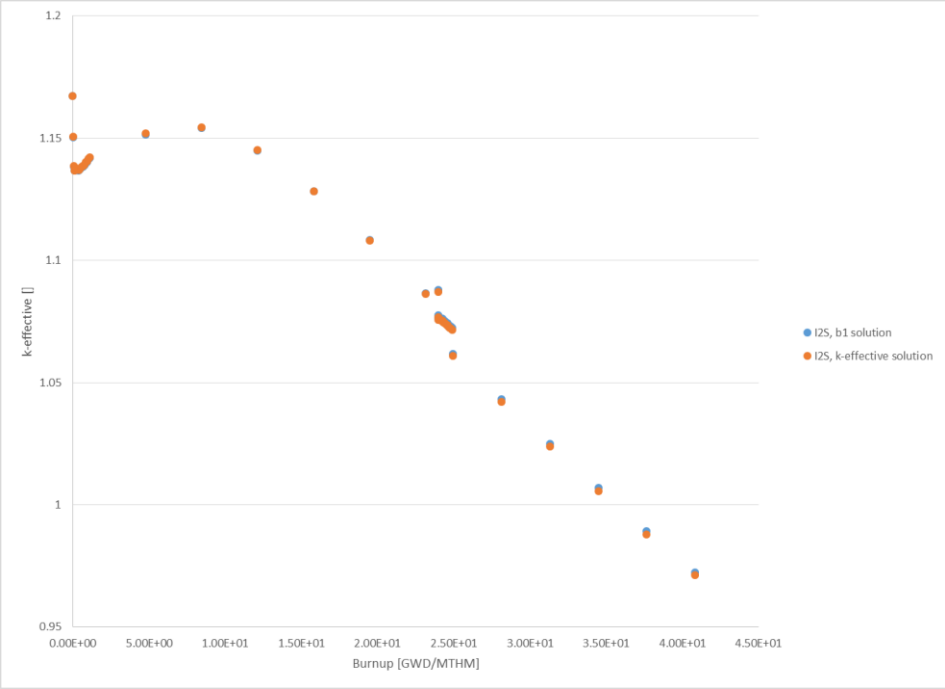

Figure 31: Burnup-dependent K-effective in 44 GWD/MTHM fuel

Where all fuel has been irradiated to 44 GWD/MTHM fuel on the 24 GWD/MTHM-20 GWD/MTHM cycle. Notice here in Figure 31 that there is a slight decrease in reactivity when

changing from the b1 to the k_{eff} method of solution at high burnups, and that the two are roughly equal at the beginning of the first cycle.

Defining $\Delta\rho$ as ρ_{b1}-ρ_{keff}, where ρ_{b1} and ρ_{keff} are the excess reactivities from the b1 and k_{eff} solution methods, respectively, the difference is shown in Figure 32 as:

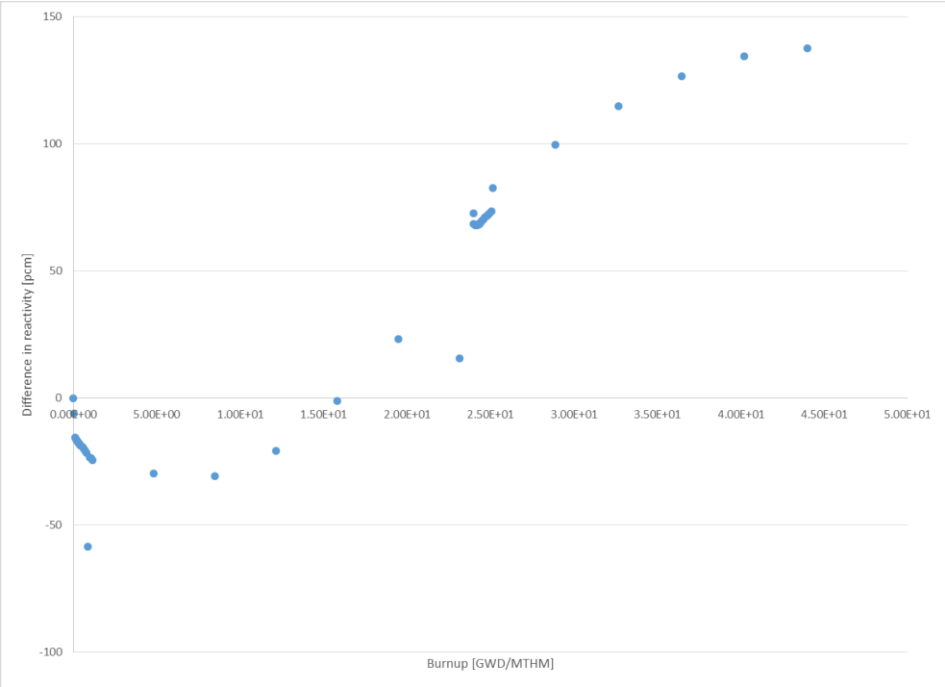

Figure 32: Difference in reactivity between b1 and k-effective methods of solution for I²S-LWR fuel irradiated to 44 GWD/MTHM

Notice that the k_{eff} solution method has the higher reactivity up until & including 15.8 GWD/MTHM burnup, after which the b1 solution method produces the higher reactivity; starting at a burnup of 23.1 GWD/MTHM, or shortly before the first refueling, the reactivity difference continually increases with burnup, with a maximum difference of 231 pcm at the discharge burnup of 44 GWD/MTHM. This difference is non-trivial from a reactor kinetics perspective, but small relative to k_{eff} that there is no reason to expect an impact on solution accuracy.

6.2 Decay Heat Results

6.2.1 Transition to I²S-LWR

Looking first at a conventional PWR, the decay heat curve for a 44 GWD/MTHM 2-batch core is shown below in figure 33:

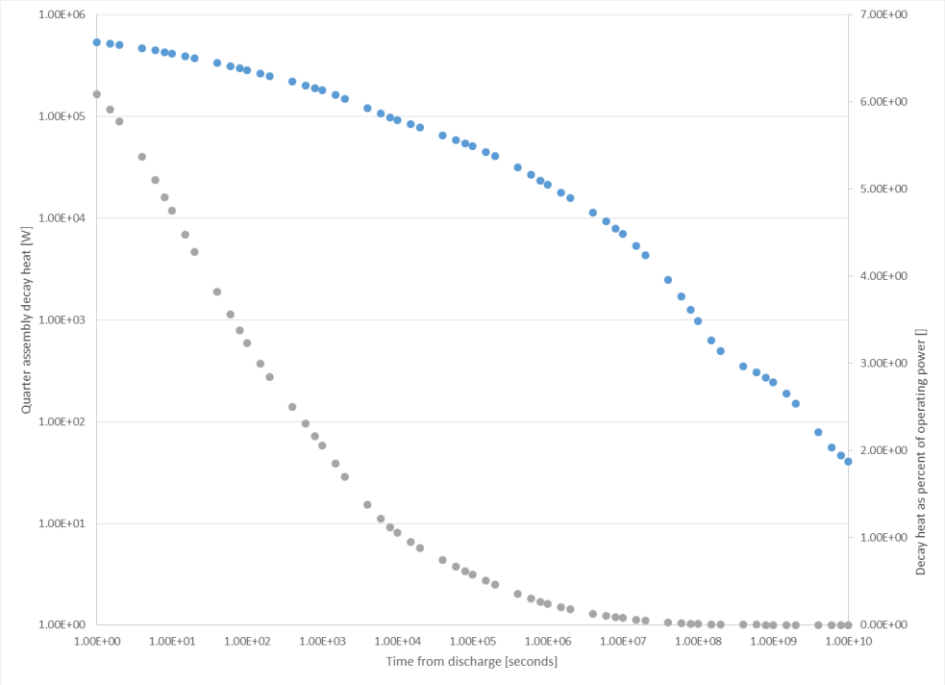

Figure 33: Absolute (blue) and percent (gray) decay heat from PWR oxide fuel irradiated to 44 GWD/MTHM

Of note here is the good agreement with ANS-5.1-2005: 6.09% of operating power is present 1 second after shutdown, compared with 6.12% from the ANS standard, assuming the ISO standard of 202.2 MeV/fission [18]. It should also be noted that, for the rest of this thesis, decay heat refers to quarter assembly decay heat unless otherwise specified

To determine the impact of changes from a traditional PWR to I²S-LWR, the changes made will be implemented in two phases; first, the oxide fuel will be replaced with silicide, keeping burnup and specific power constant, and the lattice size will then be changed from 17x17 to 19x19 lattice, with the accompanying change from zircaloy to stainless steel clad. This

will let one see how much of the changes in decay heat are due to the change in fuel composition, and how much is due to the changes in geometry.

Making the first step in this change, from oxide to silicide fuel, yields a similar decay heat curve in Figure 34:

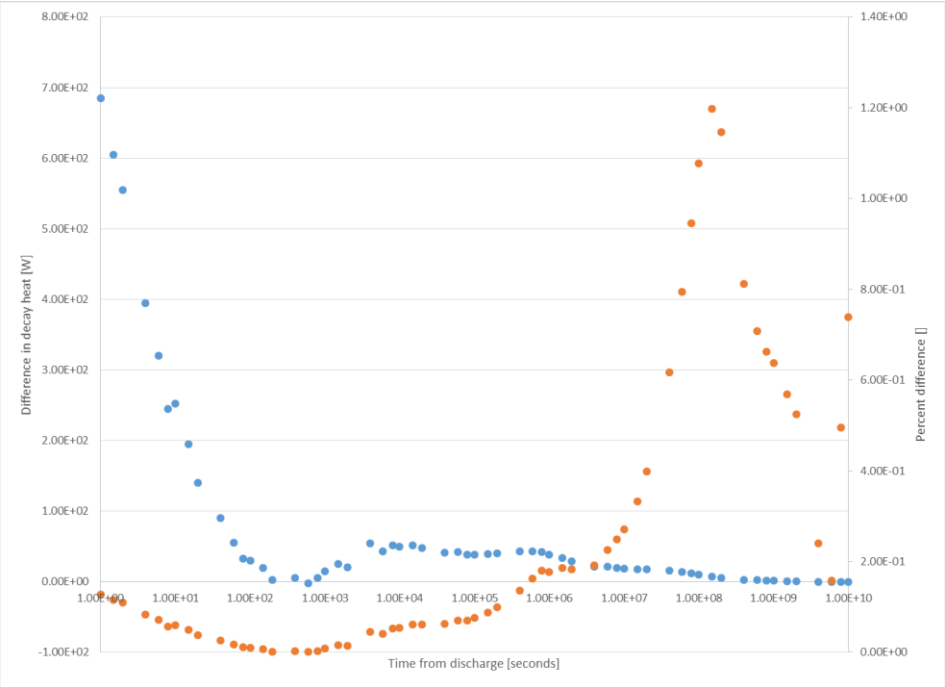

Figure 34: Absolute (blue) and percent (orange) difference in decay heat from UO2- and U3Si2- fuelled traditional PWRs

Several things should be noted from the transition to silicide fuel depicted above in Figure 34. First and foremost is that the decay heat increases from oxide to silicide at all times except 600 seconds (10 minutes) after discharge, when the decay heat from the otherwise identical oxide fueled PWR is 2.5 W higher than in its silicide fueled counterpart. Furthermore, whether speaking in absolute or percentage terms, the difference in decay heat between silicide and oxide fueled PWR lattices is quite small, at no more than 700 kW or 1.2%, respectively.

Now changing the geometry from 17x17 to 19x19, and the clad from zircaloy to stainless steel, the differences in decay heat are shown below in Figure 35:

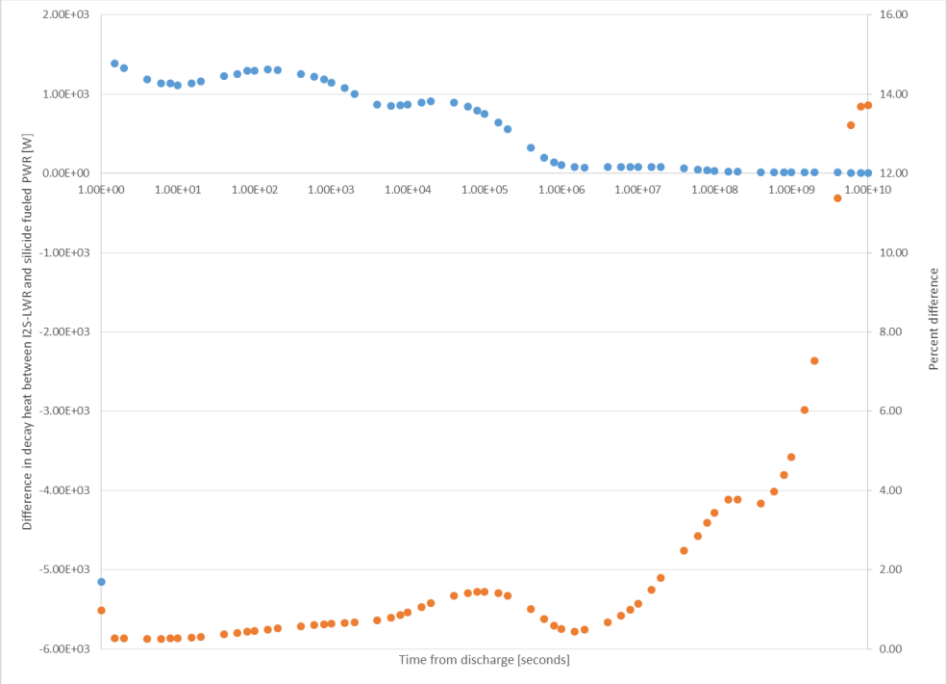

Figure 35: Absolute (blue) and percent (orange) difference in decay heat between traditional PWR and I2S-LWR

Notwithstanding the lower decay heat one second after discharge, decay heat is greater in I^2S-LWR than in a silicide fueled PWR. This is to be expected, owing to the greater uranium mass and consequently the higher operating power. Also to be noted is the greater percent difference between I^2S-LWR and a silicide fueled PWR: Whereas the difference in the transition from oxide to silicide fuel reaches a maximum of 1.20% at $1.5 * 10^8$ seconds after discharge and then decreases, the difference is 3.77 % at this same time in the transition from silicide fueled traditional PWR to I^2S-LWR, and continually increases starting at $4 * 10^8$ seconds after discharge, up to 13.7% difference at 10^{10} seconds after discharge.

Gamma ray decay heat has also been measured for all 3 designs, and is plotted for a traditional PWR in figure 36.

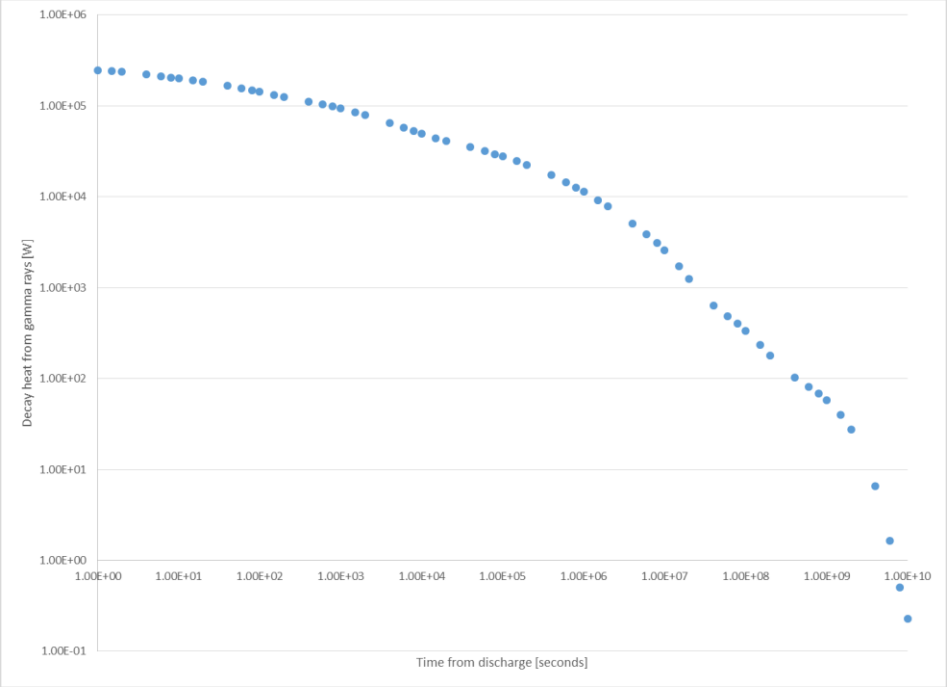

Figure 36: Gamma ray decay heat for AP1000 fuel irradiated to 44 GWD/MTHM

Since the change in decay heat due to the change from traditional PWR to I^2S-LWR was much greater than that due to the change from oxide to silicide fuel, for the sake of conciseness the transition from traditional PWR to I^2S-LWR was consolidated into one step, directly comparing I^2S-LWR to a traditional PWR. The results of this comparison are summarized in Figure 37.

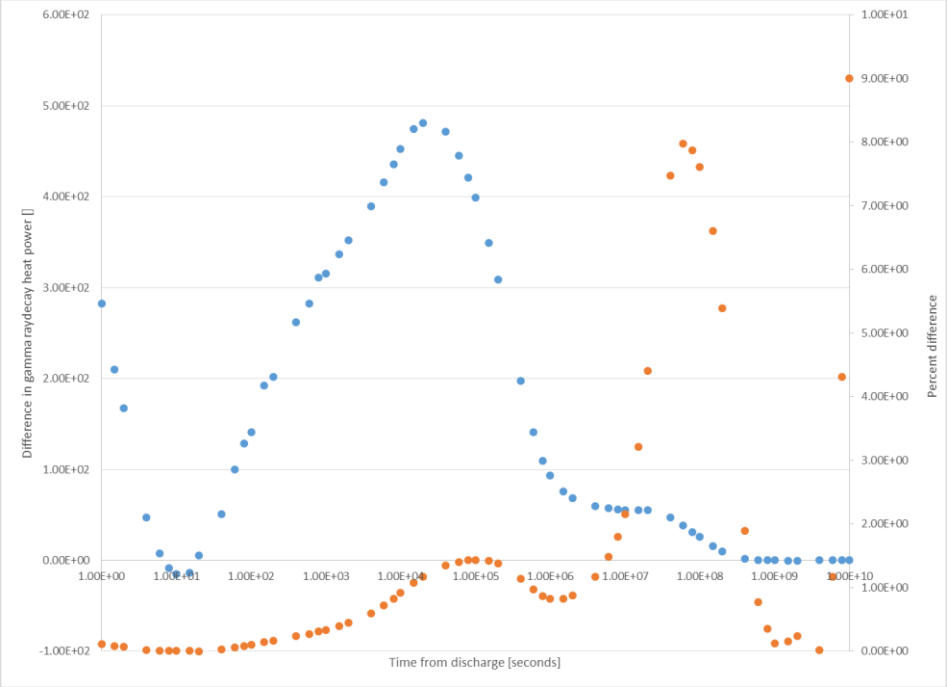

Figure 37: Absolute (blue) and percent (orange) difference in gamma heating between oxide-fueled traditional PWR and I^{2}S-LWR

The trends in gamma ray heat are not the same as those from the total decay heat, suggesting that the change in total and gamma ray decay heat are not directly related. Whereas the difference in total decay heat continually went down, here it increases from 10 to 10^5 seconds, and percent difference peaks at $6 * 10^7$ seconds after discharge and then falling until 10^9 seconds, followed by a smaller increase, whereas the percent difference continually increases from $8 * 10^5$ seconds after discharge up to 9%.

Looking at the fraction of decay heat due to gamma rays, seen below in figure 38, the fraction is constant for all three of a traditional PWR with oxide fuel, the same PWR with silicide fuel, and the I^{2}S-LWR, up to $8 * 10^6$ seconds. From there, the fraction of heating due to gamma rays is greater in I^{2}S-LWR 10^7 to $2 * 10^8$ seconds, after which it is greatest in the silicide fueled traditional PWR. From this, it can be inferred that the silicide fuel increases decay heat due to rays.

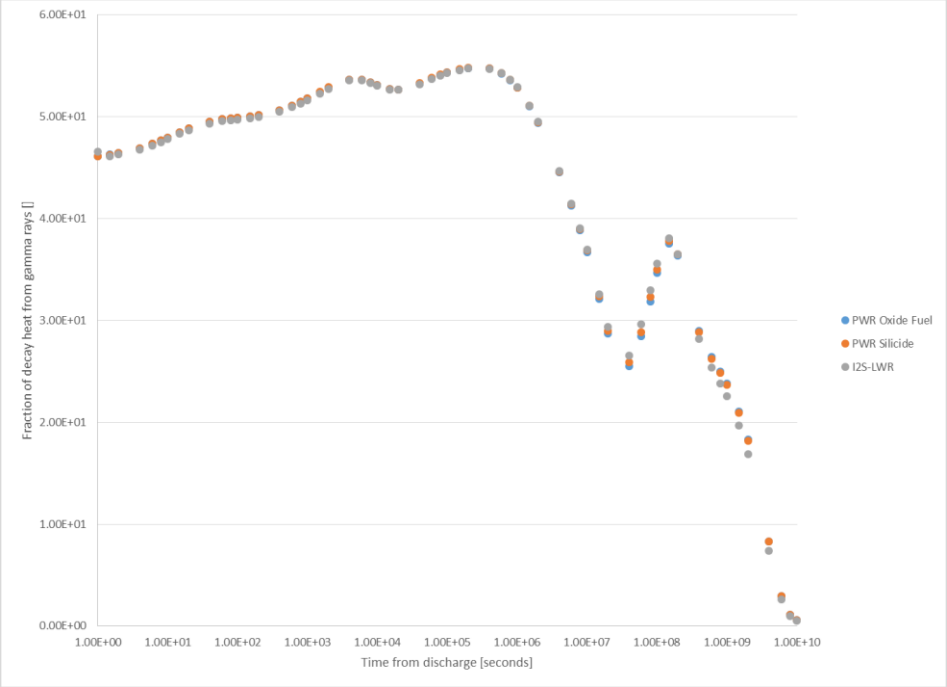

Figure 38: Fraction of decay heat from gamma rays in 44 GWD/MTHM fuel

6.2.2 Sensitivity to Enrichment

To determine sensitivity of decay heat to enrichment, the 44 GWD/MTHM discharge burnup case for the I^{2}S-LWR, with cycle burnups of 24 and 20 GWD/MTHM, was also modelled at an enrichment of 4.45 w/o, with fuel composition as given in Table 4 above and all other parameters unchanged.

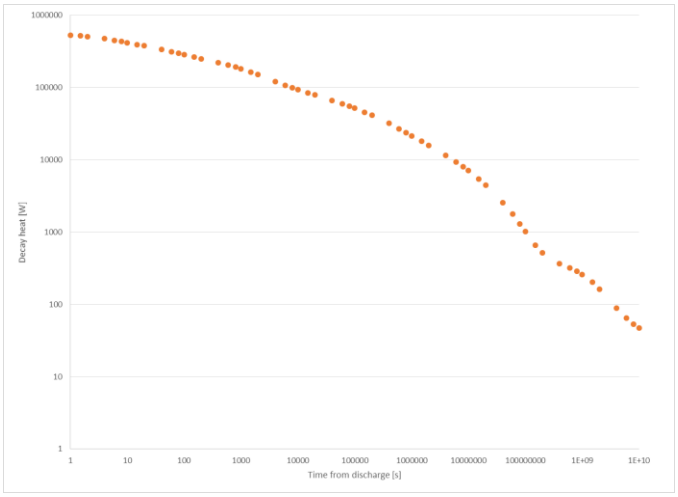

Figure 39: Decay heat from 4.95 w/o, 44 GWD/MTHM fuel from I^{2}S-LWR

It should be noted that the differences between the 4.95 and 4.45 w/o cases are so small that the curves could not be displayed on the same graph; as such, figure 39 is a plot of only the 4.95 w/o case while figure 40 displays the changes in decay heat due to the change in enrichment.

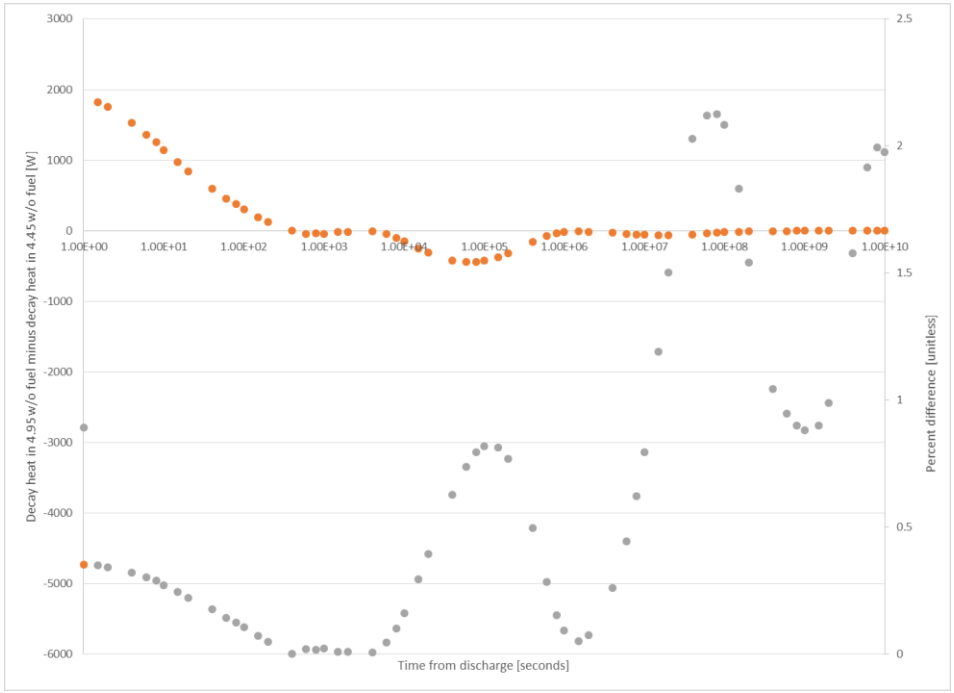

Figure 40: Difference between decay heat from 4.95 & 4.45 w/o I^2S-LWR fuel in watts(orange) & percentage (gray)

Looking at the difference between the two enrichments in Figure 40, one sees almost no difference. The effects of fuel enrichment here are less than 2.1%, and less than 5 kW, dropping to less than 1 kW after only 20 seconds from discharge, over the entire range of times surveyed. In figure 40 above, the difference is defined as decay heat from the 4.45 w/o case minus decay heat from the 4.95 w/o case, while the percent difference is given by the equation:

$$Percent\ difference = 100 * \frac{|DH_{4.95} - DH_{4.45}|}{DH_{4.95}}$$

Equation 15: Percent difference in decay heat

Where $DH_{4.95}$ and $DH_{4.45}$ are the decay heats from the 4.95 and 4.45 w/o enrichments, respectively.

The same trends are also apparent if only gamma-ray emissions are considered. Once again, only the 4.95 w/o case has been plotted since, due to the similarities between the 4.45 and 4.95 w/o cases, they would be indistinguishable and it is more informative to plot the difference between the two cases, which is plotted in figure 41, while gamma ray decay heat from the 4.95 w/o case is plotted in Figure 42. Looking at gamma-ray emissions in figure 41, the difference between 4.45 w/o and 4.95 w/o is once again negligible, with differences not exceeding 3.5 % or 1.59 kW. Once again, differences between the two cases increase with time from discharge; unlike the total decay heat, however, the percent difference is ~0% immediately after discharge, and uncertainties do not exceed 1% until $8 * 10^9$ seconds after discharge. Additionally, the gamma ray decay heat from 4.45 w/o fuel is less than that from 4.95 w/o fuel

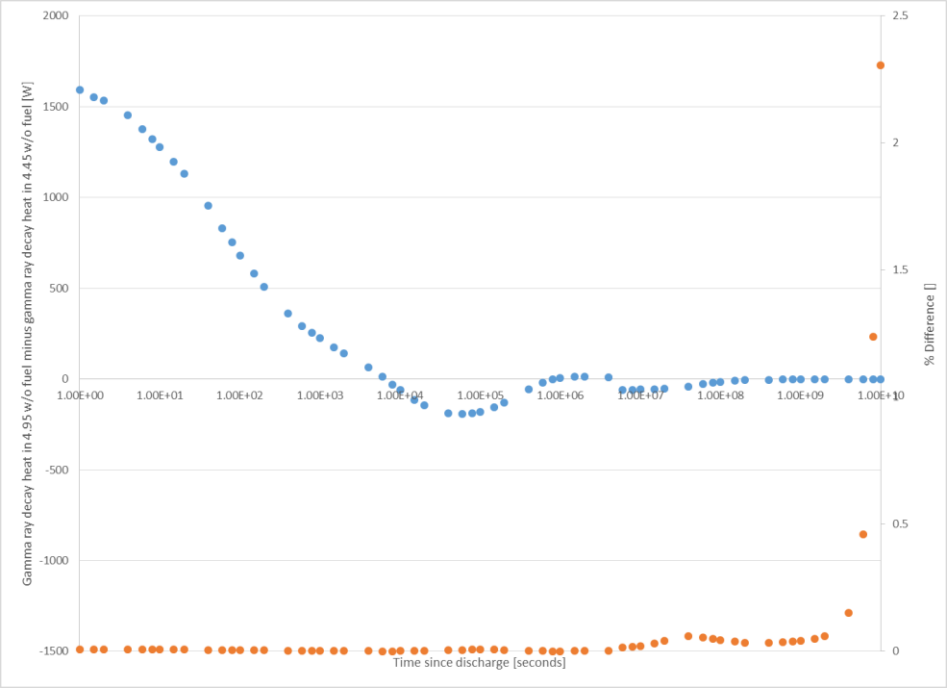

Figure 41: Percent (orange) and absolute (blue) difference in gamma ray emissions

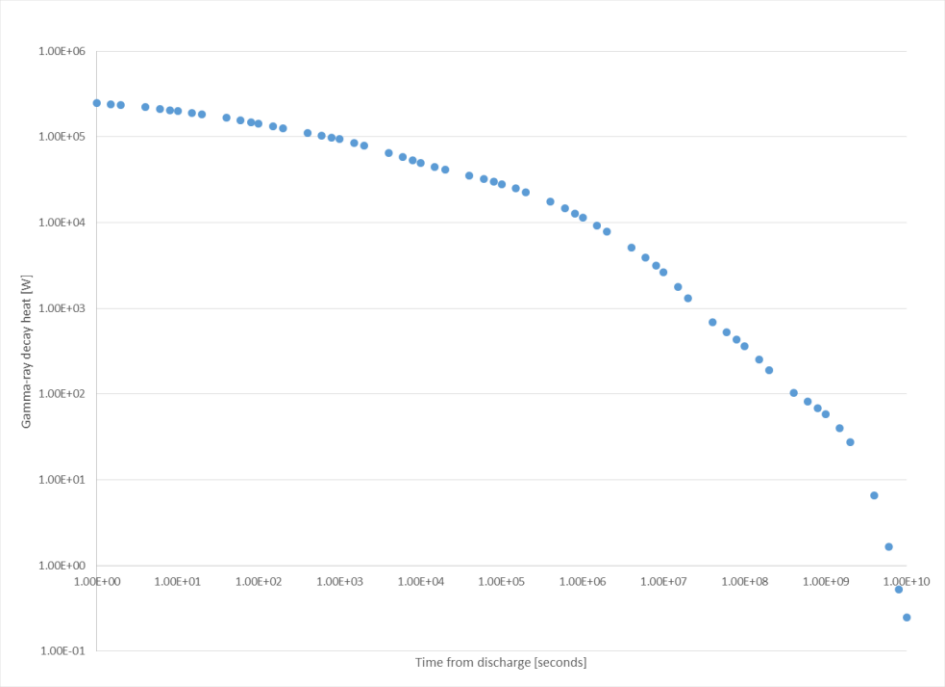

Figure 42: Gamma ray decay heat from 4.95 w/o, 44 GWD/MTHM I²S-LWR fuel

For the comparison between 4.95 w/o and 6.50 w/o fuel, rather than model the 44 GWD/MTHM case, a single-cycle 70 GWD/MTHM case will be compared, as 6.50 w/o fuel would not be used with lower-burnup fuel management strategies. As such, direct comparisons between 4.45 w/o and 6.50 w/o fuel are not possible.

The decay heat curve for 6.50 w/o fuel irradiated to 70 GWD/MTHM is shown in Figure 42. Once again, the decay heat curves for the 6.50 w/o and 4.95 w/o cases, both irradiated to 70 GWD/MTHM, are so similar that they are not plotted on the same graph; instead, only the 6.50 w/o case will be plotted, as it does not appear elsewhere in this document.

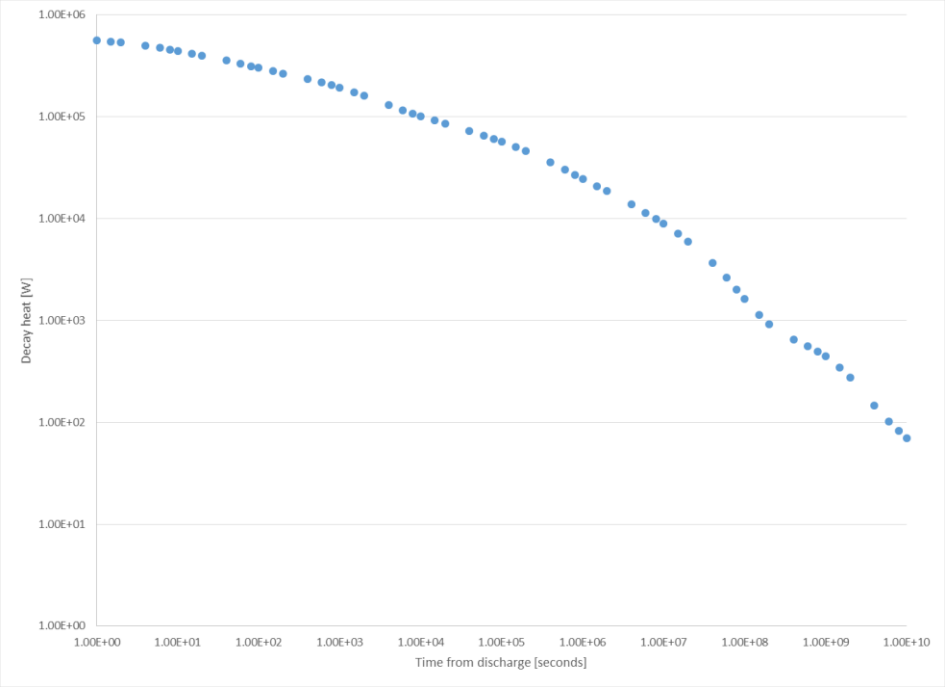

Figure 43: Decay heat from 6.50 w/o I^2S-LWR fuel irradiated to 70 GWD/MTHM

Figure 43 shows decay heat from the 6.50 w/o, 40 MW/MT, 70 GWD/MTHM case, while Figure 44 shows the percent and absolute differences between the 6.50 and 4.95 w/o enriched fuels; here, the difference is defined as the decay heat from the 6.50 w/o fuel, minus the decay heat from the 4.95 w/o fuel. As would be expected, the absolute difference in decay heat between the two cases decreases with time. Looking at the percentage difference, however, trends are different from the 4.45 vs 4.95 w/o case, implying that the difference is nonlinear.

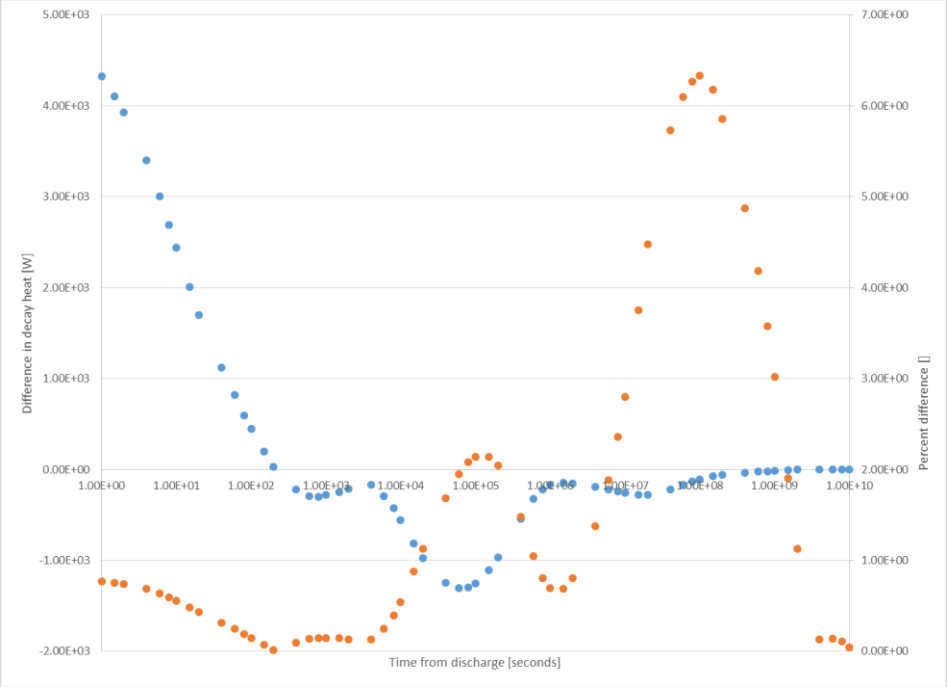

Figure 44: Percent (orange) and absolute (blue) difference in decay heat between 6.50 and 4.95 w/o fuel

Looking now only at gamma ray emissions in Figure 45, some but not all of the trends from overall decay heat are still present; in particular, gamma ray decay heat from the lower-enriched fuel being considered becomes greater than that from the higher-enriched case at 6 * 10^3 seconds from discharge and this difference becomes more negative around 10^7 seconds after discharge. However, 4.95 w/o fuel has the higher gamma ray decay heat in both cases from 8 * 10^5 to 4 * 10^6 seconds after discharge, regardless of the other enrichment under consideration.

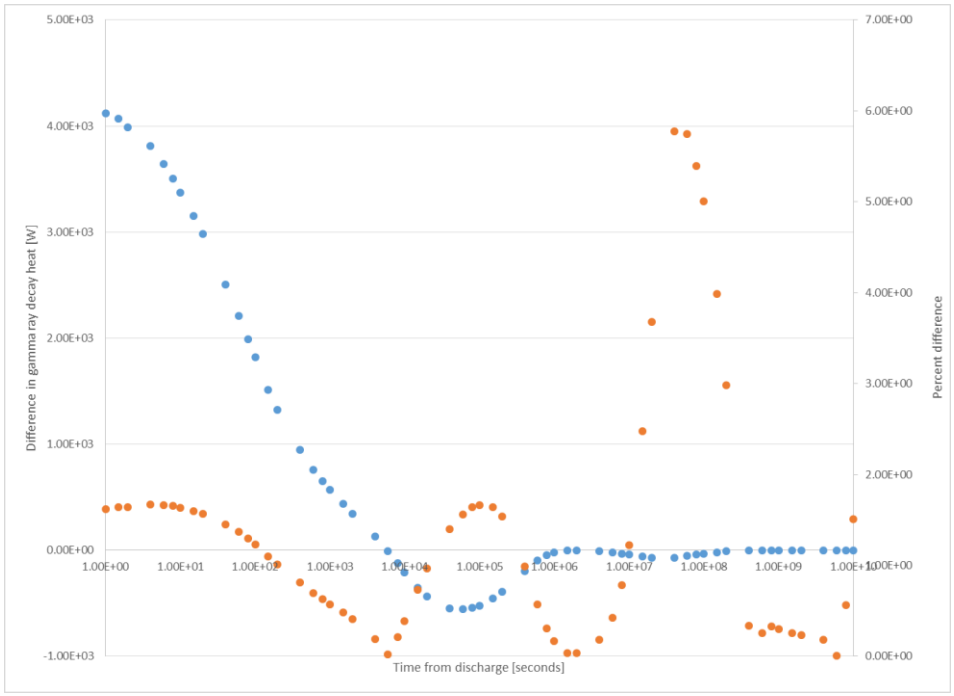

Figure 45: Absolute (blue) and percent (orange) difference in gamma ray decay heat between 4.95 and 6.50 w/o I^2S-LWR fuel irradiated to 70 GWD/MTHM

Now finally looking at the fraction of decay heat coming from gamma rays in Figure 46,

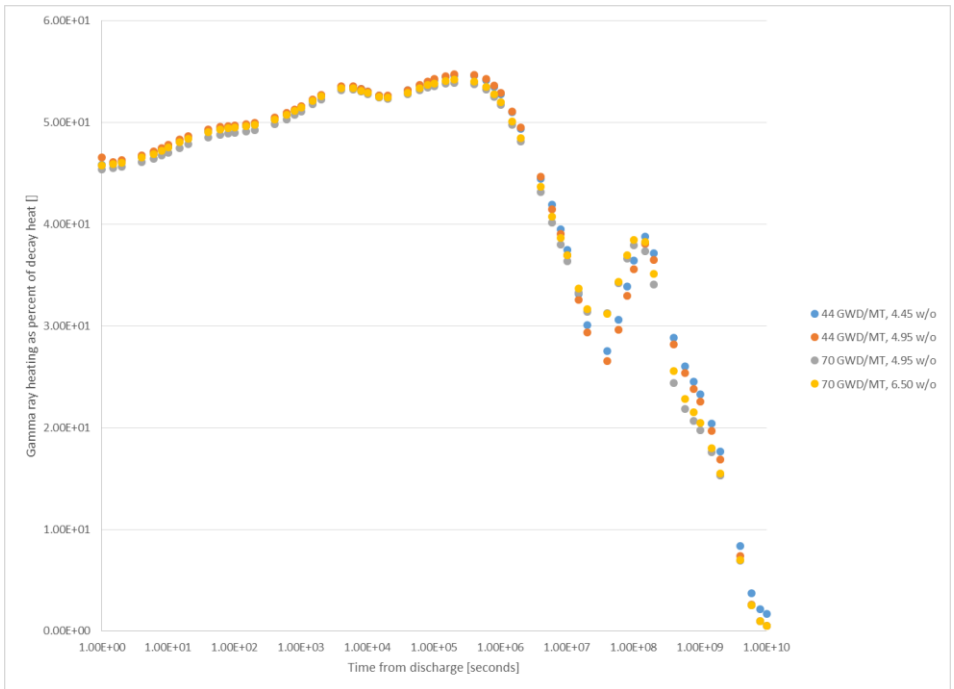

Figure 46: Fraction of decay heat coming from gamma rays, enrichment study

Notice that, while the fraction coming from gamma rays is similar up to $1.5 * 10^7$ seconds (~173 days), there is a divergence based on the fuel management strategy & associated burnup. While the 70 GWD/MT case has a higher fraction of decay heat from gamma rays for both enrichments from $2 * 10^7$ to $1 * 10^8$ seconds after discharge, starting at $1.5 * 10^8$ seconds the fraction is greater for the 2-batch, 44 GWD/MTHM case. Additionally, for both burnups, a lower enrichment corresponds to a higher fraction of decay heat from gamma rays.

6.2.3 Sensitivity to Discharge Burnup & Operating Time

Another consideration is the sensitivity to discharge burnup and, by extension, operating time at constant power. To this end, 4.95 w/o fuel was irradiated at a constant specific power of 40 MW/MTHM to discharge burnups of 40 GWD/MTHM, 50 GWD/MTHM, 60 GWD/MTHM and 70 GWD/MTHM, corresponding to operating times of 1000, 1250, 1500, and 1750 days, respectively, as summarized in Table 9.

Table 9: Listing of cases for burnup sensitivity studies

Specific power	Discharge Burnup	Operating time [days]
40 MW/MTHM	40 GWD/MTHM	1000
40 MW/MTHM	50 GWD/MTHM	1250
40 MW/MTHM	60 GWD/MTHM	1500
40 MW/MTHM	70 GWD/MTHM	1750

The decay heat from these 4 cases is plotted in [30] 47:

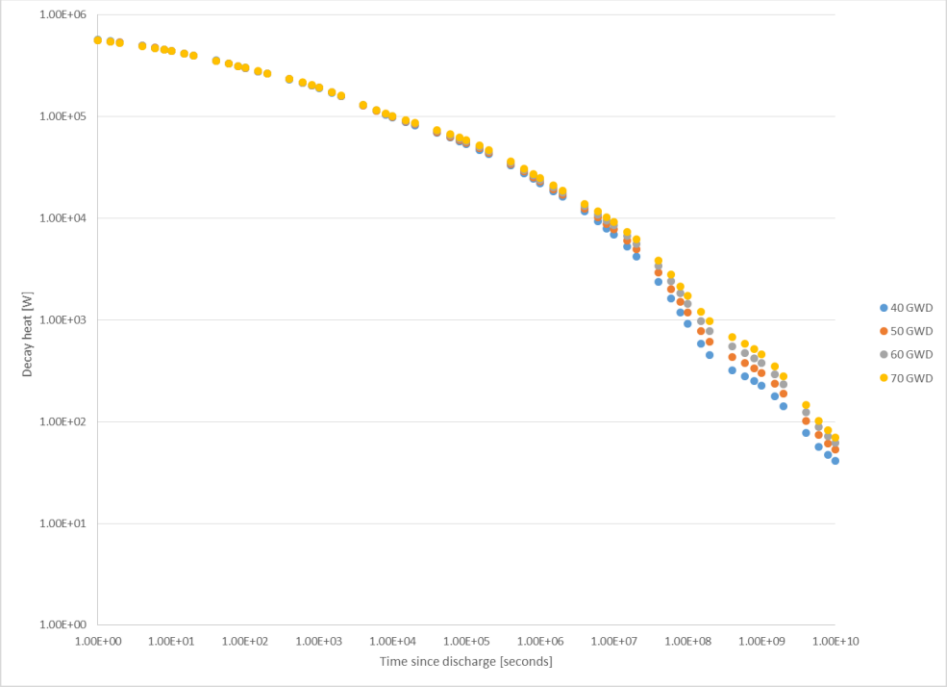

Figure 47: Decay heat from discharged I²S-LWR, constant power

Here one can see, in contrast to the results from section 6.2.4, that the difference between the cases examined is most pronounced at long (>10^5 seconds) times, whereas the decay heat curves in 6.2.4 converged at long (>10^7) times after discharge with larger differences immediately after discharge. While these differences are clearly non-zero, it will first be examined as a percent difference to examine the significance of this difference. Since 40 GWD/MTHM is considered the "baseline" case for this sensitivity study, as it is close to the 44 GWD/MTHM case considered for an operated I^2S-LWR, all comparisons will be to this case.

Looking at the absolute difference, shown in figure 48, the difference between the two cases, defined as decay heat for the case being compared minus decay heat for the 40 GWD/MTHM case, one sees that the difference between the 70 GWD/MTHM and 40 GWD/MTHM cases is greater than that between the 60 GWD/MTHM and 40 GWD/MTHM,

which in turn is greater than the difference between the 50 GWD/MTHM and 40 GWD/MTHM cases, and that this difference never exceeds 8 kW.

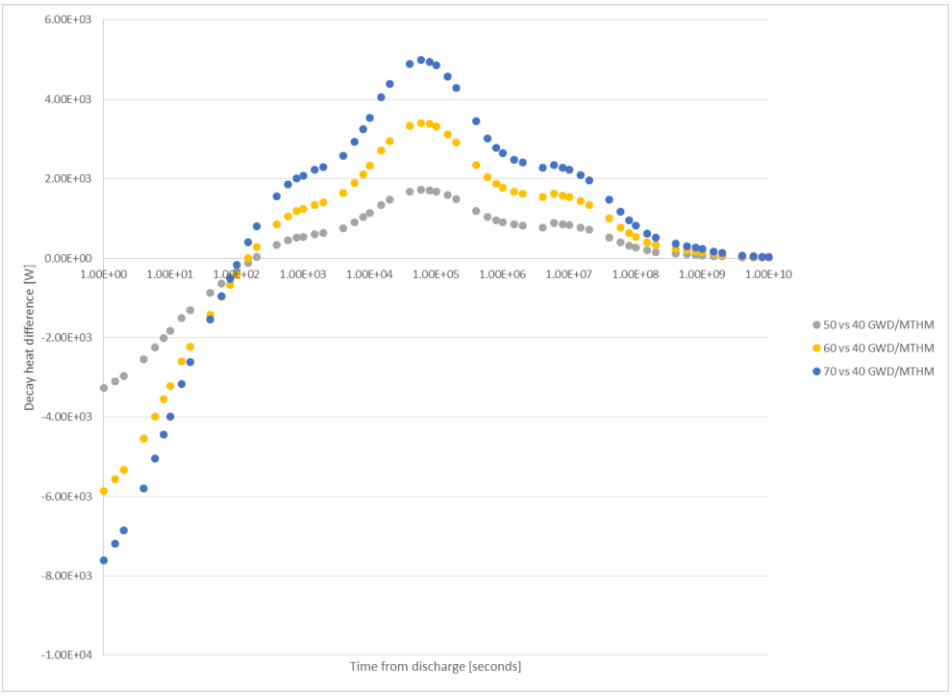

Figure 48: Absolute difference in decay heat, constant specific power, varying burnup

However, the percent difference below in Figure 49 shows growing discrepancies beginning at 10^4 seconds, and reaching a difference as large as 112% at a time of $2 * 10^8$ seconds after discharge. Judging from these results, it is clear that discharge burnup is relevant.

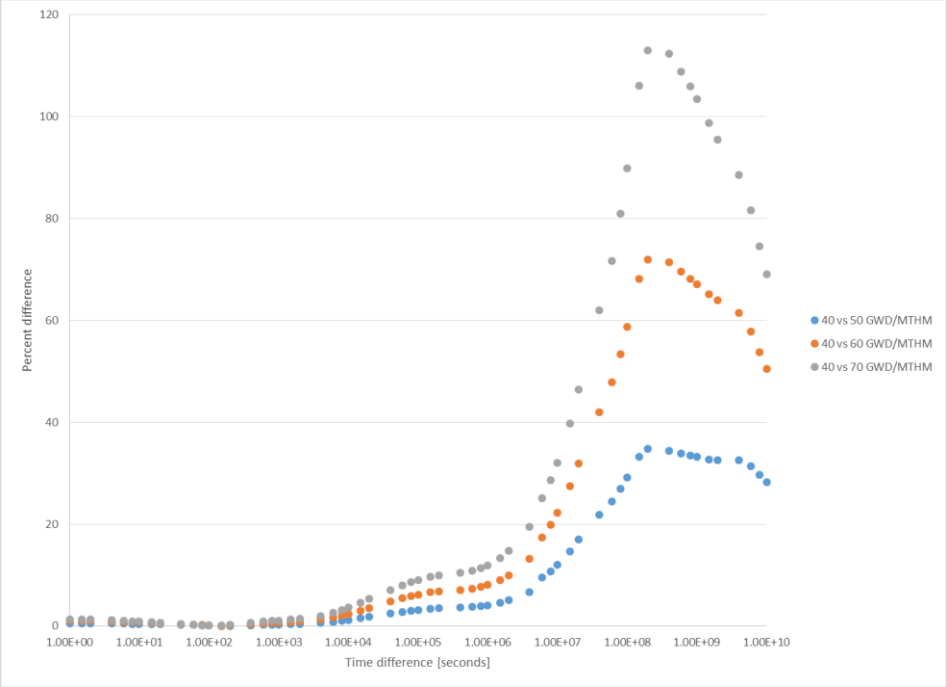

Figure 49: Percent difference in decay heat

From a practical perspective, however, this large percent difference is acceptable: The 8 kW difference occurs 1 second after discharge, compared to 5600 kW in freshly discharged fuel, or a difference of ~1.41%. While the percentage differences increase with time after discharge, the raw difference decreases. In summary, decay heat from a one-batch operated at constant power, but varying discharge burnup, has non-trivial but practically negligible variations in decay heat with burnup.

6.2.4 Sensitivity to Operating Power

Continuing from the previous section, the 40 GWD/MTHM and 60 GWD/MTHM cases were also compared at specific powers of 20 and 62.5 MW/MTHM; these cases are summarized in Table 10, which also includes the 40 MW/MTHM cases for both burnups to provide an additional basis for comparison.

Table 10: Operating power histories for burnup sensitivity study

Discharge Burnup [GWD/MTHM]	Specific Power [MW/MTHM]	Operating time [days]
40	20	2000
40	40	1000
40	62.5	640
60	20	3000
60	40	1500
60	62.5	960

Since section 6.2.5 discusses the sensitivity of decay heat to burnup at fixed specific power, this section will exclusively consider sensitivity of decay heat to specific power at fixed burnup. Looking first at the 40 GWD/MTHM burnup case, the following decay heat curves are obtained:

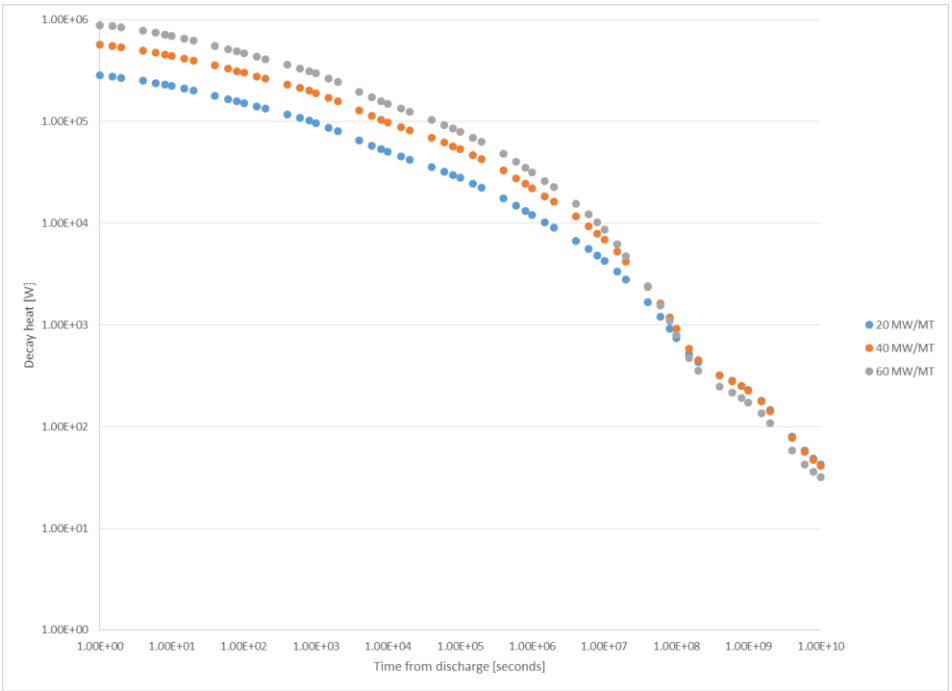

Figure 50:Decay heat curves for 40 GWD/MTHM I²S-LWR fuel at varying specific powers

There is, as would be expected, a dependence on specific operating power, as seen above in Figure 50. Normalizing to operating power, however, this difference largely disappears, as seen in figure 51:

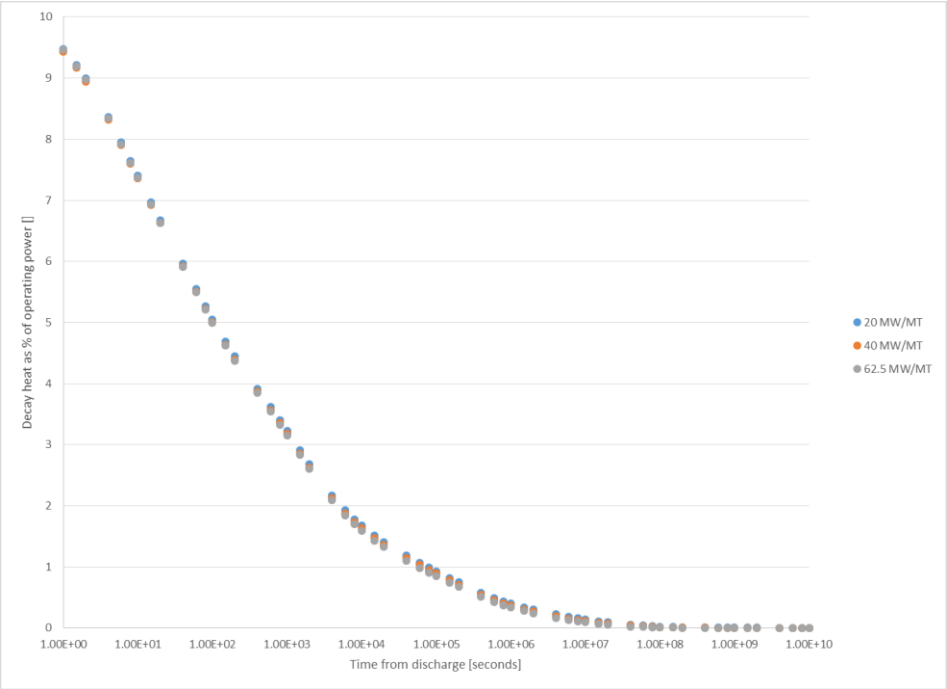

Figure 51: Decay heat as percentage of operating power for 40 GWD/MTHM I²S-LWR fuel

Once again, once the difference in operating power is accounted for, the difference in decay heat is significantly reduced. Taking the percent difference from the 40 MW/MT case, however, shows a nonzero difference: percent difference increases with time, with the percent difference of the 40 MW/MT case compared to the 20 and 62.5 MW/MT case diverging at $4 * 10^7$ seconds, with differences reaching 107% at $6 * 10^9$ seconds from discharge for 20 MW/MT and 51.8% at $4 * 10^9$ seconds from discharge for the 62.5 MW/MT case.

However, the absolute difference, defined as the power from the decay heat from the 20 or 62.5 MW/MT case subtracted from the decay heat from the 40 MW/MT case, decreases with time, as seen in Figure 52. This is common sense, as decay heat decreases with time.

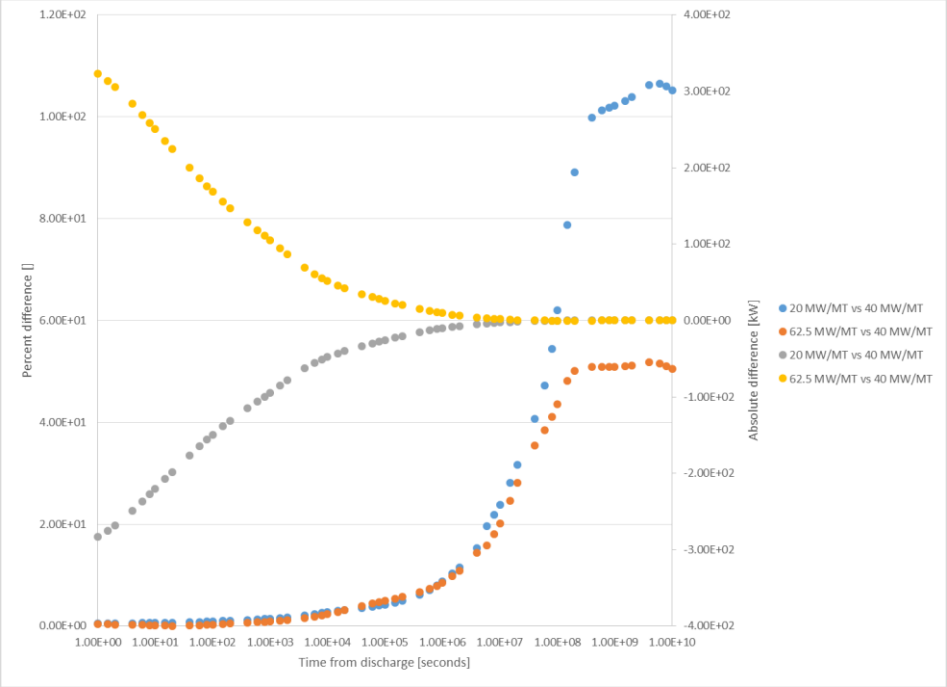

Figure 52: Percent (blue, orange) and absolute (yellow, gray) differences in decay heat in 40 GWD/MTHM I²S-LWR fuel

For the 60 GWD/MTHM case, the same trends are apparent: Decay heat increases with operating power immediately after discharge, with this difference decreasing over time. However, unlike the 40 GWD/MTHM case, here all 3 specific powers result in comparable heat beyond $4 * 10^8$ seconds from discharge, as seen in Figure 46, rather than a lower decay heat from the higher-burnup fuel.

Decay heat only from gamma rays will now be considered. Generating the same curves as seen in figure 50, one gets:

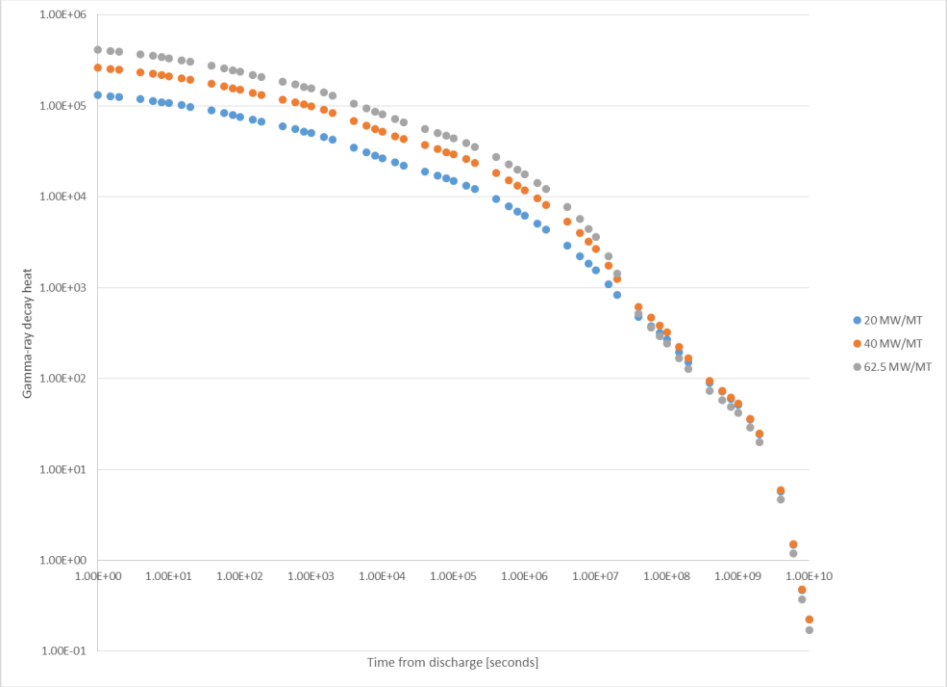

Figure 53: Gamma-ray decay heat in discharged I²S-LWR fuel irradiated to 40 GWD/MTHM

Here in Figure 53, the 62.5 MW/MT specific power case has the highest decay heat out to $2 * 10^7$ seconds, and it has the lowest gamma ray decay heat starting at 10^8 seconds; in between, it has a lower decay heat than the 40 MW/MT case, and a higher gamma ray decay heat than the 20 MW/MT case. One final comment is that, starting at $4 * 10^8$ seconds, the gamma ray decay heat is roughly the same from both the 20 and 40 MW/MT cases. Dividing by operating power and normalizing to the 40 MW/MT case using equation 16 below, the percent differences are plotted in Figure 54:

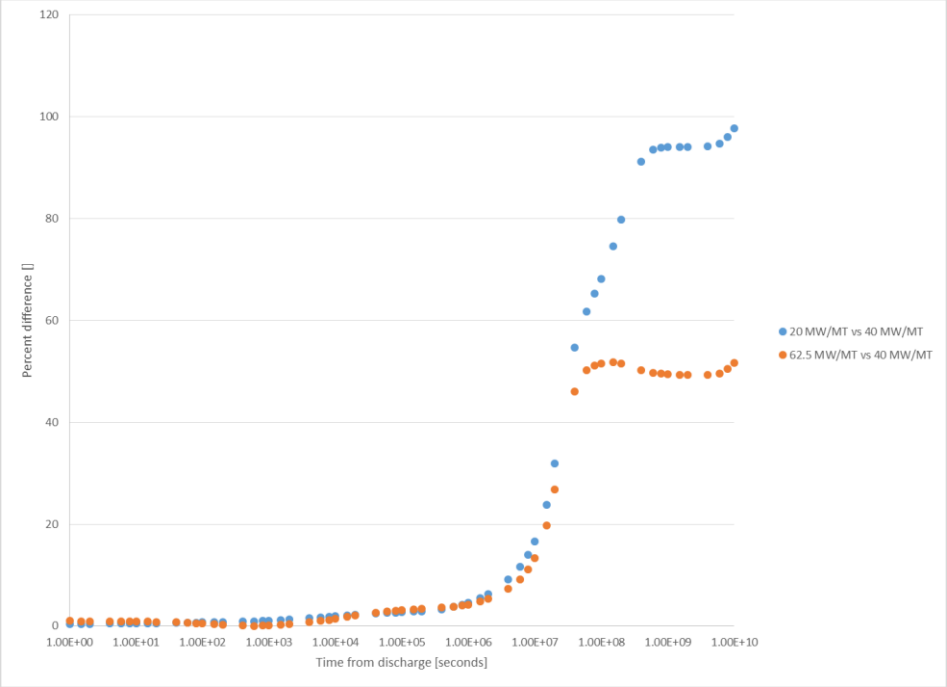

Figure 54: Comparison of percent difference in gamma ray decay heat from 40 GWD/MTHM I^2S-LWR fuel

Here, though the 20 and 62.5 MW/MT agree immediately after discharge, they diverge starting at $4 * 10^7$ seconds (~462 days), with a higher percent difference in the 20 MW/MT case. This divergence is possibly because, whereas a transition from 40 to 62.5 MW/MT is a change of 56.25 %, the change from 20 to 40 MW/MT is a doubling. Once again, as expected, the absolute difference decreases with time after discharge.

Now looking at the fraction of decay heat due to gamma rays below in Figure 55, several trends are apparent: While the fraction of decay heat from gamma rays is slightly higher in 62.5 MW/MT fuel even 1 second after discharge, this difference is much larger from $4 * 10^4$ to $2 * 10^7$ seconds, and the 20 MW/MT case has the largest share of decay heat of gamma rays among the operating powers studied from $4 * 10^7$ to $2 * 10^8$ seconds, beyond which all three have roughly the same fraction of decay heat due to gamma rays.

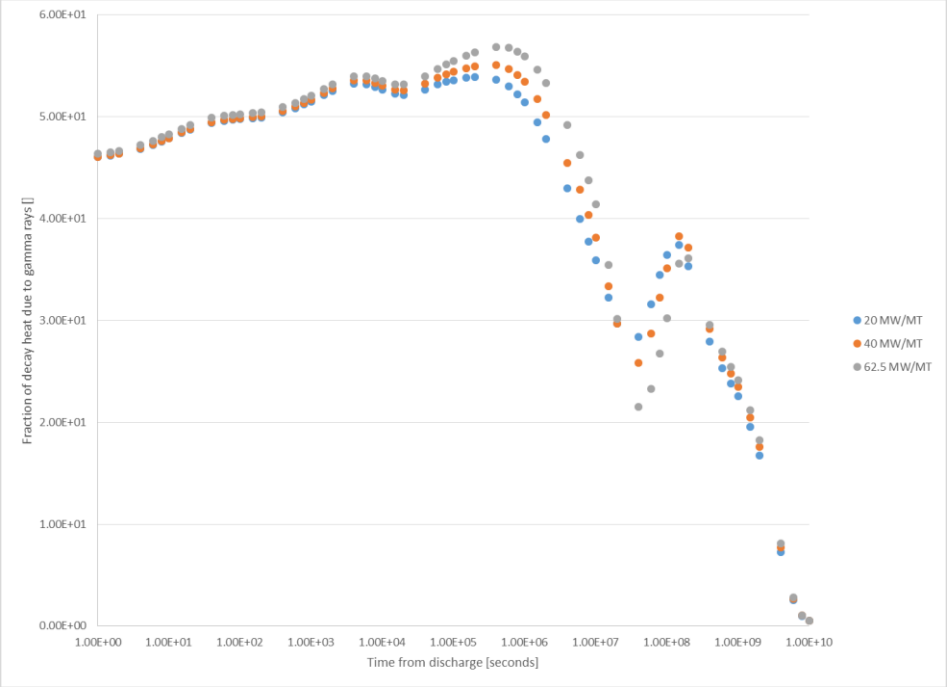

Figure 55: Fraction of decay heat due to gamma rays in 40 GWD/MTHM I²S-LWR fuel

Considering now fuel with the same specific power, but now irradiated to 60 GWD/MTHM, the following decay heat measurements are obtained in Figure 56:

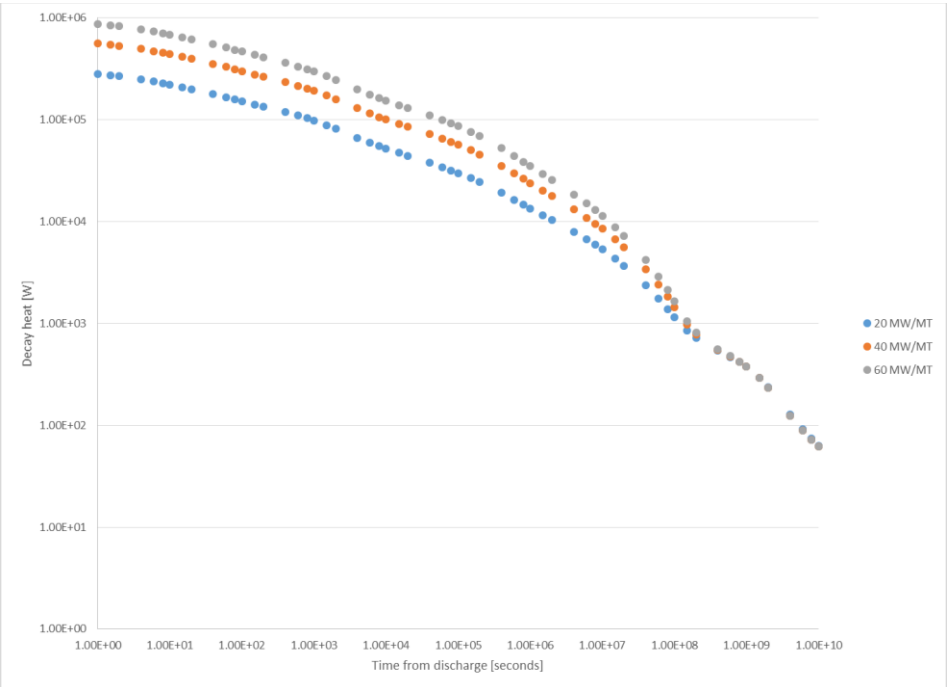

Figure 56: Decay heat as a function of time for 60 GWD/MTHM I²S-LWR fuel

Normalizing for operating power in Figure 57, one actually sees that the 62.5 MW/MT case actually has a slightly lower decay heat as a percentage of operating power.

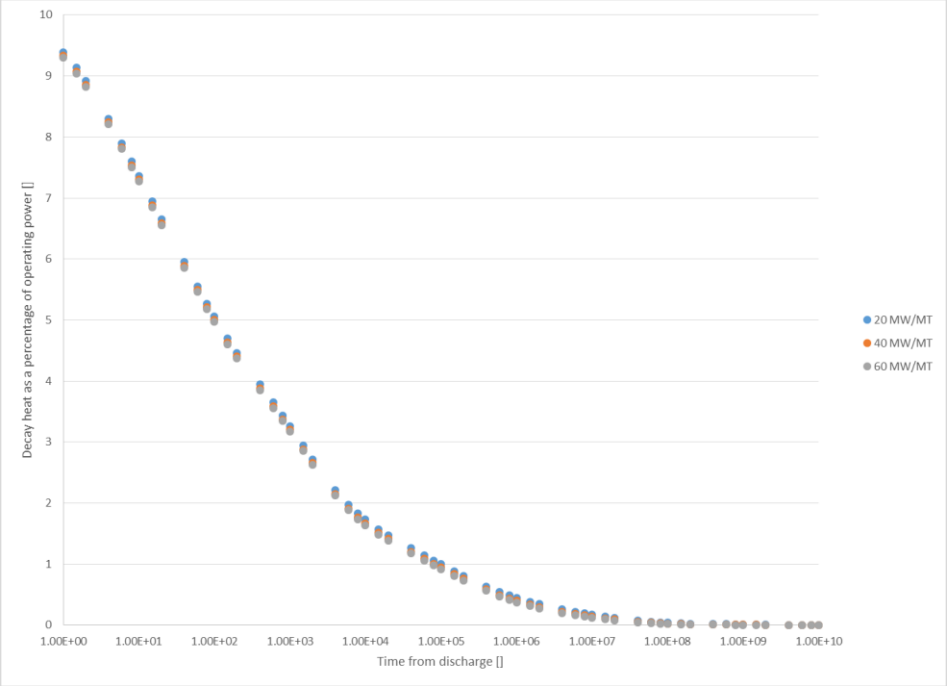

Figure 57: Decay heat as a percent of operating power for 60 GWD/MTHM I^{2}S-LWR fuel

Looking at percent differences now in Figure 58, one sees that the percent difference in fractional power remaining is much greater for the 20 MW/MT case than in the 60 MW/MT case meaning that, even at constant burnup and fixed operating power, decay heat divided by operating power is not the same across operating powers.

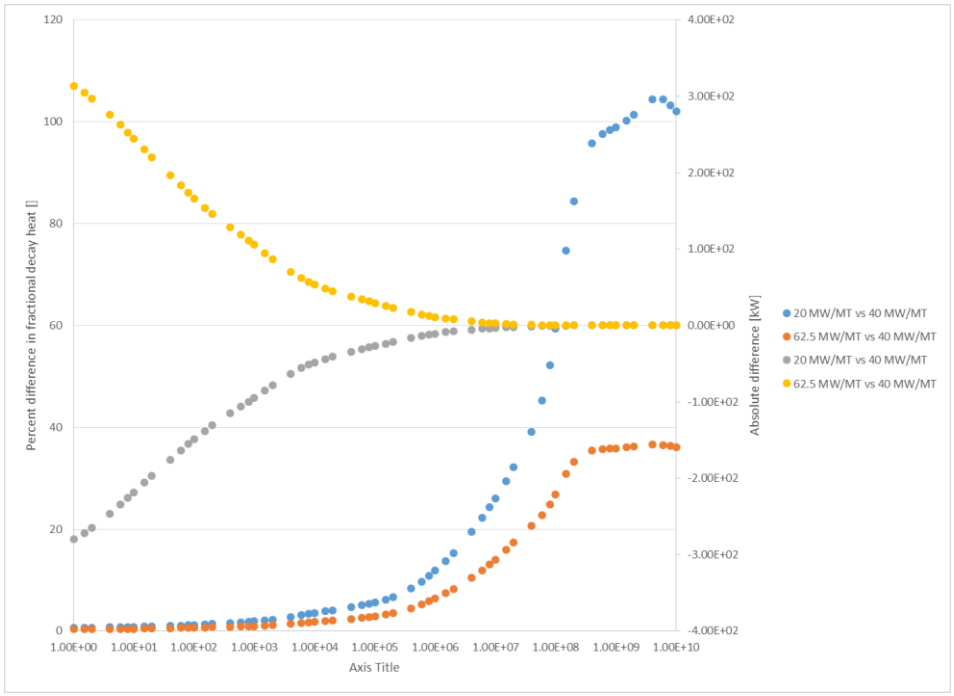

Figure 58: Percent (orange, blue) and absolute (yellow, gray) difference in baseline and 20 MW/MT and 60 MW/MT operating power in 60 GWD/MTHM fuel

Performing now the same analysis for gamma-ray decay heat:

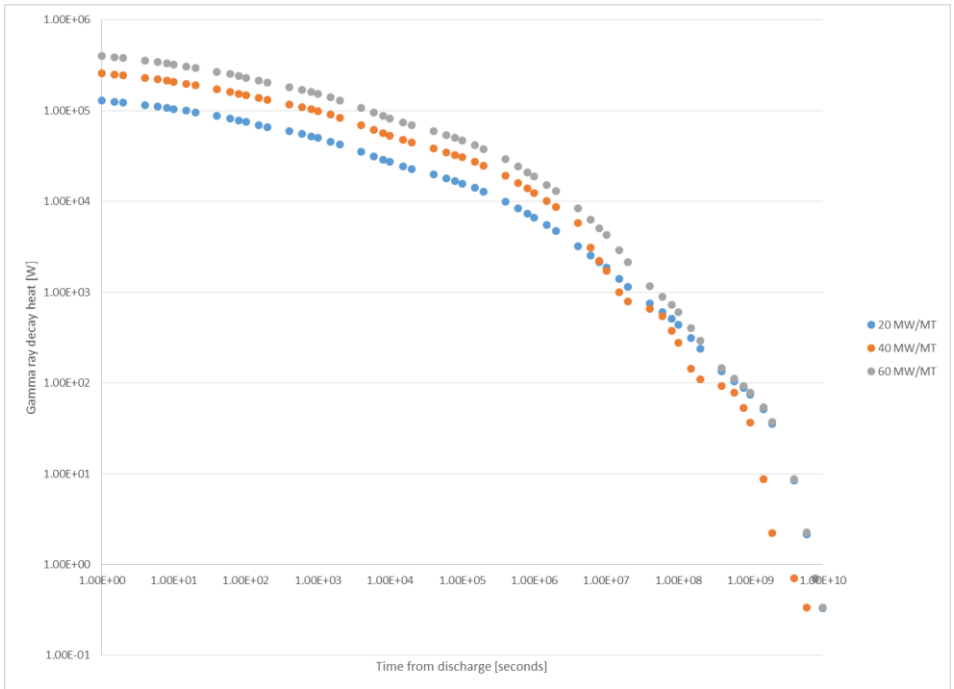

Figure 59: Gamma ray decay heat from I²S-LWR fuel irradiated to 60 GWD/MTHM

Here, it is observed in Figure 59that the lowest decay heat is from the 40 MW/MT case starting at 8 * 10^6 seconds after discharge, rather than the roughly comparable total decay heats for all 3 operating powers at 60 GWD/MTHM, or the 20 MW/MT found for the 40 GWD/MTHM case. Normalizing and finding the percent difference from the 40 GWD/MTHM case, the following is obtained in Figure 60:

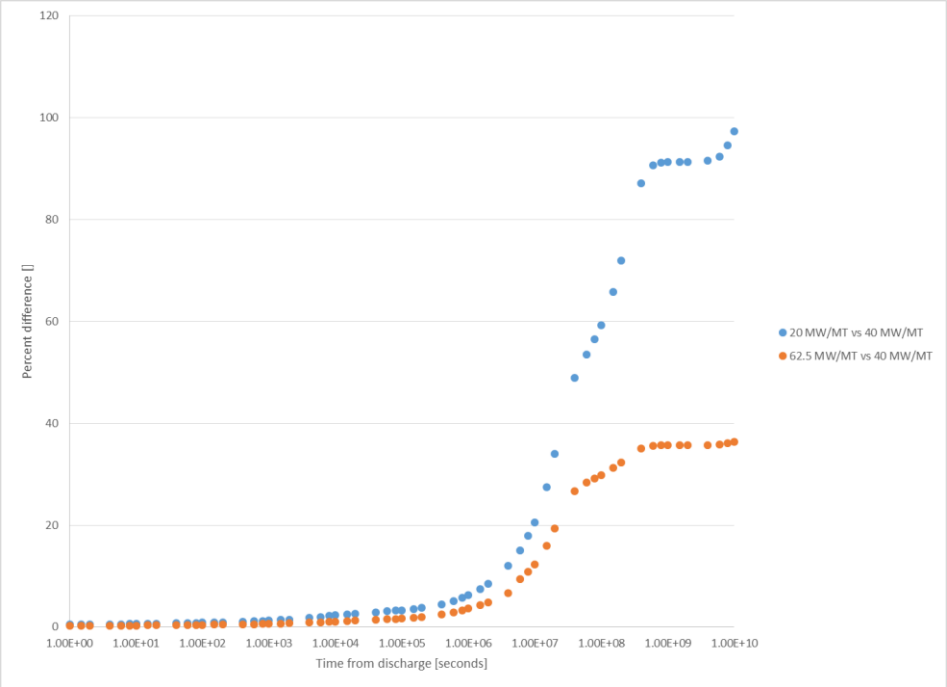

Figure 60: Percent difference in gamma ray heat compared with 40 MW/MT case

Another interesting parameter is the fraction of decay heat coming from gamma rays: Looking at the Figure 61 below, the fraction is roughly identical up to 2 * 10^3 seconds, after which the 62.5 MW/MT fuel has the highest gamma fraction, which continues up to 8 * 10^6 seconds and again from 8* 10^7 to 1.5 * 10^8 seconds; outside of these ranges, the 20 MW/MT fuel has the greatest fraction of decay heat from gamma rays. It should be noted that the 40 MW/MT case never has the highest or lowest fraction, that is, its fraction of decay heat from gamma rays always falls between the fractions found in 20 and 62.5 MW/MT.

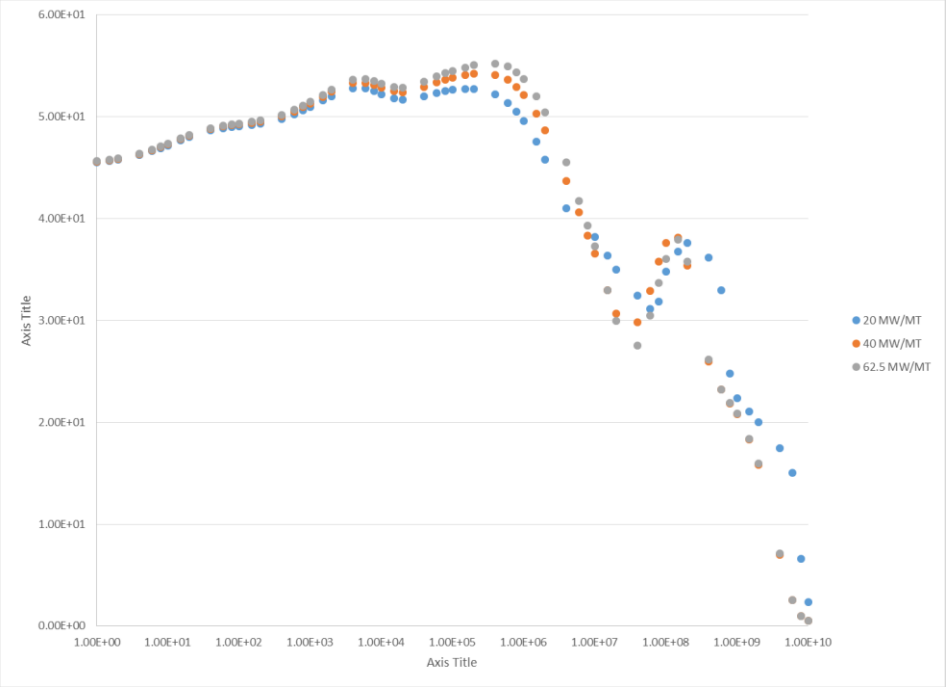

Figure 61: Fraction of decay heat coming from gamma rays, 60 GWD/MTHM burnup

6.2.5 Sensitivity to Specific Power Oscillations

The 44 GWD/MTHM baseline case was subjected to the specific power oscillations described in Table 8, and the associated decay heat curves were generated, as shown in Figure 62.

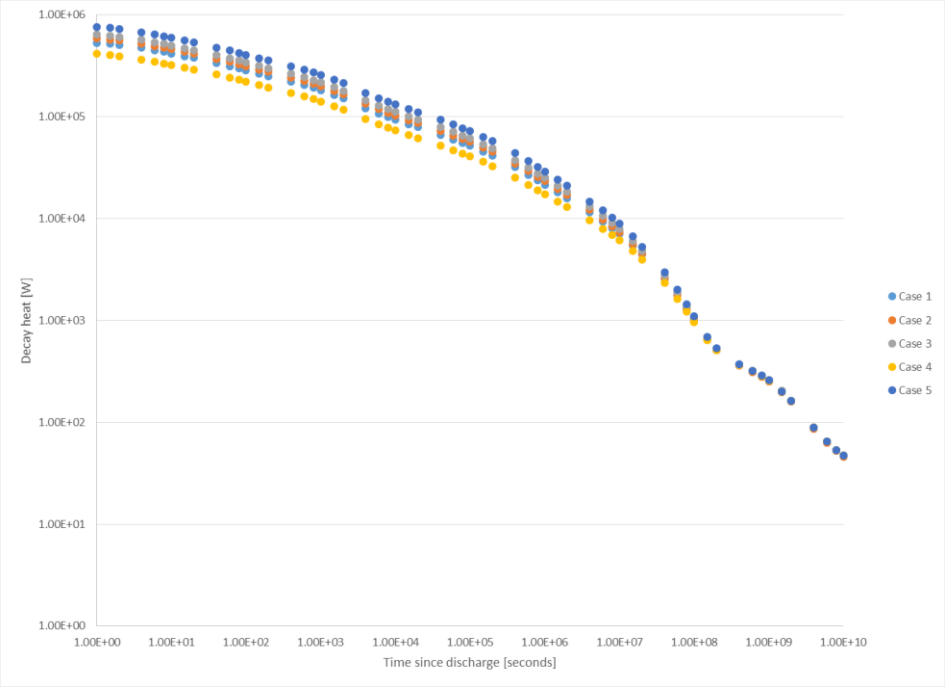

Figure 62: Decay heat curves for I²S-LWR at constant 44 GWD/MT burnup, varying specific power

Where the case numbering is the same as is given in Table 8. Clearly, the power oscillations have an impact on decay heat, even with constant burnup and cycle length. This is to be expected since, as discussed in the literature search, ANS 5.1-2005 bases its decay heat curves on MeV/s/fission, i.e. decay heat per unit operating power. If the fraction of decay heat remaining, i.e. the decay heat at some time arbitrary *t* for some fuel management strategy divided by the second cycle operating power for that fuel management strategy, then normalized decay heat at fixed burnup is insensitive to operating power. Computing this for all fuel management strategies, one gets the following plot for normalizing decay heat:

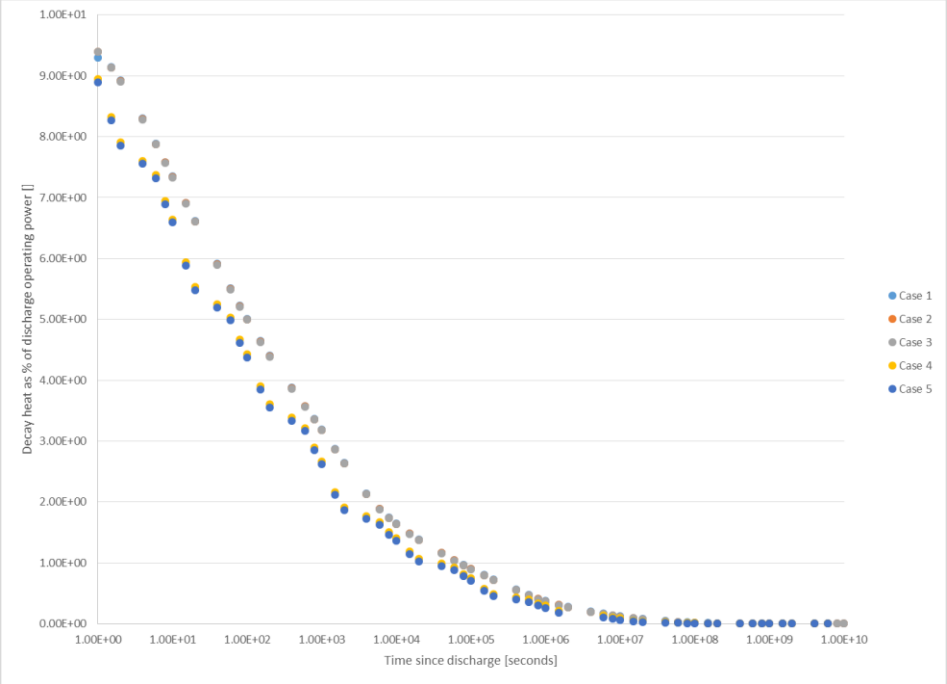

Figure 63: Decay heat for I²S-LWR fuel irradiated to 44 GWD/MTHM

Notice that there are now 2 curves here in figure 63, rather than five in figure 62, or the 1 that would be expected if operating power alone determined decay heat.

To look at the sensitivity of cases 2 and 3 to the different fuel management strategy, it is necessary to introduce the percent difference variable, defined as

$$PD_{n,t} = 100 * \frac{\left|\frac{DH_{n,t}}{PO_{2,n,t}} - \frac{DH_{1,t}}{PO_{2,1,t}}\right|}{\frac{DH_{1,t}}{PO_{2,1,t}}}$$

Equation 16: Percent difference in fractional decay heat

Where $PD_{n,t}$ is the percent difference between case *n* and case 1 at time *t*, where n=2,3,4,5, and $DH_{n,t}$ is the decay heat for case *n* at time *t*, and $PO_{2,n,t}$ is the second cycle operating power for case *n*.

Plotting each of these percent differences, the following is obtained:

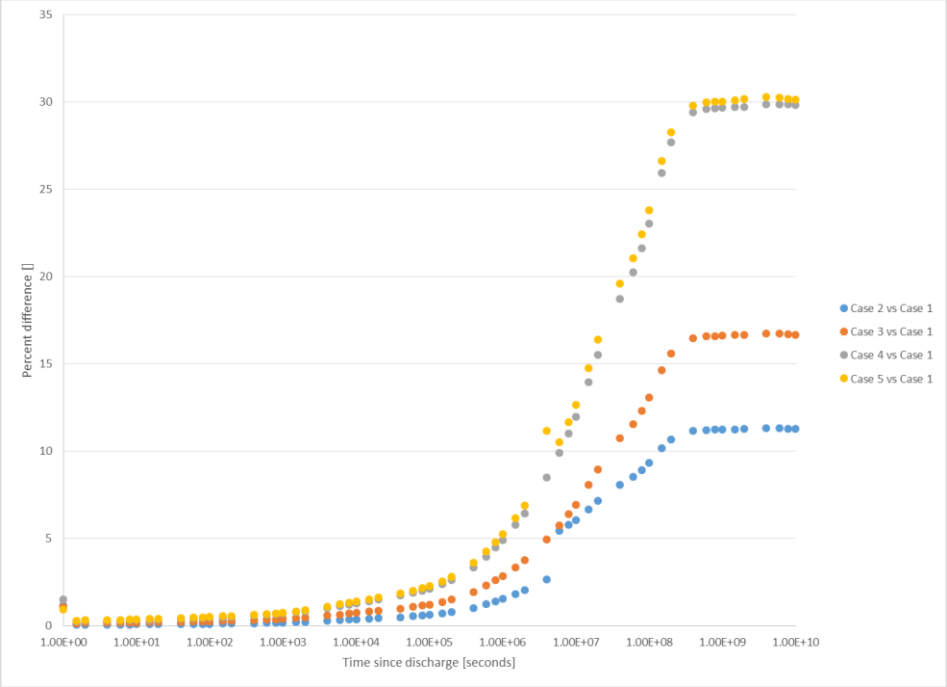

Figure 64: Percent difference in normalized decay heat

Looking at Figure 64, 2 things are apparent: The largest difference between the baseline is consistently case 5, while case 4, which operates on a first cycle burnup of 28.6 GWD/MT and second cycle burnup of 15.4 GWD /MT, compared to the reference case of 24 GWD /MT and 20 GWD /MT, undergoes the wildest "swings" in difference: The difference between cases 4 and 1 decreases more rapidly, and is as low as $1.27 * 10^{-3}$ % , before the difference increases. Unfortunately, these trends in percent error mean that the difference in cycle operating powers are not sufficient to predict normalized decay heat. While the normalized decay heat in figure X was very similar between cases 4 and 5, and also between cases 2 and 3, suggesting that the change in cycle operating power could determine fractional decay heat, the differing percent errors, and different trends in percent error, mean that second-cycle operating power at fixed burnup is insufficient to determine decay heat in this case.

As an additional exercise, comparing the decay heat without normalizing yields the following:

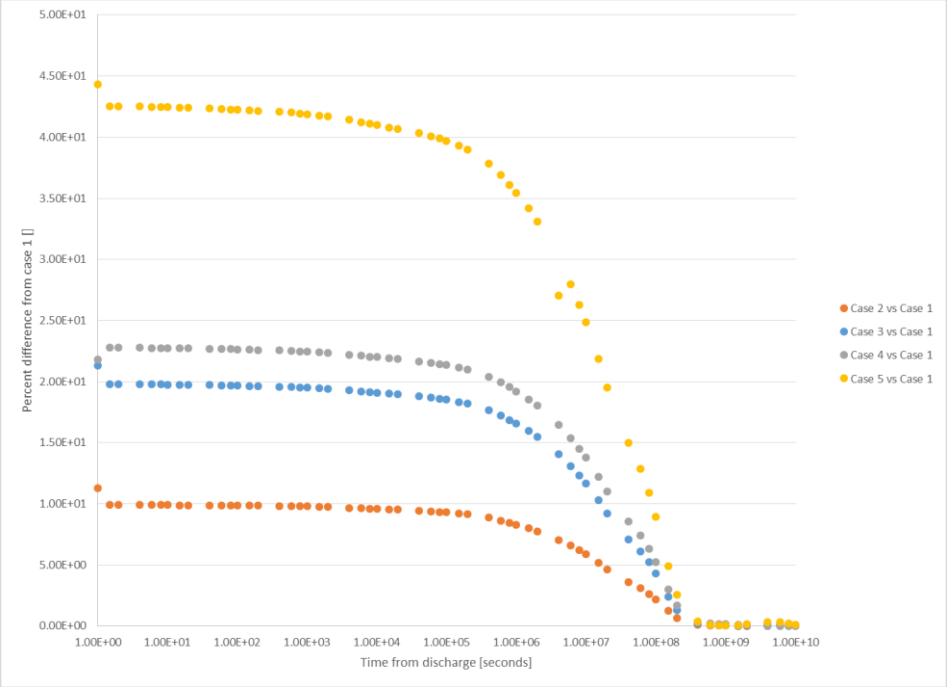

Figure 65: Difference from baseline fuel management strategy for 44 GWD/MTHM I^{2}S-LWR fuel

Here, as expected, the percent difference decreases with time. Additionally, the percent increases with larger differences in second cycle burnup when compared to the 20 GWD/MTHM in the baseline case. It should be noted that, while cases 3 and 4 have a large difference in second cycle burnup at 24 and 15.4 GWD/MTHM, respectively, comparing to the baseline 20 GWD/MTHM the differences from that case are 4 and 4.6 GWD/MTHM, respectively, explaining their similarity.

Performing these same analyses for gamma rays, one obtains the following:

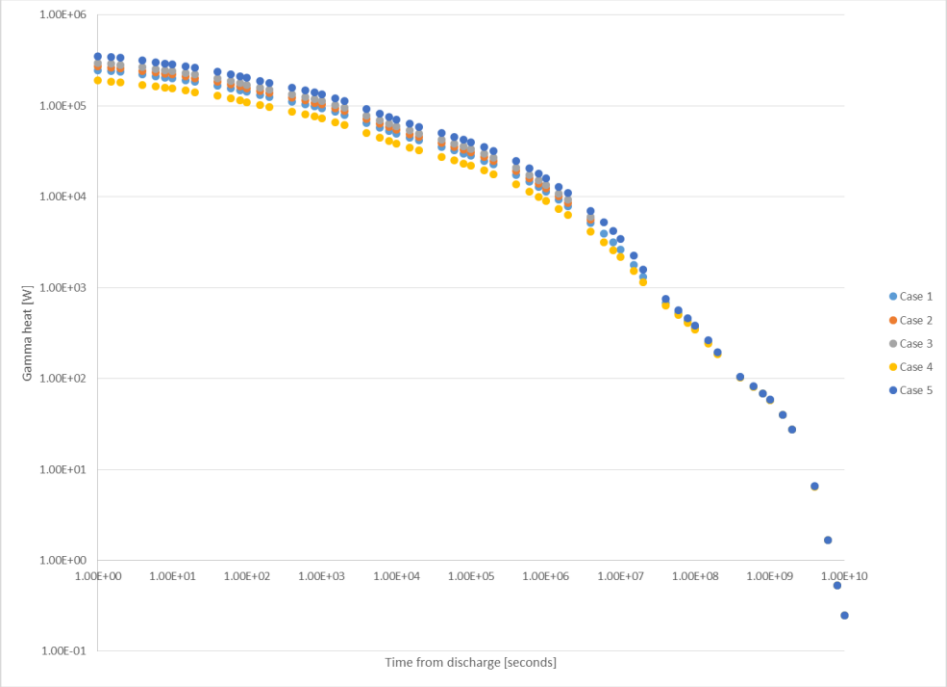

Figure 66: Gamma ray decay heat from 44 GWD/MTHM I²S-LWR fuel at varying specific powers

The same trends are observed here in Figure 66 as in the total decay heat: While decay heat converges to the same value long (> 10^8 seconds) after discharge, there are larger differences shortly after discharge, with higher second-cycle burnup corresponding to higher gamma ray decay heat immediately after discharge. Normalizing now to operating power, since one would not expect differing operating powers to result in the same decay heat, the following is obtained:

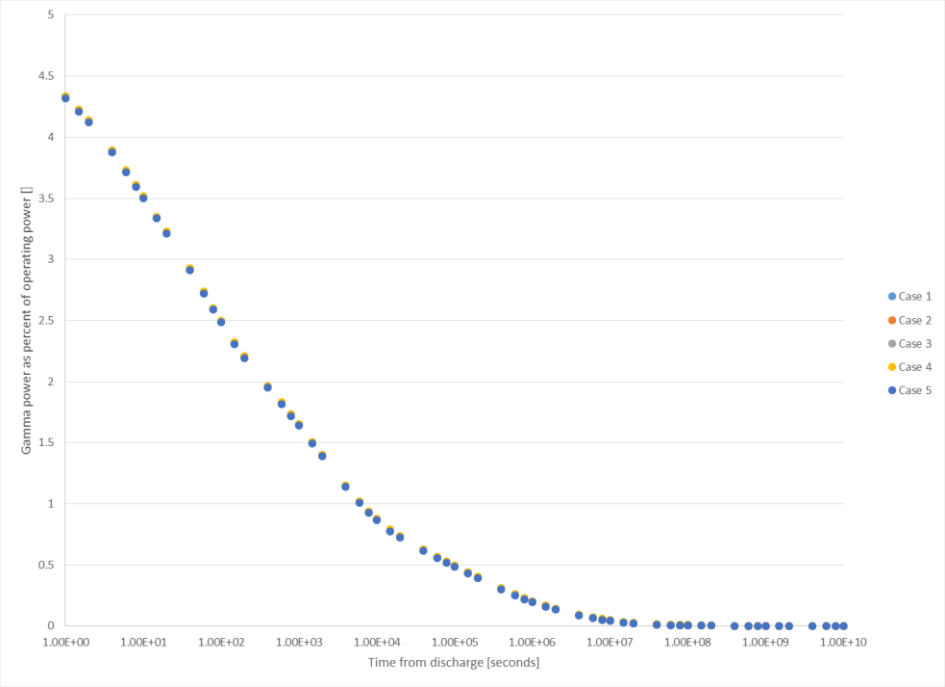

Figure 67: Gamma ray decay heat per unit operating power at discharge for 44 GWD/MTHM I²S-LWR Fuel

Here, unlike total decay heat, there is no apparent difference in between the 5 fuel management strategies considered, meaning that charged particle decays may perhaps account for the difference in decay heats not explained by the difference in operating powers. To examine this possibility, the percent difference, defined as

$$PD_{n,t} = 100 * \frac{\left|\frac{DH_{\gamma,n,t}}{PO_{2,n,t}} - \frac{DH_{\gamma,1,t}}{PO_{2,1,t}}\right|}{\frac{DH_{1,t}DH_{\gamma,1,t}}{PO_{2,1,t}}}$$

Equation 17: Percent difference in fractional decay heat

Where $PD_{n,t}$ is the percent difference between cases 1 and case *n* at time *t*, where n=2,3,4,5, and $DH\gamma_{n,t}$ is the gamma ray decay heat for case *n* at time *t*, and $PO_{2,n,t}$ is the second cycle operating power for case *n*.

Unfortunately, while the absolute difference in gamma ray decay heat divided by operating power decreased, the percent differences are largely the same and follow the same

trends as total decay heat: The difference between Case 1 and Case 4 or 5 is similar, and the largest percent difference of those studied, reaching just under 30 (29.9%) difference at 10^{10} seconds. Whereas for total decay heat the difference first exceeds 1% at $4 * 10^3$ seconds from discharge, here it first exceeds 1% at 10^5 seconds from discharge. In summary, while normalized gamma-ray decay heat is less sensitive to operating power than total decay heat at short times from discharge, the percent differences in the two follow similar long-term trends and uncertainties at times long after discharge.

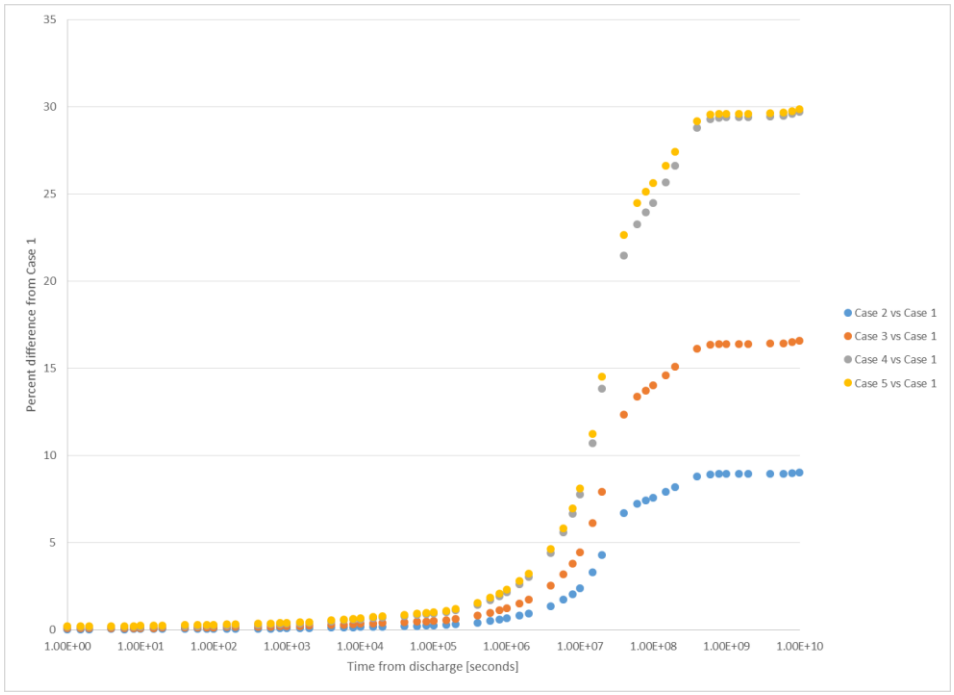

Figure 68: Percent difference in gamma ray decay heats for 44 GWD/MTHM I²S-LWR fuel

And considering the percent difference in unnormalized gamma ray decay heat, one sees in Figure 69 trends similar to those seen above in total decay heat in Figure 65: The primary determinant of difference from Case 1 is the difference in discharge burnups, while the difference in all cases tends towards 0 as time increases.

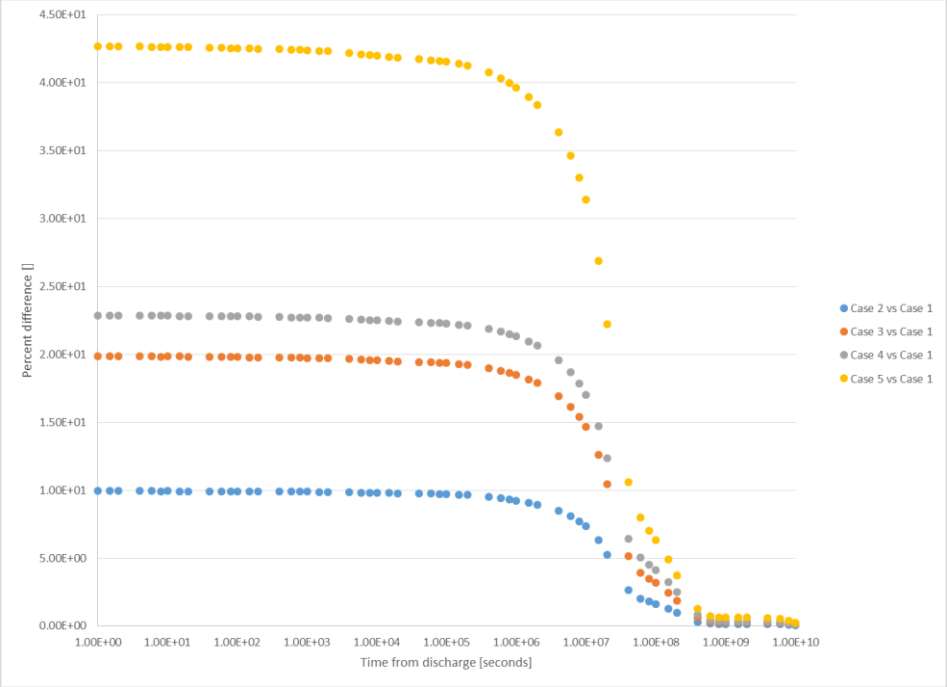

Figure 69: Percent difference from case 1 in unnormalized gamma ray heat, specific power study

6.2.6 Sensitivity to Fuel Management Strategy

The fuel management strategy likely to be used in a real I^2S-LWR power plant is a "2.5-batch" core, in which one half of all assemblies are in a 2-batch, 44 GWD/MTHM discharge burnup cycle with cycle burnups of 24 and 20 GWD/MTHM, while the other half are in a 3-batch, 54 GWD/MTHM discharge burnup cycle with cycle burnups of 22, 18, and 14 GWD/MTHM. This sensitivity study is unique in that multiple variables have been simultaneously changed, as both discharge burnup and operating power are different across the two cases being examined.

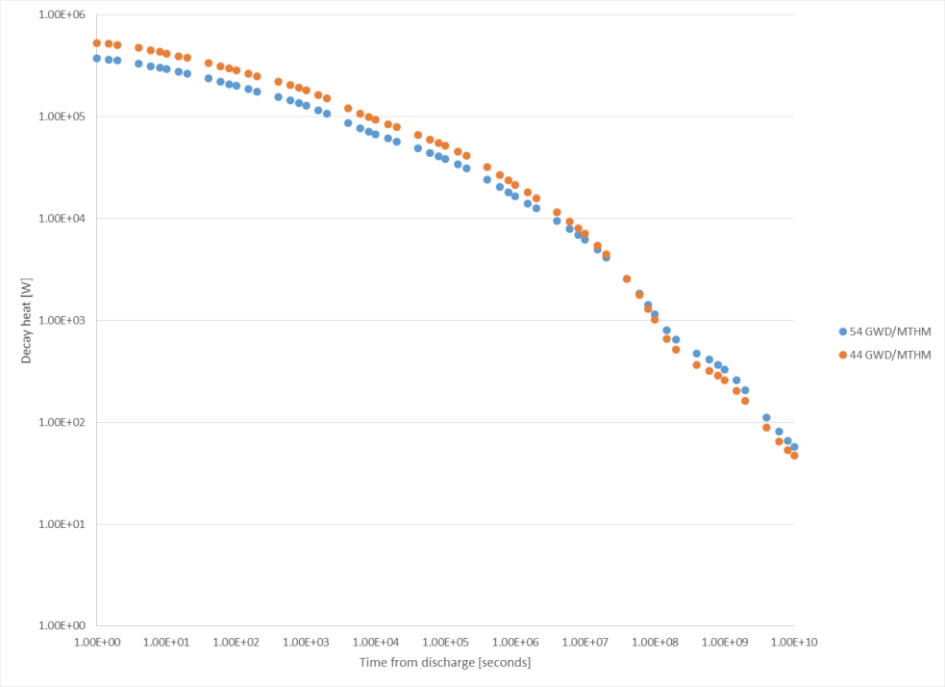

Figure 70: Comparison of decay heat for 2- and 3- batch I²S-LWR fuel

It should be noted here that the decay heat at discharge is greater for the 44 GWD/MTHM case, as would be expected owing to its higher last-cycle operating power, but decay heat is greater for the 54 GWD/MTHM case starting at a time of 60 * 10^7 seconds after discharge, and is greater at all subsequent times; this confirms the earlier hypothesis that burnup has an impact on decay heat.

Looking at the difference between the two, as shown below in Figure 71, the 44 GWD/MTHM case has a greater decay heat up to 6 * 10^7 seconds from discharge, after which the 54 GWD/MTHM fuel has higher decay heat. However, the difference here is small, never exceeding 135 W.

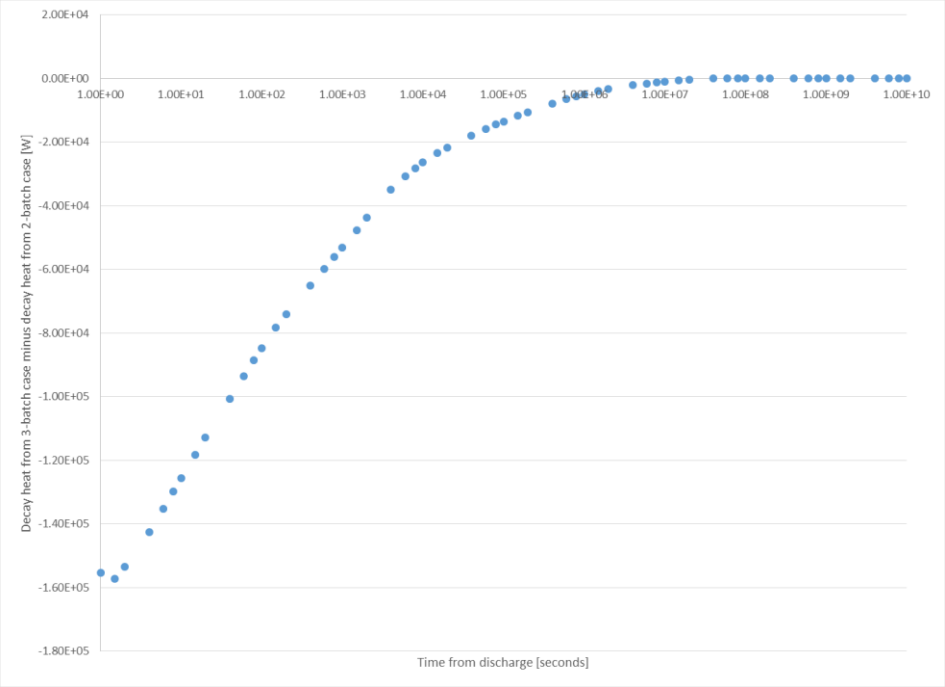

Figure 71: Absolute difference in decay heat, 3- vs 2- batch cases

Normalizing for operating power, one gets two similar decay heat curves in Figure 72, as would be expected.

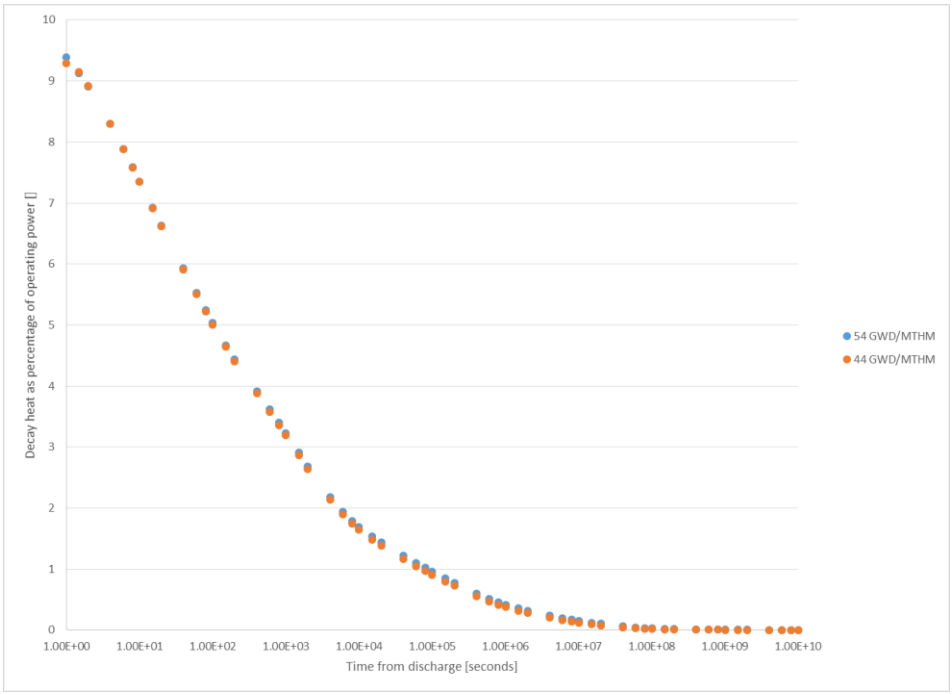

Figure 72: Normalized decay heat, I²S-LWR multibatch

And now looking at the percent difference in normalized decay heat between the 44 and 54 GWD/MTHM. Since a difference in decay heat between the two cases was both observed and expected, there will not be a comparison of non-normalized decay heats performed. Looking at figure 73 below, there is a significant difference; the percent difference in normalized decay heats exceeds 5% at 6 *10^4 seconds (16.67 hours) and 10% at 10^6 seconds (11.57 days) after discharge. From this, it is clear that the prior operating history must still be considered in determining decay heat, even though much of the decay heat is from the most recent cycle.

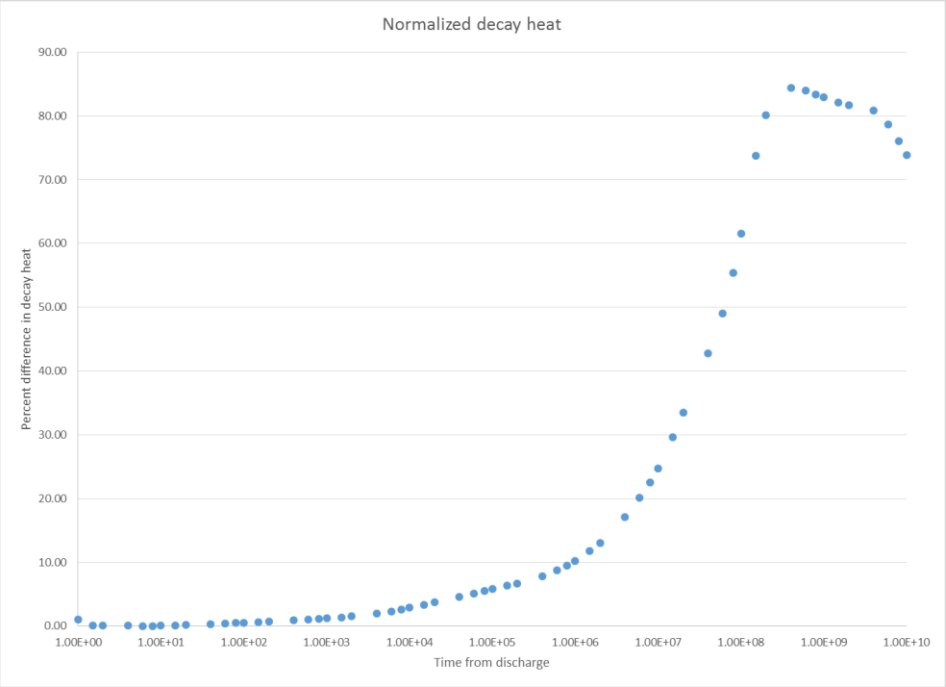

Figure 73: Percent difference in normalized decay heat

And now performing these same analyses for gamma ray decay heat only, the trend for gamma ray decay heat is found to be slightly higher for 44 GWD/MTHM than 54 GWD/MTHM fuel, as seen in Figure 74:

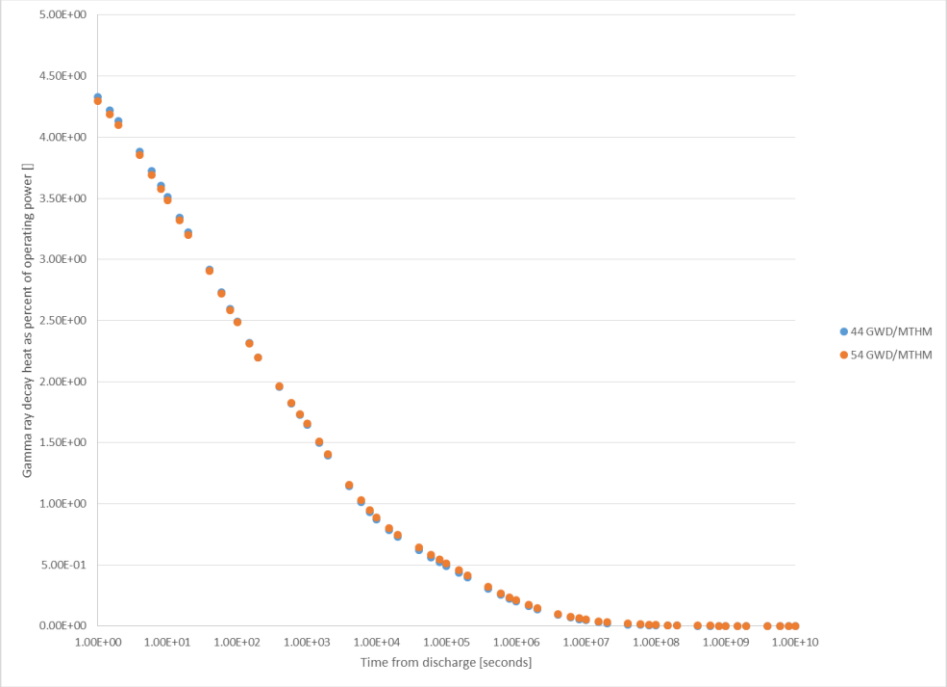

Figure 74: Decay heat as a function of operating power, 2- and 3- batch I²S-LWR fuel

And now, looking at the percent differences of the 54 GWD/MTHM case compared with the 44 GWD/MTHM baseline, shown below in Figure 75:

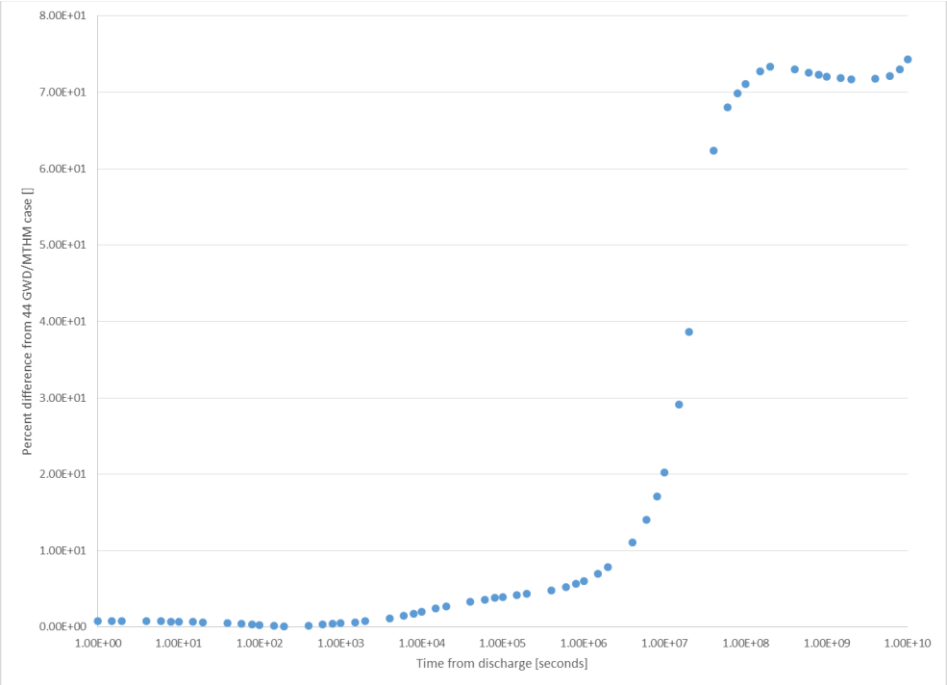

Figure 75: Percent difference in gamma ray decay heat for 54 and 44 GWD/MTHM I²S-LWR fuel

Here, the percent error is lower than it is for total decay heat despite similar trends in normalized total and gamma ray decay heat, with a percent difference no greater than 74.4%, a value reached at 10^{10} seconds after discharge compared with a maximum difference of 84.4% for total decay heat, reached $4 * 10^{8}$ seconds after discharge. As the percent error is different, both in magnitude and time-dependent behavior, for total & gamma ray decay heat, it follows that the fraction of decay heat coming from gamma rays also depends on fuel management strategy.

6.2.7 Single-pin analysis and isotopic decay heat

So far, all analyses performed have been of a quarter assembly, and only considering the decay heat or gamma heat due to all nuclides present. However, it is also useful to identify the principle isotopes contributing to the decay heat, and to find their contribution at each time after discharge. Due to the large amount of time needed to extract this data for an entire quarter assembly, this analysis will only be performed for a single pin. Analyzing fuel pin 1, using the notation of Figure 9, the following was found:

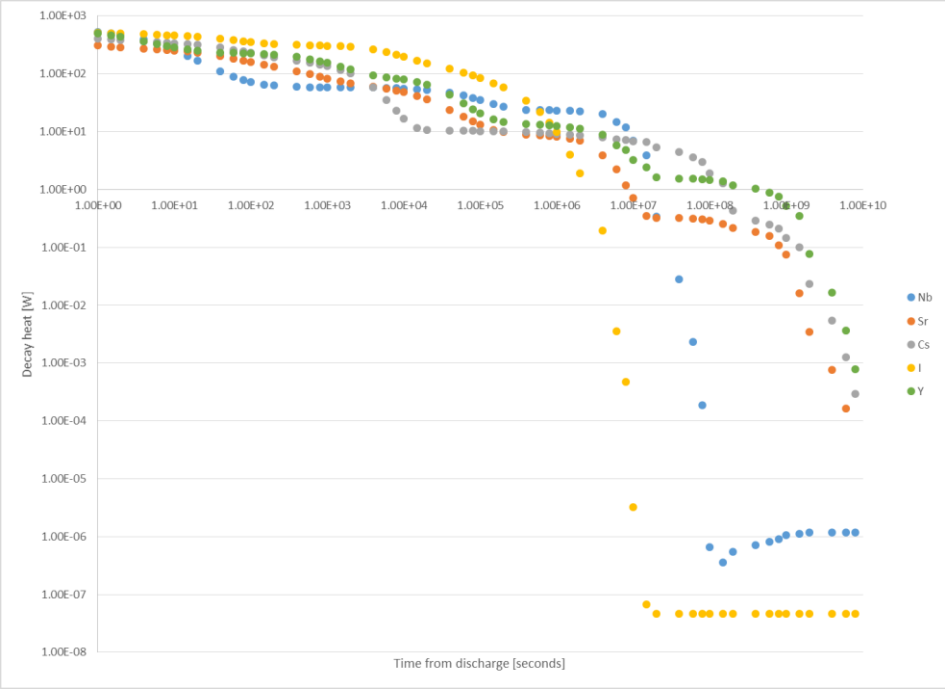

Figure 76: Total Decay heat by isotope from I²S-LWR fuel pin irradiated to 44 GWD/MTHM

It should be noted that only the largest contributors to decay heat are plotted in Figure 76, and the decay heat from these does not add up to the total decay heat from this pin. Iodine is the largest source of decay heat up to 6 * 10^6 seconds, niobium from 6 * 10^6 to 2*10^7 seconds, cesium from 4 * 10^7 seconds to 10^8 seconds, and Yttrium at all times after then.

Now looking only at gamma ray emissions, one obtains the following:

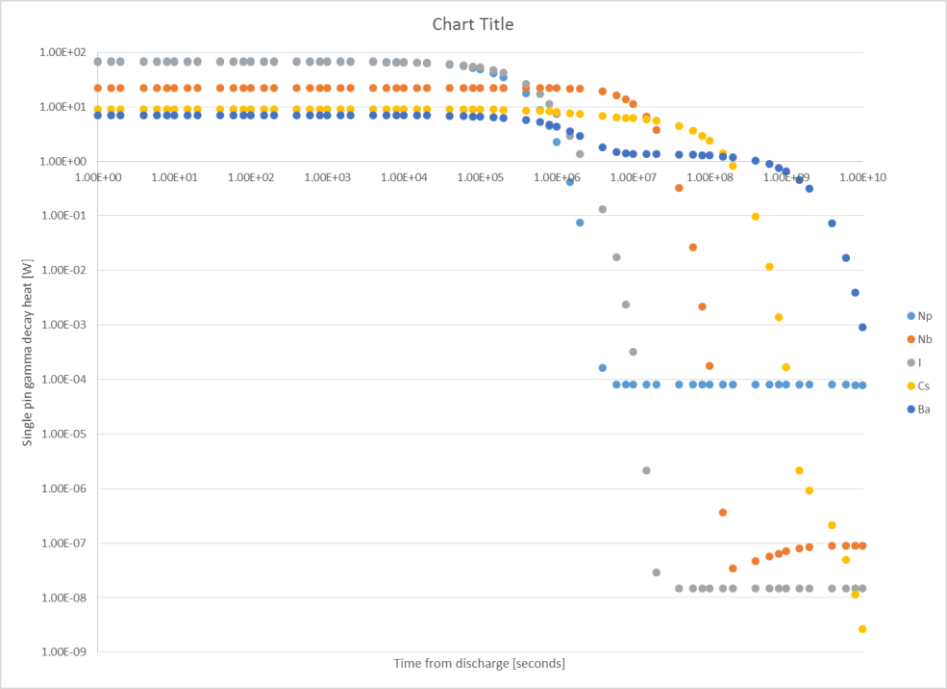

Figure 77: Gamma ray Decay heat by isotope from I²S-LWR fuel pin irradiated to 44 GWD/MTHM

Note that the isotopes tracked are not the same in both cases, as not all principle contributors to decay heat are gamma emitters, and vice-versa. Here, the contribution from I is roughly equal to that from Np until 8 * 10^4 seconds from discharge, after which I is the largest contributor to gamma ray decay heat. Nb is then the largest contributor to gamma heating from then until 2 * 10^7 seconds; Cs is then the largest source of decay heat up to 1.5 * 10^8 seconds, beyond which Ba is the primary source of gamma heating.

6.3 Comparison to ANS 5.1-2005

6.3.1 Generation of power data

For the sake of conciseness and practicality, only the multibatch fuel management strategies have been benchmarked against ANS 5.1-2005. One major limitation in this analysis is that the ANS standard requires the contribution from each isotope to the operating power, which is not provided by SCALE; further, the standard does not have data for fission in ^{240}Pu, ^{242}Pu, or ^{242}Am. Therefore, it will be assumed that all fissions occur in one of ^{235}U, ^{238}U, ^{239}Pu, or ^{241}Pu. Further, it will be assumed that power from a particular isotope is constant over the fuel cycle, using the beginning-of-cycle data to determine the fraction of power coming from that isotope Using nuclear data from [10] and [28], the data shown in Table 11 and 12 are obtained for the 2- and 3- batch cases:

Table 11: Contribution to operating power by isotope, 2-batch case

Nuclide	Contribution to power, start of cycle 1 [%]	Contribution to power, start of cycle 2 [%]
^{235}U	98.8	69.4
^{238}U	1.12	1.44
^{239}Pu	0	24.8
^{241}Pu	0	4.34

Table 12: Contribution to operating power by isotope, 3-batch case

Nuclide	Contribution to power, start of cycle 1 [%]	Contribution to power, start of cycle 2 [%]	Contribution to power, start of cycle 3 [%]
^{235}U	98.8	71.6	53.5
^{238}U	1.12	1.41	1.70
^{239}Pu	0	23.3	35.0
^{241}Pu	0	3.72	9.74

Additionally, finding decay heat from ANS-5.1-2005 is based not on burnup but rather operating power. Using a quarter-assembly heavy metal loading of 0.1507 MT [3], the operating power for a quarter assembly on each fuel management strategy is obtained and listed in table 13.

Table 13: Power histories for I²S-LWR fuel assembly

Case	First cycle power [MW]	Second cycle power [MW]	Third cycle power [MW] (3-batch only)
2-batch	6.856	5.714	N/A
3-batch	6.285	5.142	4.000

All necessary data for using ANS 5.1-2005 has now been obtained. As mentioned above, the 2- and 3- batch cycle depletion models assume an 18-month cycle length, with 20 days of downtime for refueling & maintenance included in this 18 months.

As an aside, neutron capture in fission products can still occur after shutdown, and decay heat may need to be corrected as a result. While ANS-5.1-2014 introduces a correction factor *G(t)* [19], defined as the ratio of actual decay heat to decay heat ignoring capture in fission products, uncorrected decay heat has not been plotted here, as G is so close to 1; specifically, it never exceeds 1.000006 and quickly tends to 1, so that the differences introduced by it are much smaller than the

uncertainty in the ANS standard and its inclusion has no practical influence on decay heat. As such, *G(t)* will be neglected in the following analyses.

6.3.2 Analysis of 2-batch case

Assuming a constant 200 MeV/fission, the decay heat is calculated and plotted against SCALE results in figure 67. Notably, since the reactor was operating at non-constant operating powers, it is not possible to tabulate decay heat here in MeV/fission, only in watts. Here, several trends are apparent: From $4 * 10^3$ to $4 * 10^5$ seconds, ANS and SCALE diverge, though within 1 standard deviation. As discussed in the literature search, SCALE tends to underestimate decay heat, so this is expected if undesirable. More interesting is that the decay heat at $4 * 10^7$ seconds, or roughly 462 days, after discharge, differs beyond the margin of error, as do all values for $6 * 10^8$ to $8 * 10^9$ seconds (19-254 years) from discharge, though consistently less than the results obtained from SCALE as would be expected given the Standard's history of underestimating decay heat. Also of note is the standard's overprediction of decay heat at 10^{10} seconds from discharge. While the calculated value is still within 1 standard deviation, it is surprising as ANS Standard is not generally known to overestimate decay heat.

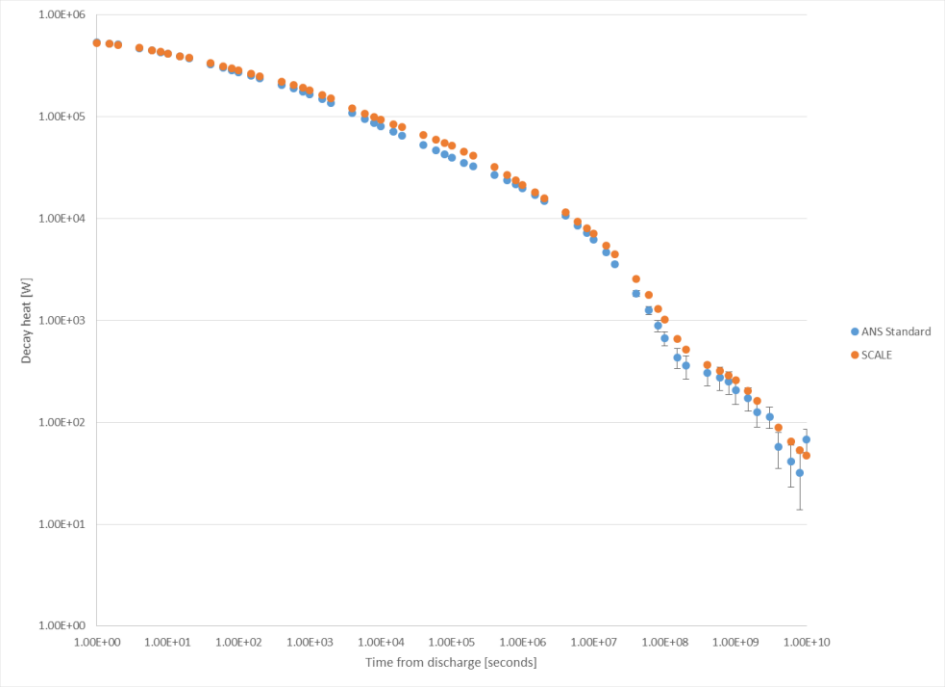

Figure 78: SCALE results vs ANS 2014 Standard, 44 GWD/MTHM decay heat

Looking at the difference between the two decay heats in Figures 78 and 79, one sees that starting at 10 seconds from discharge and at all times after that until $4 * 10^8$ seconds, decay heat from SCALE is greater than that predicted by the ANS standard, and the overpredictions by the ANS standard are always within 1 standard deviation.

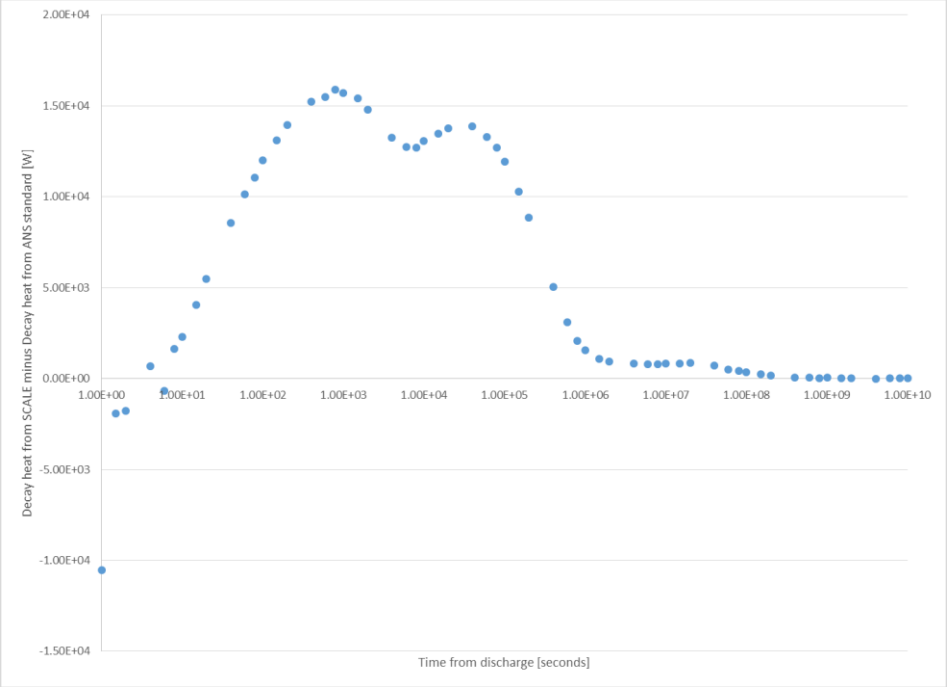

Figure 79: Difference in decay heat for SCALE and ANS standard, 2-batch I^{2}S-LWR core

6.3.3 Analysis of 3-batch case

Performing the same analyses as above, the decay heat curves for the 3-batch case are plotted below. Once again, the decay heat curves are in agreement immediately after discharge and diverge beyond one standard deviation at long times after discharge, though here the divergence begins at $4 * 10^9$ seconds after discharge, or roughly 127 years.

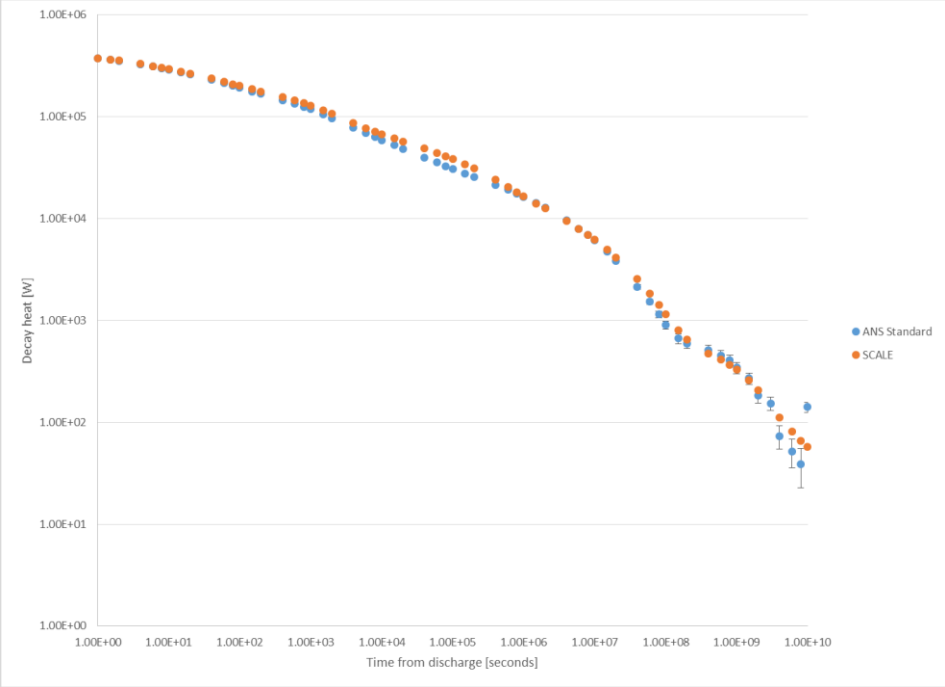

Figure 80: Decay heat for 3-batch I²S-LWR fuel, SCALE results vs ANS standard

Looking at Figure 80, the ANS Standard once again underpredicts decay heats long after discharge, outside the uncertainty and consistent with the Standard's known problems.

Looking now at the difference between the SCALE and ANS standards and defining the difference as decay heat from SCALE minus predicted decay heat so that most of the values are positive, the results are plotted in Figure 81. The trends here are quite similar, with the maximum differences between SCALE and ANS results at 800 seconds after discharge, regardless of fuel management strategy, and a second, smaller difference reaching its maximum at 40000 seconds, or 11.11 hours, after discharge, and then decreasing thereafter. There is, however, a brief period from $1.5 * 10^6$ to $6 * 10^7$ seconds from discharge where, while the results agree within 1 standard deviation, the ANS Standard unexpectedly has overestimated decay heat at these times.

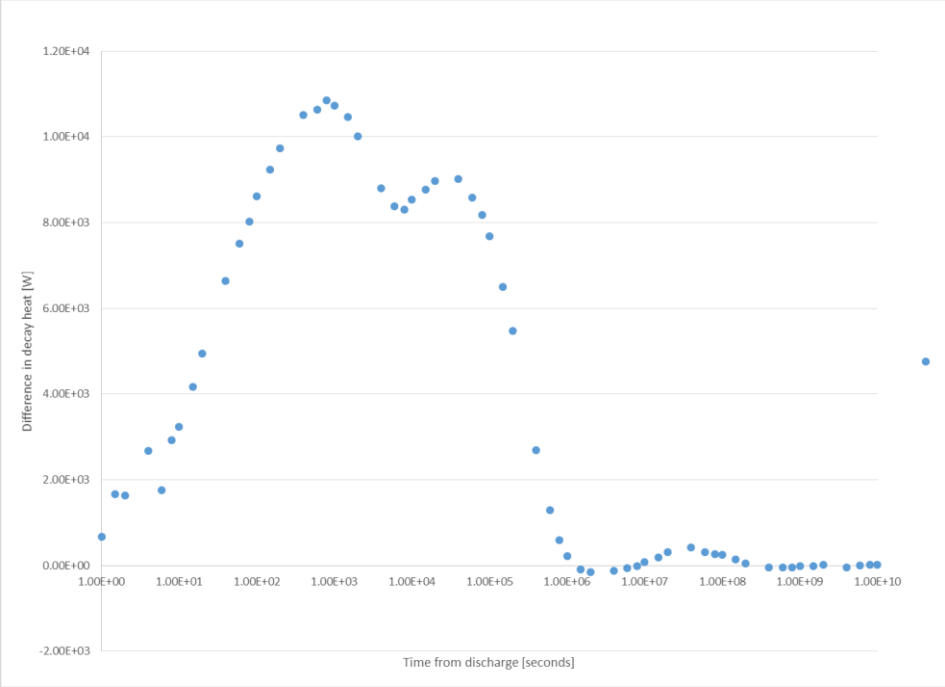

Figure 81: Difference between SCALE and ANS Standard for decay heat of 54 GW/MTHM I²S-LWR fuel

6.3.4 Sensitivity to power data

As mentioned above, the power contributed from each isotope was assumed to be constant over each cycle, using contributions from the beginning of that cycle to find the power by isotope. As ^{235}U and ^{238}U are depleted over the entire cycle, while ^{239}Pu and ^{241}Pu concentrations increase over time, using beginning-of-cycle data overestimates contributions from uranium and underestimates those from plutonium, assuming that they contribute no power in the first cycle. Since the F(t,∞) function in ANS-5.1 varies between isotopes, the power distribution by isotope will also determine, in part, the decay heat. To determine the sensitivity to power data, the data found in section 6.3.1 will be re-generated, this time using end-of-cycle fuel composition, and the decay heat will be re-calculated using the ANS standard. As this is just a sensitivity study, rather than an attempt to match the results from the ANS Standard and SCALE results, this section will not consider mid-cycle fuel composition, as the fuel composition, and by extension decay heat, would fall somewhere between the results using beginning- and end-of-cycle data.

For the 2-batch case, this results in the isotopic power distribution shown in Table 14:

Table 14: End-of-cycle contribution by isotope to operating power, 2-batch I²S-LWR fuel

Isotope	Contribution to power, end of cycle 1 [%]	Contribution to power, end of cycle 2 [%]
^{235}U	69.4	49.9
^{238}U	1.44	1.77
^{239}Pu	24.8	37.1
^{241}Pu	4.34	11.3

While the 3-batch case has the distribution shown in Table 15:

Table 15: End-of-cycle contribution by isotope to operating power, 3-batch I²S-LWR fuel

Isotope	Contribution to power, end of cycle 1 [%]	Contribution to power, end of cycle 2 [%]	Contribution to power, end of cycle 3 [%]
^{235}U	71.6	53.5	40.8
^{238}U	1.41	1.70	1.96
^{239}Pu	23.3	35.0	42.5
^{241}Pu	3.72	9.76	14.8

As expected, the change in when isotopic data was taken has resulted in a larger share of power produced from ^{239}Pu and ^{241}Pu, with a corresponding decrease in power from ^{235}U and ^{238}U; notably, ^{239}Pu rather than ^{235}U has the single largest contribution to operating power at the end of the third cycle, whereas ^{235}U produced more power than ^{239}Pu and ^{241}Pu combined when beginning of cycle data was used. While the isotopic distribution has changed, the total cycle power is the same here as given in section 6.3.1.

Considering first the two-batch case, below in Figure 82 is the ANS Standard decay heat results using end of cycle data compared with the same SCALE results used in section 6.3.2:

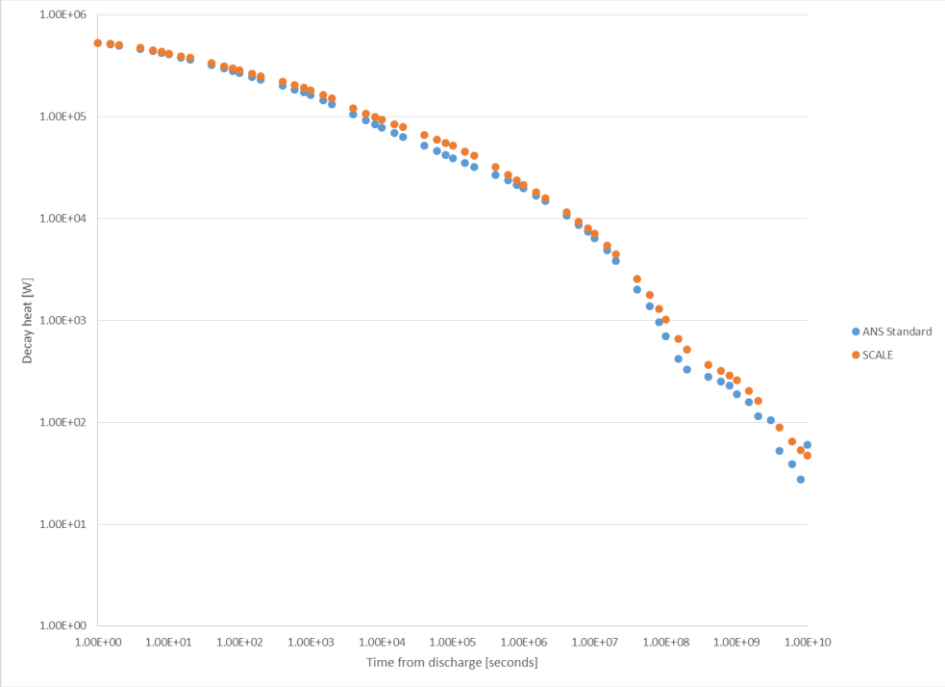

Figure 82: Decay heat for 44 GWD/MTHM I^{2}S-LWR fuel, ANS-5.1 using end of cycle compositions vs SCALE results

These results are similar, but not identical, to the ones obtained using beginning-of-cycle power data. To better examine the impact of using end-of-cycle data, the difference between SCALE and the ANS standard is plotted below for both sets of ANS results.

Looking first at the 2-batch case in figure 82 and the comparison in Figure 83, the beginning-of-cycle data provides the better fit from 1.5 seconds to 4 * 10^5 seconds, beyond which it is in good agreement with the end-of-cycle data. That the end-of-cycle data is a better fit at 1 second, and an underestimate rather than an overestimate of decay heat, is probably due to the lower decay heat in MeV/Fission immediately for ^{239}Pu and ^{241}Pu. Since there is already good agreement between SCALE and the ANS standard at times up to 4 * 10^5 seconds, the ANS standard's known problems with underestimating decay heat, including the underestimates long after discharge found in this thesis, are not fixed by the use of end-of-cycle data, and the lower decay heat found with by using end-of-cycle data actually increases the problem of underestimates in the ANS standard.

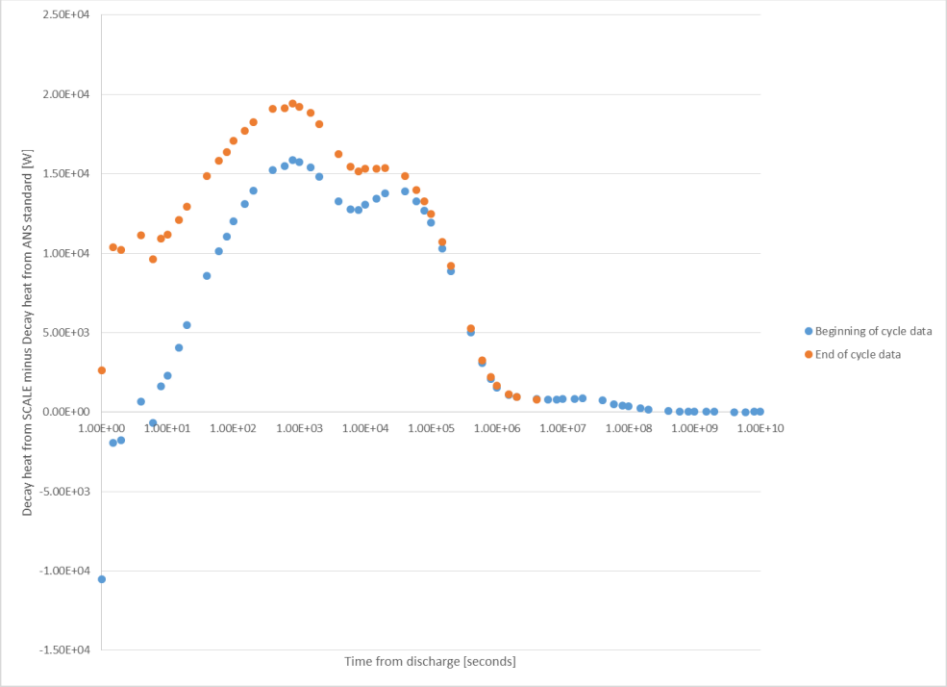

Figure 83: Comparison of differences from SCALE decay heat results, I²S-LWR 2-batch fuel

Now doing the same for the 3-batch case:

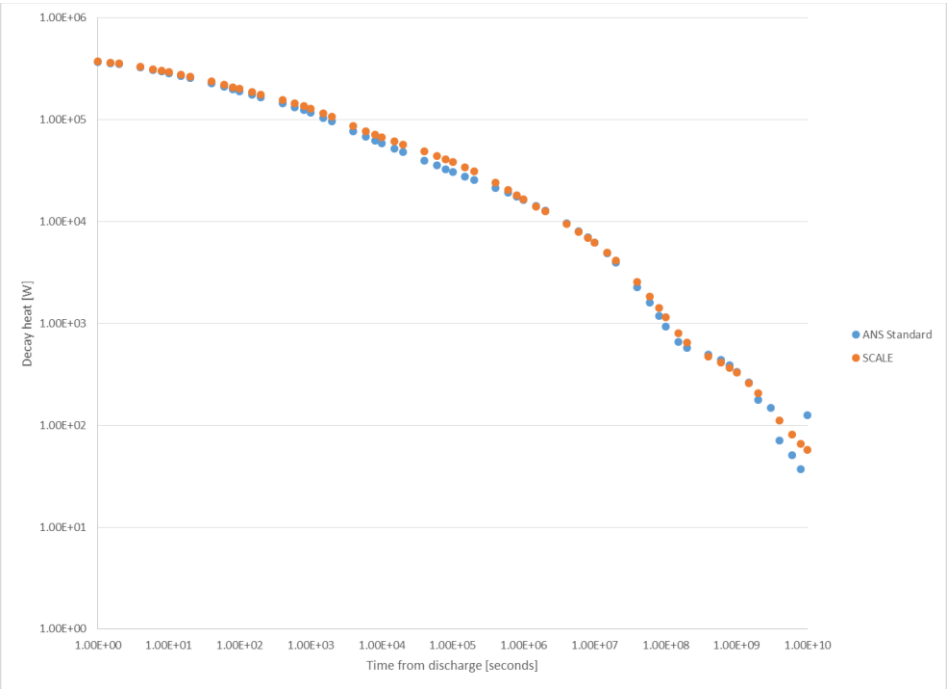

Figure 84: Decay heat for 54 GWD/MTHM I²S-LWR fuel, ANS-5.1 using end of cycle compositions vs SCALE results

Once again there is good agreement exact at very long times after discharge, with the divergence occurring here at 4 * 10^9 seconds after discharge. Looking at a comparison of SCALE decay heat minus decay heat found using the ANS standard for the two isotopic data cases in Figure 85, one obtains:

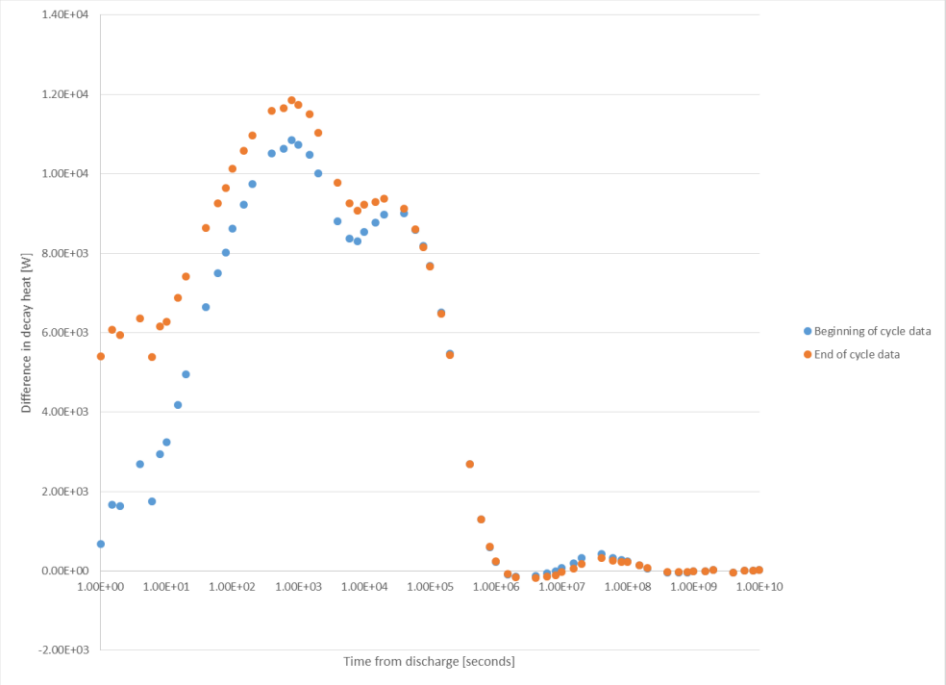

Figure 85:Comparison of differences from SCALE decay heat results, I²S-LWR 3-batch fuel

Unlike the 2-batch case, the ANS Standard is more inaccurate at 1 second after discharge; whereas ANS overestimated decay heat at 1 second in the 2 batch case using beginning of cycle data, here it underestimates it, and the underestimate is even greater when end-of-cycle data is used. While the difference in decay heat is smaller, and convergence occurs sooner at 4 * 10^4 seconds compared with 4 * 10^5 seconds in the 2-batch case, ANS-5.1 underestimates decay heat using end-of-cycle data even more than it does with beginning of cycle data. The convergence at 4 * 10^4 seconds is also of little use, as it means the ANS standard is still inaccurate at long (> 4 * 10^9 seconds) times after discharge. Once again, end-of-cycle data provides a worse approximation to decay heat and there is no reason to use it in place of beginning-of-cycle data.

6.4 Covariance Studies

From the results of Section 6.2, the main drivers of decay heat are burnup and operating power. To determine the versatility and applicability of these results, it is useful to know whether burnup and operating power are covariant, that is, whether a change in burnup will introduce the same percent difference in decay heat even at different powers, or vice-versa. If this is the case, then the percent difference in decay heat from a change in burnup ΔP should be the same at any power. If decay heat is defined as some function *F(BU,P)*, where *P* refers to the power, then the following expression should be satisfied if the two variables are not covariant:

$$\frac{F(BU, P + \Delta P) - F(BU, P)}{F(BU, P)} = C * \frac{F(BU', P + \Delta P) - F(BU', P)}{F(BU', P)}$$

Equation 18: Non-covariant relation of decay heat as a function of burnup & power

Where BU' and BU need not be equal, and C is not dependent on time. To examine this claim, the operating power sensitivity results from section 6.2.4 are revisited: Examining the change from operating power of 40 to 62.5 MW/MT, and then finding the percent difference in normalized operating power & the ratio between the two, the graph below is generated:

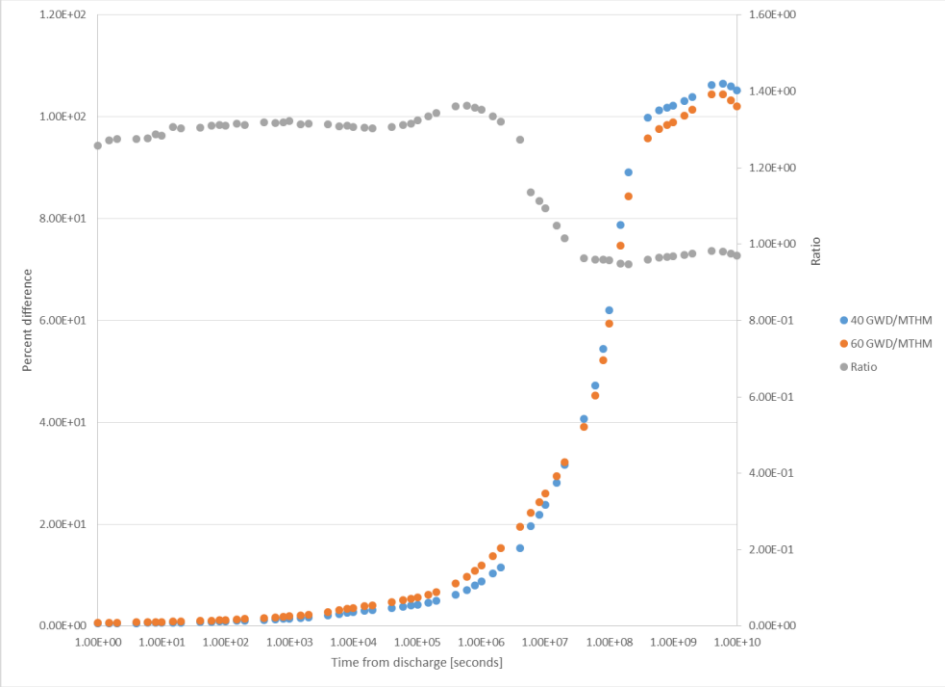

Figure 86: Comparison of percent difference (blue, orange) and the ratio of percent differences (gray) for covariance study

The "ratio" data, shown as the gray line in figure 86, corresponds to the parameter *C* from the above equation. Not only is the ratio not equal to 1 throughout, but it is non-constant. As such, there is a nonzero covariance between operating power and burnup. From a practical perspective, this means that a change in burnup or operating power will not result in the decay heat increasing or decreasing by a factor over all times, and it is inappropriate to extrapolate data from cases in this study to other, even largely similar power and burnup histories. In particular, since the ratio is very sensitive to time from 1 to 15 seconds, and again 10^5 to 10^7 seconds after discharge, it has no applicability even for rough estimates, as the former range of times covers shutdown and accidents, while the latter covers used-fuel storage applications.

7 Conclusions and Future Work

For short-term transient or accident analyses, an I^2S-LWR assembly produces slightly more decay heat, necessitating greater cooling per assembly as a result. However, as I^2S-LWR assemblies are larger than those for the AP1000, and the I^2S-LWR has fewer assemblies per reactor than the AP1000, this increase in needed cooling is small. Additionally, as the fraction of decay heat in gamma rays is comparable to that from a traditional PWR, there are no novel shielding concerns presented by the transition to I^2S-LWR. Looking at used-fuel storage applications, one of the major consequences of changing from oxide to silicide fuel is an increase in the decay heat due to gamma rays, necessitating additional shielding. Further, the higher decay heat at the same specific power & burnup as a traditional PWR is still present at longer time scales, necessitating additional cooling. Finally, owing to the higher concentration of Plutonium and Americium in I^2S-LWR, gamma spectra will be different from those of a traditional PWR, and unique criticality safety/reactivity control concerns are also presented.

As is the case with traditional LWR fuel, decay heat in I^2S-LWR fuel is determined by both burnup and operating power, and sensitivity to burnup is not eliminated by high-burnup or multibatch fuel management approaches. As covariance between operating power and decay heat is nonzero, operating power histories not discussed in this thesis would need to have the depletion & decay heat calculations redone, as the change in decay heat due to a change in burnup is a function of operating power, and vice-versa, meaning it is not adequate to simply multiply decay heat from a known case by a constant.

The ANS-5.1-2005 standard and computed results from SCALE are in agreement within the margin of error for silicide fuel in the I^2S-LWR up to $4*10^7$ seconds, or 462 days from discharge in the 44 GWD/MTHM case and $4 * 10^9$ seconds or roughly 127 years from discharge

in the 54 GWD/MTHM case, at which point they are not in agreement within 1σ of the ANS standard calculated values but within 2σ for the 44 GWD/MTHM case; for the 54 GWD/MTHM case even this was not valid. As was discussed in the literature search, the ANS standard has been known to provide an underestimate of decay heat even when applied to a typical LWR operating history. This was also the case here, as the ANS standard underestimated decay heat when it disagreed with results from SCALE. The sole exception to this was the decay heat measured at 10^{10} seconds from discharge, which may be explained by the way in which extrapolation beyond 10^{10} seconds, which is discouraged by the ANS standard, was needed to find decay heat at $F(10^{10} + T, \infty)$. While using beginning-of-cycle data is not entirely accurate when performing ANS Standard calculations, end-of-cycle data is even less accurate, further underestimating decay heat, and as such should not be used.

Future research in this area could cover any number of topics. Further sensitivity studies to burnup & fuel management strategy could be performed, as many other fuel-management strategies were proposed, but discarded, and could be used to improve or validate the model developed in this thesis. An improved treatment of fission in ^{238}U, ^{239}Pu and ^{241}Pu could also be used in applying the ANS standard: The model used in this thesis assumed that the fraction of power coming from each isotope was constant over each cycle in-core and ignored fission in ^{242}Am, ^{240}Pu, and ^{242}Pu, when the plutonium accumulation results discussed in 6.1.3 show that such an assumption is invalid. The constant plutonium density assumption would have the larger impact, due to the fission threshold and high resonance absorption cross section of ^{240}Pu and ^{242}Pu.

From a computational modeling perspective, more accurate approaches could be used. This thesis made numerous assumptions that are not entirely valid: The zero-current assumption is not exactly valid, particularly at end of cycle, when there is a net current into once- or twice- burned

assemblies, and when fuel is freshly inserted; at that time, there is a net current from fresh fuel assemblies to already burned ones. These could be rectified with a quarter-core, rather than a quarter-assembly model. Further assessment of uncertainty is also warranted: Since all depletion studies in this thesis were performed with NEWT, no attempts were made to correct for error introduced by NEWT itself. Benchmarking these results against MCNP, or even KENO, the Monte Carlo module within SCALE, would be useful to determine whether, or to what extent, results vary based on the code package used, and to determine what, if any, effects would be introduced by using a 3-D vs. 2-D model. MCNP has the added benefit of being continuous energy: SCALE's energy group structure was chosen specifically for a traditional LWR, so it may do a poor job of modelling the different spectrum in the I^2S-LWR.

On a somewhat related note, additional reactor physics modelling is also necessary to use these models for reactor safety during accidents, as fission power is still non-zero immediately after shutdown due to delayed neutrons.

Additionally, an interesting next step for this work could be burnup credits assessment, one of the other major concerns for used fuel storage or disposal: As this thesis has established, the I^2S-LWR has a different spectrum and actinide production from a traditional PWR, and as such the reactivity of I^2S-LWR fuel would also have a different relationship with burnup than traditional PWR fuel, both during irradiation and after discharge. This would require that the quarter assembly studied in this thesis be re-created in 3D, however, as axial effects cannot be captured by the 2D model used here, and Monte Carlo depletion would need to be instead used for the ability to model systems without simplified or approximate geometry, as S_N codes require spatial discretization.

Appendix A: Sample Depletion File for I^{2}S-LWR

This is a sample input file for I^{2}S-LWR depletion. Lines that changed between cases are in **bold**.

```
=t-depl parm=(addnux=3)
i2s sn depletion
v7-238
read composition
 atomfuelrod1    1  12.2  2
                        92000 3
                        14000 2
                  0.965 900
                        92234 0.0383461158
                        92235 4.95
                        92238 95.01165388   end
 wtptodssteel    2  7.25  7
                        24000 21
                        13000 5
                        42000 3
                        6000 0.08
                        14000 0.7
                        25000 0.4
                        26000 69.82
                   1 650   end
 h2o        4 den=0.71347 1 579.25   end
 h2o        5 den=0.71347 1 579.25   end
 atomfuelrod2    10  12.2  2
                        92000 3
                        14000 2
```

```
                0.965 900
                        92234 0.0383461158
                        92235 4.95
                        92238 95.01165388   end
atomifbapin5    55  6.085  2
                        40000 1
                        5000 2
                1 300
                        5010 60
                        5011 40   end
h2o         81 den=0.71347 1 579.25   end
h2o         119 den=0.71347 1 579.25   end
wtptodssteel    132  7.25  7
                        24000 21
                        13000 5
                        42000 3
                        6000 0.08
                        14000 0.7
                        25000 0.4
                        26000 69.82
                1 650   end
wtptodssteel    273  7.25  7
                        24000 21
                        13000 5
                        42000 3
                        6000 0.08
                        14000 0.7
                        25000 0.4
                        26000 69.82
```

1 700 end

end composition

read celldata

latticecell squarepitch fuelr=0.4083 1 gapr=0.4165 0 cladr=0.4571 2 hpitch=0.6053 4 end

multiregion cylindrical left_bdy=reflected right_bdy=reflected end

10 0.4083

55 0.4088

0 0.4165

132 0.4571

81 0.6830079098

end zone

end celldata

read depletion

1 7 8 9 11 12 14 15 16 19 20 21 23 26 29 31 33 36 37 40 41 42 44 45 46 54 10 13 17 18 22 24 25 27 28 30 32 34 35

38 39 43 47 48 49 50 51 52 53

flux 55 56 57 58 59 60 61 62 63 64 65 66 67 68 69 70 71 72 73 74 75 76 77 end

assign 1 7 8 9 11 12 14 15 16 19 20 21 23 26 29 31 33 36 37 40 41 42 44 45 46 54 end

assign 10 13 17 18 22 24 25 27 28 30 32 34 35 38 39 43 47 48 49 50 51 52 53 end

assign 55 56 57 58 59 60 61 62 63 64 65 66 67 68 69 70 71 72 73 74 75 76 77 end

end depletion

read burndata

power=45.49763003 burn=10 nlib=10 end

power=45.49763003 burn=16 nlib=8 end

power=45.49763003 burn=502 nlib=6 down=20 end

power=37.91469194 burn=10 nlib=10 end

power=37.91469194 burn=16 nlib=8 end

power=37.91469194 burn=501 nlib=6 end

end burndata

read opus

symnuc=ag-109 am-241 am-242 am-242m am-243 cm-242 cm-243 cm-244 cm-245

cs-133 cs-137 eu-152 eu-153 gd-155 i-129 i-131 mo-95 nd-143 nd-145 np-235

np-236 np-237 np-238 np-239 np-240 pu-238 pu-239 pu-240 pu-241 pu-242 pu-243 pu-244 rh-103 ru-101

sr-90 tc-99 u-234 u-235 u-236 u-237 u-238 u-239 end

units=watts

time=years

nrank=40

matl=1 7 8 9 10 11 12 13 14 15 16 17 18 19 20 21 22 23 24 25 26 27 28

29 30 31 32 33 34 35 36 37 38 39 40 41 42 43 44 45 46 47 48 49 50 51 52

53 54 55 56 57 58 59 60 61 62 63 64 65 66 67 68 69 70 71 72 73 74 75 76

77 end

new case

symnuc=am-241 am-242 am-242m am-243 b-10 cf-252 cm-241 cm-242 cm-243

cm-244 cm-245 cm-246 cm-247 cm-248 he-3 np-235 np-236 np-237

np-238 np-239 np-240 pu-238 pu-239 pu-240

pu-241 pu-242 pu-243 u-234 u-235 u-236 u-238 u-237 u-239 pu-236

pu-244 np-238 np-239 sm-149 xe-135 end

units=atom

time=years

nrank=39

new case

symnuc=am-241 cs-133 cs-137 co-59 eu-152 eu-153 i-129 i-131 sr-90 tc-99 end

units=gamwatts

time=years

nrank=10

```
end opus
read model
read parameter
 drawit=yes
 echo=yes
 epsinner=1e-04
 epsouter=1e-04
 prtmxtab=yes
 solntype=b1
 sn=4
 timed=yes
end parameter
read materials
  mix=1 pn=1 end
  mix=2 pn=1 end
  mix=4 pn=1 end
  mix=5 pn=1 end
  mix=7 pn=1 end
  mix=8 pn=1 end
  mix=9 pn=1 end
  mix=10 pn=1 end
  mix=11 pn=1 end
  mix=12 pn=1 end
  mix=13 pn=1 end
  mix=14 pn=1 end
  mix=15 pn=1 end
  mix=16 pn=1 end
  mix=17 pn=1 end
  mix=18 pn=1 end
```

mix=19 pn=1 end

mix=20 pn=1 end

mix=21 pn=1 end

mix=22 pn=1 end

mix=23 pn=1 end

mix=24 pn=1 end

mix=25 pn=1 end

mix=26 pn=1 end

mix=27 pn=1 end

mix=28 pn=1 end

mix=29 pn=1 end

mix=30 pn=1 end

mix=31 pn=1 end

mix=32 pn=1 end

mix=33 pn=1 end

mix=34 pn=1 end

mix=35 pn=1 end

mix=36 pn=1 end

mix=37 pn=1 end

mix=38 pn=1 end

mix=39 pn=1 end

mix=40 pn=1 end

mix=41 pn=1 end

mix=42 pn=1 end

mix=43 pn=1 end

mix=44 pn=1 end

mix=45 pn=1 end

mix=46 pn=1 end

mix=47 pn=1 end

mix=48 pn=1 end

mix=49 pn=1 end

mix=50 pn=1 end

mix=51 pn=1 end

mix=52 pn=1 end

mix=53 pn=1 end

mix=54 pn=1 end

mix=55 pn=1 end

mix=56 pn=1 end

mix=57 pn=1 end

mix=58 pn=1 end

mix=59 pn=1 end

mix=60 pn=1 end

mix=61 pn=1 end

mix=62 pn=1 end

mix=63 pn=1 end

mix=64 pn=1 end

mix=65 pn=1 end

mix=66 pn=1 end

mix=67 pn=1 end

mix=68 pn=1 end

mix=69 pn=1 end

mix=70 pn=1 end

mix=71 pn=1 end

mix=72 pn=1 end

mix=73 pn=1 end

mix=74 pn=1 end

mix=75 pn=1 end

mix=76 pn=1 end

```
 mix=77 pn=1 end
 mix=81 pn=1 end
 mix=119 pn=1 end
 mix=132 pn=1 end
 mix=273 pn=1 end
end materials
read geometry
unit 1
com="fuel rod 1"
 cylinder 1   0.4083  sides=20
 cylinder 2   0.4165  sides=20
  cylinder 3   0.4571 sides=20
 cuboid 4    0.6053   -0.6053    0.6053   -0.6053
 media 1 1 1
 media 0 1 2 -1
 media 2 1 3 -2
 media 4 1 4 -3
 boundary 4 6 6
unit 2
com="fuel rod 2"
 cylinder 1   0.4083  sides=20
 cylinder 2   0.4165  sides=20
  cylinder 3   0.4571 sides=20
 cuboid 4    0.6053   -0.6053    0.6053   -0.6053
 media 7 1 1
 media 0 1 2 -1
 media 2 1 3 -2
 media 4 1 4 -3
 boundary 4 6 6
```

```
unit 3
com="fuel rod 3"
 cylinder 1   0.4083  sides=20
 cylinder 2   0.4165  sides=20
  cylinder 3   0.4571 sides=20
 cuboid 4    0.6053   -0.6053    0.6053   -0.6053
 media 8 1 1
 media 0 1 2 -1
 media 2 1 3 -2
 media 4 1 4 -3
 boundary 4 6 6
unit 4
com="fuel rod 4"
 cylinder 1   0.4083  sides=20
 cylinder 2   0.4165  sides=20
  cylinder 3   0.4571 sides=20
 cuboid 4    0.6053   -0.6053    0.6053   -0.6053
 media 9 1 1
 media 0 1 2 -1
 media 2 1 3 -2
 media 4 1 4 -3
 boundary 4 6 6
unit 5
com="fuel rod 5"
 cylinder 1   0.4083  sides=20
 cylinder 2   0.4088 sides=20
 cylinder 3   0.4165  sides=20
  cylinder 4   0.4571  sides=20
 cuboid 5    0.6053   -0.6053    0.6053   -0.6053
```

```
 media 10 1 1
 media 55 1 2 -1
 media 0 1 3 -2
 media 132 1 4 -3
 media 81 1  5 -4
 boundary 5 8 8
unit 6
com="fuel rod 6"
 cylinder 1   0.4083  sides=20
 cylinder 2   0.4165  sides=20
  cylinder 3   0.4571 sides=20
 cuboid 4    0.6053   -0.6053    0.6053   -0.6053
 media 11 1 1
 media 0 1 2 -1
 media 2 1 3 -2
 media 4 1 4 -3
 boundary 4 6 6
unit 7
com="fuel rod 7"
 cylinder 1   0.4083  sides=20
 cylinder 2   0.4165  sides=20
  cylinder 3   0.4571 sides=20
 cuboid 4    0.6053   -0.6053    0.6053   -0.6053
 media 12 1 1
 media 0 1 2 -1
 media 2 1 3 -2
 media 4 1 4 -3
 boundary 4 6 6
unit 8
```

```
com="fuel rod 8"
 cylinder 1   0.4083  sides=20
 cylinder 2   0.4088 sides=20
 cylinder 3   0.4165  sides=20
  cylinder 4   0.4571  sides=20
 cuboid 5    0.6053   -0.6053    0.6053   -0.6053
 media 13 1 1
 media 56 1 2 -1
 media 0 1 3 -2
 media 132 1 4 -3
 media 81 1  5 -4
 boundary 5 8 8
unit 9
com="fuel rod 9"
 cylinder 1   0.4083  sides=20
 cylinder 2   0.4165  sides=20
  cylinder 3   0.4571 sides=20
 cuboid 4    0.6053   -0.6053    0.6053   -0.6053
 media 14 1 1
 media 0 1 2 -1
 media 2 1 3 -2
 media 4 1 4 -3
 boundary 4 6 6
unit 10
com="fuel rod 10"
 cylinder 1   0.4083  sides=20
 cylinder 2   0.4165  sides=20
  cylinder 3   0.4571 sides=20
 cuboid 4    0.6053   -0.6053    0.6053   -0.6053
```

```
 media 15 1 1
 media 0 1 2 -1
 media 2 1 3 -2
 media 4 1 4 -3
 boundary 4 6 6
unit 11
com="fuel rod 11"
 cylinder 1   0.4083  sides=20
 cylinder 2   0.4165  sides=20
  cylinder 3   0.4571 sides=20
 cuboid 4    0.6053   -0.6053    0.6053   -0.6053
 media 16 1 1
 media 0 1 2 -1
 media 2 1 3 -2
 media 4 1 4 -3
 boundary 4 6 6
unit 12
com="fuel rod 12"
 cylinder 1   0.4083  sides=20
 cylinder 2   0.4088 sides=20
 cylinder 3   0.4165  sides=20
  cylinder 4   0.4571  sides=20
 cuboid 5    0.6053   -0.6053    0.6053   -0.6053
 media 17 1 1
 media 57 1 2 -1
 media 0 1 3 -2
 media 132 1 4 -3
 media 81 1  5 -4
 boundary 5 8 8
```

```
unit 13
com="fuel rod 13"
 cylinder 1   0.4083  sides=20
 cylinder 2   0.4088 sides=20
 cylinder 3   0.4165  sides=20
  cylinder 4   0.4571  sides=20
 cuboid 5    0.6053   -0.6053    0.6053   -0.6053
 media 18 1 1
 media 58 1 2 -1
 media 0 1 3 -2
 media 132 1 4 -3
 media 81 1  5 -4
 boundary 5 8 8
unit 14
com="fuel rod 14"
 cylinder 1   0.4083  sides=20
 cylinder 2   0.4165  sides=20
  cylinder 3   0.4571 sides=20
 cuboid 4    0.6053   -0.6053    0.6053   -0.6053
 media 19 1 1
 media 0 1 2 -1
 media 2 1 3 -2
 media 4 1 4 -3
 boundary 4 6 6
unit 15
com="fuel rod 15"
 cylinder 1   0.4083  sides=20
 cylinder 2   0.4165  sides=20
  cylinder 3   0.4571 sides=20
```

```
 cuboid 4    0.6053   -0.6053    0.6053   -0.6053
 media 20 1 1
 media 0 1 2 -1
 media 2 1 3 -2
 media 4 1 4 -3
 boundary 4 6 6
unit 16
com="fuel rod 16"
 cylinder 1   0.4083  sides=20
 cylinder 2   0.4165  sides=20
  cylinder 3   0.4571 sides=20
 cuboid 4    0.6053   -0.6053    0.6053   -0.6053
 media 21 1 1
 media 0 1 2 -1
 media 2 1 3 -2
 media 4 1 4 -3
 boundary 4 6 6
unit 17
com="fuel rod 17"
 cylinder 1   0.4083  sides=20
 cylinder 2   0.4088 sides=20
 cylinder 3   0.4165  sides=20
  cylinder 4   0.4571  sides=20
 cuboid 5    0.6053   -0.6053    0.6053   -0.6053
 media 22 1 1
 media 59 1 2 -1
 media 0 1 3 -2
 media 132 1 4 -3
 media 81 1  5 -4
```

```
 boundary 5 8 8
unit 18
com="fuel rod 18"
 cylinder 1   0.4083  sides=20
 cylinder 2   0.4165  sides=20
  cylinder 3   0.4571 sides=20
 cuboid 4    0.6053   -0.6053    0.6053   -0.6053
 media 23 1 1
 media 0 1 2 -1
 media 2 1 3 -2
 media 4 1 4 -3
 boundary 4 6 6
unit 19
com="fuel rod 19"
 cylinder 1   0.4083  sides=20
 cylinder 2   0.4088 sides=20
 cylinder 3   0.4165  sides=20
  cylinder 4   0.4571  sides=20
 cuboid 5    0.6053   -0.6053    0.6053   -0.6053
 media 24 1 1
 media 60 1 2 -1
 media 0 1 3 -2
 media 132 1 4 -3
 media 81 1  5 -4
 boundary 5 8 8
unit 20
com="fuel rod 20"
 cylinder 1   0.4083  sides=20
 cylinder 2   0.4088 sides=20
```

```
 cylinder 3   0.4165  sides=20
  cylinder 4   0.4571  sides=20
 cuboid 5    0.6053   -0.6053    0.6053   -0.6053
 media 25 1 1
 media 61 1 2 -1
 media 0 1 3 -2
 media 132 1 4 -3
 media 81 1  5 -4
 boundary 5 8 8
unit 21
com="fuel rod 21"
 cylinder 1   0.4083  sides=20
 cylinder 2   0.4165  sides=20
  cylinder 3   0.4571 sides=20
 cuboid 4    0.6053   -0.6053    0.6053   -0.6053
 media 26 1 1
 media 0 1 2 -1
 media 2 1 3 -2
 media 4 1 4 -3
 boundary 4 6 6
unit 22
com="fuel rod 22"
 cylinder 1   0.4083  sides=20
 cylinder 2   0.4088 sides=20
 cylinder 3   0.4165  sides=20
  cylinder 4   0.4571  sides=20
 cuboid 5    0.6053   -0.6053    0.6053   -0.6053
 media 27 1 1
 media 62 1 2 -1
```

```
 media 0 1 3 -2
 media 132 1 4 -3
 media 81 1  5 -4
 boundary 5 8 8
unit 23
com="fuel rod 23"
 cylinder 1   0.4083  sides=20
 cylinder 2   0.4088 sides=20
 cylinder 3   0.4165  sides=20
  cylinder 4   0.4571  sides=20
 cuboid 5    0.6053   -0.6053    0.6053   -0.6053
 media 28 1 1
 media 63 1 2 -1
 media 0 1 3 -2
 media 132 1 4 -3
 media 81 1  5 -4
 boundary 5 8 8
unit 24
com="fuel rod 24"
 cylinder 1   0.4083  sides=20
 cylinder 2   0.4165  sides=20
  cylinder 3   0.4571 sides=20
 cuboid 4    0.6053   -0.6053    0.6053   -0.6053
 media 29 1 1
 media 0 1 2 -1
 media 2 1 3 -2
 media 4 1 4 -3
 boundary 4 6 6
unit 25
```

```
com="fuel rod 25"
 cylinder 1   0.4083  sides=20
 cylinder 2   0.4088 sides=20
 cylinder 3   0.4165  sides=20
  cylinder 4   0.4571  sides=20
 cuboid 5    0.6053   -0.6053    0.6053   -0.6053
 media 30 1 1
 media 64 1 2 -1
 media 0 1 3 -2
 media 132 1 4 -3
 media 81 1  5 -4
 boundary 5 8 8
unit 26
com="fuel rod 26"
 cylinder 1   0.4083  sides=20
 cylinder 2   0.4165  sides=20
  cylinder 3   0.4571 sides=20
 cuboid 4    0.6053   -0.6053    0.6053   -0.6053
 media 31 1 1
 media 0 1 2 -1
 media 2 1 3 -2
 media 4 1 4 -3
 boundary 4 6 6
unit 27
com="fuel rod 27"
 cylinder 1   0.4083  sides=20
 cylinder 2   0.4088 sides=20
 cylinder 3   0.4165  sides=20
  cylinder 4   0.4571  sides=20
```

```
 cuboid 5    0.6053   -0.6053    0.6053   -0.6053
 media 32 1 1
 media 65 1 2 -1
 media 0 1 3 -2
 media 132 1 4 -3
 media 81 1  5 -4
 boundary 5 8 8
unit 28
com="fuel rod 28"
 cylinder 1   0.4083  sides=20
 cylinder 2   0.4165  sides=20
  cylinder 3   0.4571 sides=20
 cuboid 4    0.6053   -0.6053    0.6053   -0.6053
 media 33 1 1
 media 0 1 2 -1
 media 2 1 3 -2
 media 4 1 4 -3
 boundary 4 6 6
unit 29
com="fuel rod 29"
 cylinder 1   0.4083  sides=20
 cylinder 2   0.4088 sides=20
 cylinder 3   0.4165  sides=20
  cylinder 4   0.4571  sides=20
 cuboid 5    0.6053   -0.6053    0.6053   -0.6053
 media 34 1 1
 media 66 1 2 -1
 media 0 1 3 -2
 media 132 1 4 -3
```

```
 media 81 1  5 -4
 boundary 5 8 8
unit 30
com="fuel rod 30"
 cylinder 1   0.4083  sides=20
 cylinder 2   0.4088 sides=20
 cylinder 3   0.4165  sides=20
  cylinder 4   0.4571  sides=20
 cuboid 5    0.6053   -0.6053    0.6053   -0.6053
 media 35 1 1
 media 67 1 2 -1
 media 0 1 3 -2
 media 132 1 4 -3
 media 81 1  5 -4
 boundary 5 8 8
unit 31
com="fuel rod 31"
 cylinder 1   0.4083  sides=20
 cylinder 2   0.4165  sides=20
  cylinder 3   0.4571 sides=20
 cuboid 4    0.6053   -0.6053    0.6053   -0.6053
 media 36 1 1
 media 0 1 2 -1
 media 2 1 3 -2
 media 4 1 4 -3
 boundary 4 6 6
unit 32
com="fuel rod 32"
 cylinder 1   0.4083  sides=20
```

```
 cylinder 2   0.4165  sides=20
  cylinder 3   0.4571 sides=20
 cuboid 4    0.6053   -0.6053    0.6053   -0.6053
 media 37 1 1
 media 0 1 2 -1
 media 2 1 3 -2
 media 4 1 4 -3
 boundary 4 6 6
unit 33
com="fuel rod 33"
 cylinder 1   0.4083  sides=20
 cylinder 2   0.4088 sides=20
 cylinder 3   0.4165  sides=20
  cylinder 4   0.4571  sides=20
 cuboid 5    0.6053   -0.6053    0.6053   -0.6053
 media 38 1 1
 media 68 1 2 -1
 media 0 1 3 -2
 media 132 1 4 -3
 media 81 1  5 -4
 boundary 5 8 8
unit 34
com="fuel rod 34"
 cylinder 1   0.4083  sides=20
 cylinder 2   0.4088 sides=20
 cylinder 3   0.4165  sides=20
  cylinder 4   0.4571  sides=20
 cuboid 5    0.6053   -0.6053    0.6053   -0.6053
 media 39 1 1
```

```
 media 69 1 2 -1
 media 0 1 3 -2
 media 132 1 4 -3
 media 81 1  5 -4
 boundary 5 8 8
unit 35
com="fuel rod 35"
 cylinder 1   0.4083  sides=20
 cylinder 2   0.4165  sides=20
  cylinder 3   0.4571 sides=20
 cuboid 4    0.6053   -0.6053    0.6053   -0.6053
 media 40 1 1
 media 0 1 2 -1
 media 2 1 3 -2
 media 4 1 4 -3
 boundary 4 6 6
unit 36
com="fuel rod 36"
 cylinder 1   0.4083  sides=20
 cylinder 2   0.4165  sides=20
  cylinder 3   0.4571 sides=20
 cuboid 4    0.6053   -0.6053    0.6053   -0.6053
 media 41 1 1
 media 0 1 2 -1
 media 2 1 3 -2
 media 4 1 4 -3
 boundary 4 6 6
unit 37
com="fuel rod 37"
```

```
 cylinder 1   0.4083  sides=20
 cylinder 2   0.4165  sides=20
  cylinder 3   0.4571 sides=20
 cuboid 4    0.6053   -0.6053    0.6053   -0.6053
 media 42 1 1
 media 0 1 2 -1
 media 2 1 3 -2
 media 4 1 4 -3
 boundary 4 6 6
unit 38
com="fuel rod 38"
 cylinder 1   0.4083  sides=20
 cylinder 2   0.4088 sides=20
 cylinder 3   0.4165  sides=20
  cylinder 4   0.4571  sides=20
 cuboid 5    0.6053   -0.6053    0.6053   -0.6053
 media 43 1 1
 media 70 1 2 -1
 media 0 1 3 -2
 media 132 1 4 -3
 media 81 1  5 -4
 boundary 5 8 8
unit 39
com="fuel rod 39"
 cylinder 1   0.4083  sides=20
 cylinder 2   0.4165  sides=20
  cylinder 3   0.4571 sides=20
 cuboid 4    0.6053   -0.6053    0.6053   -0.6053
 media 44 1 1
```

```
 media 0 1 2 -1
 media 2 1 3 -2
 media 4 1 4 -3
 boundary 4 6 6
unit 40
com="fuel rod 40"
 cylinder 1   0.4083  sides=20
 cylinder 2   0.4165  sides=20
  cylinder 3   0.4571 sides=20
 cuboid 4    0.6053   -0.6053    0.6053   -0.6053
 media 45 1 1
 media 0 1 2 -1
 media 2 1 3 -2
 media 4 1 4 -3
 boundary 4 6 6
unit 41
com="fuel rod 41"
 cylinder 1   0.4083  sides=20
 cylinder 2   0.4165  sides=20
  cylinder 3   0.4571 sides=20
 cuboid 4    0.6053   -0.6053    0.6053   -0.6053
 media 46 1 1
 media 0 1 2 -1
 media 2 1 3 -2
 media 4 1 4 -3
 boundary 4 6 6
unit 42
com="fuel rod 42"
 cylinder 1   0.4083  sides=20
```

```
 cylinder 2   0.4088 sides=20
 cylinder 3   0.4165  sides=20
  cylinder 4   0.4571  sides=20
 cuboid 5    0.6053   -0.6053    0.6053   -0.6053
 media 47 1 1
 media 71 1 2 -1
 media 0 1 3 -2
 media 132 1 4 -3
 media 81 1  5 -4
 boundary 5 8 8
unit 43
com="guide tube"
 cylinder 1   0.4083  sides=10
 cylinder 2   0.4445  sides=10
 cuboid 3    0.6053   -0.6053    0.6053   -0.6053
 media 119 1 1
 media 273 1 2 -3
 media 119 1 3 -2
 boundary 3 4 4
unit 44
com="partial fuel rod 1-horizontal"
 cylinder 1   0.4083  sides=20 chord +y=0
 cylinder 2   0.4088 sides=20 chord +y=0
 cylinder 3   0.4165  sides=20 chord +y=0
  cylinder 4   0.4571  sides=20 chord +y=0
 cuboid 5    0.6053   -0.6053    0.6053       0
 media 48 1 1
 media 72 1 2 -1
 media 0 1 3 -2
```

```
 media 132 1 4 -3
 media 81 1  5 -4
 boundary 5 8 4
unit 45
com="partial fuel rod 2-horizontal"
 cylinder 1   0.4083  sides=20 chord +y=0
 cylinder 2   0.4088 sides=20 chord +y=0
 cylinder 3   0.4165  sides=20 chord +y=0
  cylinder 4   0.4571  sides=20 chord +y=0
 cuboid 5    0.6053   -0.6053    0.6053       0
 media 49 1 1
 media 73 1 2 -1
 media 0 1 3 -2
 media 132 1 4 -3
 media 81 1  5 -4
 boundary 5 8 4
unit 46
com="partial fuel rod 3-horizontal"
 cylinder 1   0.4083  sides=20 chord +y=0
 cylinder 2   0.4088 sides=20 chord +y=0
 cylinder 3   0.4165  sides=20 chord +y=0
  cylinder 4   0.4571  sides=20 chord +y=0
 cuboid 5    0.6053   -0.6053    0.6053       0
 media 50 1 1
 media 74 1 2 -1
 media 0 1 3 -2
 media 132 1 4 -3
 media 81 1  5 -4
 boundary 5 8 4
```

```
unit 47
com="partial guide tube-horizontal"
 cylinder 1   0.4083  sides=10 chord +y=0
 cylinder 2   0.4445  sides=10 chord +y=0
 cuboid 3    0.6053   -0.6053    0.6053       0
 media 119 1 1
 media 273 1 2 -1
 media 119 1 3 -2
 boundary 3 4 2
unit 48
com="partial fuel rod 4-horizontal"
 cylinder 1   0.4083  sides=20 chord +y=0
 cylinder 2   0.4088 sides=20 chord +y=0
 cylinder 3   0.4165  sides=20 chord +y=0
  cylinder 4   0.4571  sides=20 chord +y=0
 cuboid 5    0.6053   -0.6053    0.6053       0
 media 51 1 1
 media 75 1 2 -1
 media 0 1 3 -2
 media 132 1 4 -3
 media 81 1  5 -4
 boundary 5 8 4
unit 49
com="partial fuel rod 5-horizontal"
 cylinder 1   0.4083  sides=20 chord +y=0
 cylinder 2   0.4088 sides=20 chord +y=0
 cylinder 3   0.4165  sides=20 chord +y=0
  cylinder 4   0.4571  sides=20 chord +y=0
 cuboid 5    0.6053   -0.6053    0.6053       0
```

```
 media 52 1 1
 media 76 1 2 -1
 media 0 1 3 -2
 media 132 1 4 -3
 media 81 1  5 -4
 boundary 5 8 4
unit 50
com="partial fuel rod 6-horizontal"
 cylinder 1   0.4083  sides=20 chord +y=0
 cylinder 2   0.4088 sides=20 chord +y=0
 cylinder 3   0.4165  sides=20 chord +y=0
  cylinder 4   0.4571  sides=20 chord +y=0
 cuboid 5    0.6053   -0.6053    0.6053       0
 media 53 1 1
 media 77 1 2 -1
 media 0 1 3 -2
 media 132 1 4 -3
 media 81 1  5 -4
 boundary 5 8 4
unit 51
com="partial fuel rod 7-horizontal"
 cylinder 1   0.4083  sides=20 chord +y=0
 cylinder 2   0.4165  sides=20 chord +y=0
  cylinder 3   0.4571 sides=20 chord +y=0
 cuboid 4    0.6053   -0.6053    0.6053       0
 media 54 1 1
 media 0 1 2 -1
 media 2 1 3 -2
 media 4 1 4 -3
```

```
 boundary 4 6 3
unit 52
com="partial fuel rod 1-vertical"
 cylinder 1   0.4083  sides=20 chord +x=0
 cylinder 2   0.4088 sides=20 chord +x=0
 cylinder 3   0.4165  sides=20 chord +x=0
  cylinder 4   0.4571  sides=20 chord +x=0
 cuboid 5    0.6053        0    0.6053   -0.6053
 media 48 1 1
 media 72 1 2 -1
 media 0 1 3 -2
 media 132 1 4 -3
 media 81 1  5 -4
 boundary 5 4 8
unit 53
com="partial fuel rod 2-vertical"
 cylinder 1   0.4083  sides=20 chord +x=0
 cylinder 2   0.4088 sides=20 chord +x=0
 cylinder 3   0.4165  sides=20 chord +x=0
  cylinder 4   0.4571  sides=20 chord +x=0
 cuboid 5    0.6053        0    0.6053   -0.6053
 media 49 1 1
 media 73 1 2 -1
 media 0 1 3 -2
 media 132 1 4 -3
 media 81 1  5 -4
 boundary 5 4 8
unit 54
com="partial fuel rod 3-vertical"
```

```
 cylinder 1   0.4083  sides=20 chord +x=0
 cylinder 2   0.4088 sides=20 chord +x=0
 cylinder 3   0.4165  sides=20 chord +x=0
  cylinder 4   0.4571  sides=20 chord +x=0
 cuboid 5    0.6053        0    0.6053   -0.6053
 media 50 1 1
 media 74 1 2 -1
 media 0 1 3 -2
 media 132 1 4 -3
 media 81 1  5 -4
 boundary 5 4 8
unit 55
com="partial guide tube-vertical"
 cylinder 1   0.4083  sides=10 chord +x=0
 cylinder 2   0.4445  sides=10 chord +x=0
 cuboid 3    0.6053        0    0.6053   -0.6053
 media 119 1 1
 media 273 1 2 -1
 media 119 1 3 -2
 boundary 3 2 4
unit 56
com="partial fuel rod 4-vertical"
 cylinder 1   0.4083  sides=20 chord +x=0
 cylinder 2   0.4088 sides=20 chord +x=0
 cylinder 3   0.4165  sides=20 chord +x=0
  cylinder 4   0.4571  sides=20 chord +x=0
 cuboid 5    0.6053        0    0.6053   -0.6053
 media 51 1 1
 media 75 1 2 -1
```

```
 media 0 1 3 -2
 media 132 1 4 -3
 media 81 1  5 -4
 boundary 5 4 8
unit 57
com="partial fuel rod 5-vertical"
 cylinder 1   0.4083  sides=20 chord +x=0
 cylinder 2   0.4088 sides=20 chord +x=0
 cylinder 3   0.4165  sides=20 chord +x=0
  cylinder 4   0.4571  sides=20 chord +x=0
 cuboid 5    0.6053        0    0.6053   -0.6053
 media 52 1 1
 media 76 1 2 -1
 media 0 1 3 -2
 media 132 1 4 -3
 media 81 1  5 -4
 boundary 5 4 8
unit 58
com="partial fuel rod 6-vertical"
 cylinder 1   0.4083  sides=20 chord +x=0
 cylinder 2   0.4088 sides=20 chord +x=0
 cylinder 3   0.4165  sides=20 chord +x=0
  cylinder 4   0.4571  sides=20 chord +x=0
 cuboid 5    0.6053        0    0.6053   -0.6053
 media 53 1 1
 media 77 1 2 -1
 media 0 1 3 -2
 media 132 1 4 -3
 media 81 1  5 -4
```

```
 boundary 5 4 8
unit 59
com="partial fuel rod 7-vertical"
 cylinder 1   0.4083  sides=20 chord +x=0
 cylinder 2   0.4165  sides=20 chord +x=0
  cylinder 3   0.4571 sides=20 chord +x=0
 cuboid 4    0.6053        0    0.6053   -0.6053
 media 54 1 1
 media 0 1 2 -1
 media 2 1 3 -2
 media 4 1 4 -3
 boundary 4 2 4
unit 60
com="instrumentation tube/water cell"
 cuboid 1    0.6053   0    0.6053   0
 media 5 1 1
 boundary 1 2 2
unit 61
com="fuel assembly"
 cuboid 1   11.5007       0   11.5007       0
 array 1 1  place 1 1 0 0
 media 5 1 1
 boundary 1 7 7
unit 62
com="reflector-top"
 cuboid 1   11.5007       0   0.0493       0
 media 5 1 1
 boundary 1 7 7
unit 63
```

```
com="reflector-right"
 cuboid 1   0.0493       0   11.5007       0
 media 5 1 1
 boundary 1 7 7
unit 64
com="reflector-corner"
 cuboid 1   0.0493       0   0.0493       0
 media 5 1 1
 boundary 1 2 2
global unit 65
com="reflected fuel assembly"
 cuboid 1  11.55   0  11.55   0
 array 2 1  place 2 2 0 0
 media 5 1 1
 boundary 1 20 20
end geometry
read array
ara=1 nux=10 nuy=10  pinpow=yes
 com='fuel assembly aro'
 fill
  60   44   45   46   47   48   49   47   50   51
  52    1    2    3    5    7   10   13   16   20
  53    2    4    6    8   11   14   17   21   25
  54    3    6    9   12   15   18   22   26   28
  55    5    8   12   43   19   23   43   29   31
  56    7   11   15   19   24   27   30   32   34
  57   10   14   18   23   27   43   33   35   37
  55   13   17   22   43   30   33   36   38   39
  58   16   21   26   29   32   35   38   40   41
```

```
  59   20   25   28   31   34   37   39   41   42  end fill
ara=2 nux=2 nuy=2  pinpow=yes
 com=''
 fill
  64   62
  63   61  end fill
end array
read bnds
   all=mirror
end bnds
end model
end
```

Appendix B: Sample ORIGEN File

The .f71 file referenced in this sample input is NOT included due to its size (> 200 MB), and because it cannot be opened in a word processor to the best of the author's knowledge. As is the case in Appendix B, sections that change between iterations or cases are highlighted in **bold**.

'This SCALE input file was generated by
'**OrigenArp Version 6.1 Compiled on Thu Oct 7 11:31:00 2010**
#shell
copy "C:\Users\Matt\Desktop**70gwd_650.f71**" "ft71f001"
end
#origens
0$$ a11 71 e t
Decay Case
3$$ 21 1 1 238 a16 2 a33 47 e t
35$$ 0 t
54$$ a8 1 a11 2 e
56$$ a2 10 a10 0 a13 **-9065** a14 1 a15 3 a17 4 e
57** 0 a3 1e-05 e
95$$ 0 t
Case 1
0 MTU
60** 1 1.5 2 4 6 8 10 15 20 40
61** f0.05
65$$
'Gram-Atoms Grams Curies Watts-All Watts-Gamma
 3z 1 0 0 3z 3z 3z 6z

3z 1 0 0 3z 3z 3z 6z

3z 1 0 0 3z 3z 3z 6z

t

54$$ a8 1 a11 2 e

56$$ a2 10 a10 10 a14 1 a15 3 a17 4 e

57** 40 a3 1e-05 e

95$$ 0 t

Case 2

0 MTU

60** 60 80 100 150 200 400 600 800 1000 1500

61** f0.05

65$$

'Gram-Atoms Grams Curies Watts-All Watts-Gamma

3z 1 0 0 3z 3z 3z 6z

3z 1 0 0 3z 3z 3z 6z

3z 1 0 0 3z 3z 3z 6z

t

54$$ a8 1 a11 2 e

56$$ a2 10 a10 10 a14 1 a15 3 a17 4 e

57** 1500 a3 1e-05 e

95$$ 0 t

Case 3

0 MTU

60** 2000 4000 6000 8000 10000 15000 20000 40000 60000 80000

61** f0.05

65$$

'Gram-Atoms Grams Curies Watts-All Watts-Gamma

3z 1 0 0 3z 3z 3z 6z

3z 1 0 0 3z 3z 3z 6z

3z 1 0 0 3z 3z 3z 6z

t

54$$ a8 1 a11 2 e

56$$ a2 10 a10 10 a14 1 a15 3 a17 4 e

57** 80000 a3 1e-05 e

95$$ 0 t

Case 4

0 MTU

60** 100000 150000 200000 400000 600000 800000 1000000 1500000 2000000

4000000

61** f0.05

65$$

'Gram-Atoms Grams Curies Watts-All Watts-Gamma

3z 1 0 0 3z 3z 3z 6z

3z 1 0 0 3z 3z 3z 6z

3z 1 0 0 3z 3z 3z 6z

t

54$$ a8 1 a11 2 e

56$$ a2 10 a6 1 a10 10 a14 1 a15 3 a17 2 e

57** 4000000 a3 1e-05 e

95$$ 0 t

Case 5

0 MTU

60** 6000000 8000000 1e+07 1.5e+07 2e+07 4e+07 6e+07 8e+07 1e+08 1.5e+08

61** f0.05

65$$

'Gram-Atoms Grams Curies Watts-All Watts-Gamma

3z 1 0 0 3z 3z 3z 6z

3z 1 0 0 3z 3z 3z 6z

3z 1 0 0 3z 3z 3z 6z

81$$ 2 0 26 1 a7 200 e

82$$ 2 2 2 2 2 2 2 2 2 e

83**

2.0000000e+07 1.4000000e+07 1.2000000e+07 1.0000000e+07 8.0000000e+06

7.5000000e+06 7.0000000e+06 6.5000000e+06 6.0000000e+06 5.5000000e+06

5.0000000e+06 4.5000000e+06 4.0000000e+06 3.5000000e+06 3.0000000e+06

2.7500000e+06 2.5000000e+06 2.3500000e+06 2.1500000e+06 2.0000000e+06

1.8000000e+06 1.6600000e+06 1.5700000e+06 1.5000000e+06 1.4400000e+06

1.3300000e+06 1.2000000e+06 1.0000000e+06 9.0000000e+05 8.0000000e+05

7.0000000e+05 6.0000000e+05 5.1200000e+05 5.1000000e+05 4.5000000e+05

4.0000000e+05 3.0000000e+05 2.6000000e+05 2.0000000e+05 1.5000000e+05

1.0000000e+05 7.5000000e+04 7.0000000e+04 6.0000000e+04 4.5000000e+04

3.0000000e+04 2.0000000e+04 1.0000000e+04 e

84**

2.0000000e+07 1.7332990e+07 1.5683000e+07 1.4550000e+07

1.3840000e+07 1.2840000e+07 1.0000000e+07 8.1873000e+06 6.4340000e+06

4.8000000e+06 4.3040000e+06 3.0000000e+06 2.4790000e+06 2.3540000e+06

1.8500000e+06 1.5000000e+06 1.4000000e+06 1.3560000e+06 1.3170000e+06

1.2500000e+06 1.2000000e+06 1.1000000e+06 1.0100000e+06 9.2000000e+05

9.0000000e+05 8.7500000e+05 8.6110000e+05 8.2000000e+05 7.5000000e+05

6.7900000e+05 6.7000000e+05 6.0000000e+05 5.7300000e+05 5.5000000e+05

4.9952000e+05 4.7000000e+05 4.4000000e+05 4.2000000e+05 4.0000000e+05

3.3000000e+05 2.7000000e+05 2.0000000e+05 1.5000000e+05 1.2830000e+05

1.0000000e+05 8.5000000e+04 8.2000000e+04 7.5000000e+04 7.3000000e+04

6.0000000e+04 5.2000000e+04 5.0000000e+04 4.5000000e+04 3.0000000e+04

2.5000000e+04 1.7000000e+04 1.3000000e+04 9.5000000e+03 8.0300000e+03
6.0000000e+03 3.9000000e+03 3.7400000e+03 3.0000000e+03 2.5800000e+03
2.2900000e+03 2.2000000e+03 1.8000000e+03 1.5500000e+03 1.5000000e+03
1.1500000e+03 9.5000000e+02 6.8300000e+02 6.7000000e+02 5.5000000e+02
3.0500000e+02 2.8500000e+02 2.4000000e+02 2.1000000e+02 2.0750000e+02
1.9250000e+02 1.8600000e+02 1.2200000e+02 1.1900000e+02 1.1500000e+02
1.0800000e+02 1.0000000e+02 9.0000000e+01 8.2000000e+01 8.0000000e+01
7.6000000e+01 7.2000000e+01 6.7500000e+01 6.5000000e+01 6.1000000e+01
5.9000000e+01 5.3399990e+01 5.2000000e+01 5.0599990e+01 4.9200000e+01
4.8299990e+01 4.7000000e+01 4.5200000e+01 4.4000000e+01 4.2399990e+01
4.1000000e+01 3.9599990e+01 3.9099990e+01 3.8000000e+01 3.7000000e+01
3.5500000e+01 3.4599990e+01 3.3750000e+01 3.3250000e+01 3.1750000e+01
3.1250000e+01 3.0000000e+01 2.7500000e+01 2.5000000e+01 2.2500000e+01
2.1000000e+01 2.0000000e+01 1.9000000e+01 1.8500000e+01 1.7000000e+01
1.6000000e+01 1.5100000e+01 1.4400000e+01 1.3750000e+01 1.2900000e+01
1.1900000e+01 1.1500000e+01 1.0000000e+01 9.0999990e+00 8.0999990e+00
7.1500000e+00 7.0000000e+00 6.7500000e+00 6.5000000e+00 6.2500000e+00
6.0000000e+00 5.4000000e+00 5.0000000e+00 4.7500000e+00 4.0000000e+00
3.7300000e+00 3.5000000e+00 3.1500000e+00 3.0499990e+00 3.0000000e+00
2.9699990e+00 2.8700000e+00 2.7700000e+00 2.6699990e+00 2.5700000e+00
2.4699990e+00 2.3799990e+00 2.2999990e+00 2.2099990e+00 2.1200000e+00
2.0000000e+00 1.9400000e+00 1.8600000e+00 1.7700000e+00 1.6799990e+00
1.5899990e+00 1.5000000e+00 1.4500000e+00 1.4000000e+00 1.3499990e+00
1.2999990e+00 1.2500000e+00 1.2249990e+00 1.2000000e+00 1.1749990e+00
1.1500000e+00 1.1399990e+00 1.1299990e+00 1.1200000e+00 1.1100000e+00
1.0999990e+00 1.0899990e+00 1.0800000e+00 1.0700000e+00 1.0599990e+00
1.0499990e+00 1.0400000e+00 1.0300000e+00 1.0200000e+00 1.0099990e+00
1.0000000e+00 9.7500000e-01 9.5000000e-01 9.2500000e-01 9.0000000e-01

8.5000000e-01 8.0000000e-01 7.5000000e-01 7.0000000e-01 6.5000000e-01

6.2500000e-01 6.0000000e-01 5.5000000e-01 5.0000000e-01 4.5000000e-01

4.0000000e-01 3.7500000e-01 3.5000000e-01 3.2500000e-01 3.0000000e-01

2.7500000e-01 2.5000000e-01 2.2500000e-01 2.0000000e-01 1.7500000e-01

1.5000000e-01 1.2500000e-01 9.9999960e-02 8.9999970e-02 7.9999980e-02

6.9999990e-02 6.0000000e-02 5.0000000e-02 4.0000000e-02 3.0000000e-02

2.5300000e-02 9.9999980e-03 7.4999970e-03 4.9999990e-03 3.9999970e-03

3.0000000e-03 2.5000000e-03 2.0000000e-03 1.5000000e-03 1.2000000e-03

9.9999990e-04 7.4999990e-04 4.9999980e-04 9.9999990e-05 1.0000000e-05 e

t

56$$ 0 0 a10 1 e t

56$$ 0 0 a10 2 e t

56$$ 0 0 a10 3 e t

56$$ 0 0 a10 4 e t

56$$ 0 0 a10 5 e t

56$$ 0 0 a10 6 e t

56$$ 0 0 a10 7 e t

56$$ 0 0 a10 8 e t

56$$ 0 0 a10 9 e t

56$$ 0 0 a10 10 e t

54$$ a8 1 a11 2 e

56$$ a2 10 a6 1 a10 10 a14 1 a15 3 a17 2 e

57** 1.5e+08 a3 1e-05 e

95$$ 0 t

Case 6

0 MTU

60** 2e+08 4e+08 6e+08 8e+08 1e+09 1.5e+09 2e+09 4e+09 6e+09 8e+09

61** f0.05

65$$

'Gram-Atoms Grams Curies Watts-All Watts-Gamma

3z 1 0 0 3z 3z 3z 6z

3z 1 0 0 3z 3z 3z 6z

3z 1 0 0 3z 3z 3z 6z

81$$ 2 0 26 1 a7 200 e

82$$ 2 2 2 2 2 2 2 2 2 e

83**

2.0000000e+07 1.4000000e+07 1.2000000e+07 1.0000000e+07 8.0000000e+06

7.5000000e+06 7.0000000e+06 6.5000000e+06 6.0000000e+06 5.5000000e+06

5.0000000e+06 4.5000000e+06 4.0000000e+06 3.5000000e+06 3.0000000e+06

2.7500000e+06 2.5000000e+06 2.3500000e+06 2.1500000e+06 2.0000000e+06

1.8000000e+06 1.6600000e+06 1.5700000e+06 1.5000000e+06 1.4400000e+06

1.3300000e+06 1.2000000e+06 1.0000000e+06 9.0000000e+05 8.0000000e+05

7.0000000e+05 6.0000000e+05 5.1200000e+05 5.1000000e+05 4.5000000e+05

4.0000000e+05 3.0000000e+05 2.6000000e+05 2.0000000e+05 1.5000000e+05

1.0000000e+05 7.5000000e+04 7.0000000e+04 6.0000000e+04 4.5000000e+04

3.0000000e+04 2.0000000e+04 1.0000000e+04 e

84**

2.0000000e+07 1.7332990e+07 1.5683000e+07 1.4550000e+07

1.3840000e+07 1.2840000e+07 1.0000000e+07 8.1873000e+06 6.4340000e+06

4.8000000e+06 4.3040000e+06 3.0000000e+06 2.4790000e+06 2.3540000e+06

1.8500000e+06 1.5000000e+06 1.4000000e+06 1.3560000e+06 1.3170000e+06

1.2500000e+06 1.2000000e+06 1.1000000e+06 1.0100000e+06 9.2000000e+05

9.0000000e+05 8.7500000e+05 8.6110000e+05 8.2000000e+05 7.5000000e+05

6.7900000e+05 6.7000000e+05 6.0000000e+05 5.7300000e+05 5.5000000e+05

4.9952000e+05 4.7000000e+05 4.4000000e+05 4.2000000e+05 4.0000000e+05

3.3000000e+05 2.7000000e+05 2.0000000e+05 1.5000000e+05 1.2830000e+05

1.0000000e+05 8.5000000e+04 8.2000000e+04 7.5000000e+04 7.3000000e+04
6.0000000e+04 5.2000000e+04 5.0000000e+04 4.5000000e+04 3.0000000e+04
2.5000000e+04 1.7000000e+04 1.3000000e+04 9.5000000e+03 8.0300000e+03
6.0000000e+03 3.9000000e+03 3.7400000e+03 3.0000000e+03 2.5800000e+03
2.2900000e+03 2.2000000e+03 1.8000000e+03 1.5500000e+03 1.5000000e+03
1.1500000e+03 9.5000000e+02 6.8300000e+02 6.7000000e+02 5.5000000e+02
3.0500000e+02 2.8500000e+02 2.4000000e+02 2.1000000e+02 2.0750000e+02
1.9250000e+02 1.8600000e+02 1.2200000e+02 1.1900000e+02 1.1500000e+02
1.0800000e+02 1.0000000e+02 9.0000000e+01 8.2000000e+01 8.0000000e+01
7.6000000e+01 7.2000000e+01 6.7500000e+01 6.5000000e+01 6.1000000e+01
5.9000000e+01 5.3399990e+01 5.2000000e+01 5.0599990e+01 4.9200000e+01
4.8299990e+01 4.7000000e+01 4.5200000e+01 4.4000000e+01 4.2399990e+01
4.1000000e+01 3.9599990e+01 3.9099990e+01 3.8000000e+01 3.7000000e+01
3.5500000e+01 3.4599990e+01 3.3750000e+01 3.3250000e+01 3.1750000e+01
3.1250000e+01 3.0000000e+01 2.7500000e+01 2.5000000e+01 2.2500000e+01
2.1000000e+01 2.0000000e+01 1.9000000e+01 1.8500000e+01 1.7000000e+01
1.6000000e+01 1.5100000e+01 1.4400000e+01 1.3750000e+01 1.2900000e+01
1.1900000e+01 1.1500000e+01 1.0000000e+01 9.0999990e+00 8.0999990e+00
7.1500000e+00 7.0000000e+00 6.7500000e+00 6.5000000e+00 6.2500000e+00
6.0000000e+00 5.4000000e+00 5.0000000e+00 4.7500000e+00 4.0000000e+00
3.7300000e+00 3.5000000e+00 3.1500000e+00 3.0499990e+00 3.0000000e+00
2.9699990e+00 2.8700000e+00 2.7700000e+00 2.6699990e+00 2.5700000e+00
2.4699990e+00 2.3799990e+00 2.2999990e+00 2.2099990e+00 2.1200000e+00
2.0000000e+00 1.9400000e+00 1.8600000e+00 1.7700000e+00 1.6799990e+00
1.5899990e+00 1.5000000e+00 1.4500000e+00 1.4000000e+00 1.3499990e+00
1.2999990e+00 1.2500000e+00 1.2249990e+00 1.2000000e+00 1.1749990e+00
1.1500000e+00 1.1399990e+00 1.1299990e+00 1.1200000e+00 1.1100000e+00
1.0999990e+00 1.0899990e+00 1.0800000e+00 1.0700000e+00 1.0599990e+00

1.0499990e+00 1.0400000e+00 1.0300000e+00 1.0200000e+00 1.0099990e+00
1.0000000e+00 9.7500000e-01 9.5000000e-01 9.2500000e-01 9.0000000e-01
8.5000000e-01 8.0000000e-01 7.5000000e-01 7.0000000e-01 6.5000000e-01
6.2500000e-01 6.0000000e-01 5.5000000e-01 5.0000000e-01 4.5000000e-01
4.0000000e-01 3.7500000e-01 3.5000000e-01 3.2500000e-01 3.0000000e-01
2.7500000e-01 2.5000000e-01 2.2500000e-01 2.0000000e-01 1.7500000e-01
1.5000000e-01 1.2500000e-01 9.9999960e-02 8.9999970e-02 7.9999980e-02
6.9999990e-02 6.0000000e-02 5.0000000e-02 4.0000000e-02 3.0000000e-02
2.5300000e-02 9.9999980e-03 7.4999970e-03 4.9999990e-03 3.9999970e-03
3.0000000e-03 2.5000000e-03 2.0000000e-03 1.5000000e-03 1.2000000e-03
9.9999990e-04 7.4999990e-04 4.9999980e-04 9.9999990e-05 1.0000000e-05 e
t
56$$ 0 0 a10 1 e t
56$$ 0 0 a10 2 e t
56$$ 0 0 a10 3 e t
56$$ 0 0 a10 4 e t
56$$ 0 0 a10 5 e t
56$$ 0 0 a10 6 e t
56$$ 0 0 a10 7 e t
56$$ 0 0 a10 8 e t
56$$ 0 0 a10 9 e t
56$$ 0 0 a10 10 e t
54$$ a8 1 a11 2 e
56$$ a2 1 a6 1 a10 10 a14 1 a15 3 a17 2 e
57** 8e+09 a3 1e-05 e
95$$ 0 t
Case 7
0 MTU

60** 1e+10

61** f0.05

65$$

'Gram-Atoms Grams Curies Watts-All Watts-Gamma

3z 1 0 0 3z 3z 3z 6z

3z 1 0 0 3z 3z 3z 6z

3z 1 0 0 3z 3z 3z 6z

81$$ 2 0 26 1 a7 200 e

82$$ 2 e

83**

2.0000000e+07 1.4000000e+07 1.2000000e+07 1.0000000e+07 8.0000000e+06
7.5000000e+06 7.0000000e+06 6.5000000e+06 6.0000000e+06 5.5000000e+06
5.0000000e+06 4.5000000e+06 4.0000000e+06 3.5000000e+06 3.0000000e+06
2.7500000e+06 2.5000000e+06 2.3500000e+06 2.1500000e+06 2.0000000e+06
1.8000000e+06 1.6600000e+06 1.5700000e+06 1.5000000e+06 1.4400000e+06
1.3300000e+06 1.2000000e+06 1.0000000e+06 9.0000000e+05 8.0000000e+05
7.0000000e+05 6.0000000e+05 5.1200000e+05 5.1000000e+05 4.5000000e+05
4.0000000e+05 3.0000000e+05 2.6000000e+05 2.0000000e+05 1.5000000e+05
1.0000000e+05 7.5000000e+04 7.0000000e+04 6.0000000e+04 4.5000000e+04
3.0000000e+04 2.0000000e+04 1.0000000e+04 e

84**

2.0000000e+07 1.7332990e+07 1.5683000e+07 1.4550000e+07
1.3840000e+07 1.2840000e+07 1.0000000e+07 8.1873000e+06 6.4340000e+06
4.8000000e+06 4.3040000e+06 3.0000000e+06 2.4790000e+06 2.3540000e+06
1.8500000e+06 1.5000000e+06 1.4000000e+06 1.3560000e+06 1.3170000e+06
1.2500000e+06 1.2000000e+06 1.1000000e+06 1.0100000e+06 9.2000000e+05
9.0000000e+05 8.7500000e+05 8.6110000e+05 8.2000000e+05 7.5000000e+05
6.7900000e+05 6.7000000e+05 6.0000000e+05 5.7300000e+05 5.5000000e+05

4.9952000e+05 4.7000000e+05 4.4000000e+05 4.2000000e+05 4.0000000e+05
3.3000000e+05 2.7000000e+05 2.0000000e+05 1.5000000e+05 1.2830000e+05
1.0000000e+05 8.5000000e+04 8.2000000e+04 7.5000000e+04 7.3000000e+04
6.0000000e+04 5.2000000e+04 5.0000000e+04 4.5000000e+04 3.0000000e+04
2.5000000e+04 1.7000000e+04 1.3000000e+04 9.5000000e+03 8.0300000e+03
6.0000000e+03 3.9000000e+03 3.7400000e+03 3.0000000e+03 2.5800000e+03
2.2900000e+03 2.2000000e+03 1.8000000e+03 1.5500000e+03 1.5000000e+03
1.1500000e+03 9.5000000e+02 6.8300000e+02 6.7000000e+02 5.5000000e+02
3.0500000e+02 2.8500000e+02 2.4000000e+02 2.1000000e+02 2.0750000e+02
1.9250000e+02 1.8600000e+02 1.2200000e+02 1.1900000e+02 1.1500000e+02
1.0800000e+02 1.0000000e+02 9.0000000e+01 8.2000000e+01 8.0000000e+01
7.6000000e+01 7.2000000e+01 6.7500000e+01 6.5000000e+01 6.1000000e+01
5.9000000e+01 5.3399990e+01 5.2000000e+01 5.0599990e+01 4.9200000e+01
4.8299990e+01 4.7000000e+01 4.5200000e+01 4.4000000e+01 4.2399990e+01
4.1000000e+01 3.9599990e+01 3.9099990e+01 3.8000000e+01 3.7000000e+01
3.5500000e+01 3.4599990e+01 3.3750000e+01 3.3250000e+01 3.1750000e+01
3.1250000e+01 3.0000000e+01 2.7500000e+01 2.5000000e+01 2.2500000e+01
2.1000000e+01 2.0000000e+01 1.9000000e+01 1.8500000e+01 1.7000000e+01
1.6000000e+01 1.5100000e+01 1.4400000e+01 1.3750000e+01 1.2900000e+01
1.1900000e+01 1.1500000e+01 1.0000000e+01 9.0999990e+00 8.0999990e+00
7.1500000e+00 7.0000000e+00 6.7500000e+00 6.5000000e+00 6.2500000e+00
6.0000000e+00 5.4000000e+00 5.0000000e+00 4.7500000e+00 4.0000000e+00
3.7300000e+00 3.5000000e+00 3.1500000e+00 3.0499990e+00 3.0000000e+00
2.9699990e+00 2.8700000e+00 2.7700000e+00 2.6699990e+00 2.5700000e+00
2.4699990e+00 2.3799990e+00 2.2999990e+00 2.2099990e+00 2.1200000e+00
2.0000000e+00 1.9400000e+00 1.8600000e+00 1.7700000e+00 1.6799990e+00
1.5899990e+00 1.5000000e+00 1.4500000e+00 1.4000000e+00 1.3499990e+00
1.2999990e+00 1.2500000e+00 1.2249990e+00 1.2000000e+00 1.1749990e+00

1.1500000e+00 1.1399990e+00 1.1299990e+00 1.1200000e+00 1.1100000e+00
1.0999990e+00 1.0899990e+00 1.0800000e+00 1.0700000e+00 1.0599990e+00
1.0499990e+00 1.0400000e+00 1.0300000e+00 1.0200000e+00 1.0099990e+00
1.0000000e+00 9.7500000e-01 9.5000000e-01 9.2500000e-01 9.0000000e-01
8.5000000e-01 8.0000000e-01 7.5000000e-01 7.0000000e-01 6.5000000e-01
6.2500000e-01 6.0000000e-01 5.5000000e-01 5.0000000e-01 4.5000000e-01
4.0000000e-01 3.7500000e-01 3.5000000e-01 3.2500000e-01 3.0000000e-01
2.7500000e-01 2.5000000e-01 2.2500000e-01 2.0000000e-01 1.7500000e-01
1.5000000e-01 1.2500000e-01 9.9999960e-02 8.9999970e-02 7.9999980e-02
6.9999990e-02 6.0000000e-02 5.0000000e-02 4.0000000e-02 3.0000000e-02
2.5300000e-02 9.9999980e-03 7.4999970e-03 4.9999990e-03 3.9999970e-03
3.0000000e-03 2.5000000e-03 2.0000000e-03 1.5000000e-03 1.2000000e-03
9.9999990e-04 7.4999990e-04 4.9999980e-04 9.9999990e-05 1.0000000e-05 e
t
56$$ 0 0 a10 1 e t
56$$ f0 t
end
=opus
LIBUNIT=21
TYPARAMS=ELEMENTS
UNITS=WATTS
LIBTYPE=FISA
TIME=SEC
NPOSITION=9066 9067 9068 9069 9070 9071 9072 9073 9074 9075 9076 9077
9078 9079 9080 9081 9082 9083 9084 9085 9086 end
end
=opus
LIBUNIT=21

TYPARAMS=NUCLIDES

UNITS=GAMWATTS

LIBTYPE=FISA

TIME=SEC

NPOSITION=9066 9067 9068 9069 9070 9071 9072 9073 9074 9075 9076 9077

9078 9079 9080 9081 9082 9083 9084 9085 9086 end

end

#shell

copy ft71f001 "C:\Users\Matt\Desktop**i2s1b_constpower.f71**"

del ft71f001

end

Bibliography

[1] B. Petrovic, "The Integral Inherently Safe Light Water Reactor," *Nuclear Engineering International,* 28 April 2014.

[2] B. Petrovic, P. Ferroni and F. Franceschini, "Fuel Cycle Cost Trade-off Studies for I2S-LWR (Integral Inherently Safe LWR) Fuel Design Selection," Georgia Institute of Technology, Atlanta, GA, 2013.

[3] B. Petrovic, "I2S-LWR Plant Parameters List," Atlanta, 2013.

[4] Brookhaven National Laboratory, "Evaluated Nuclear Data File," 22 December 2011. [Online]. Available: http://www.nndc.bnl.gov/exfor/servlet/E4sGetTabSect?SectID=334527&req=7036&PenSectID=287452. [Accessed 16 June 2015].

[5] Brookhaven National Laboratory, "Evaluated Nuclear Data File," 22 December 2011. [Online]. Available: http://www.nndc.bnl.gov/exfor/servlet/E4sGetTabSect?SectID=339457&req=7038&PenSectID=292253. [Accessed 16 June 2015].

[6] B. Petrovic, *Private Communication,* Atlanta, 2015.

[7] Y. Yan, R. V. Strain, T. S. Bray and M. C. Billone, "High temperature oxidation of irradiated Limerick BWR cladding," Argonne National Laboratory, Argonne, 2001.

[8] Brookhaven National Laboratory, "Evaluated Nuclear Data File," 22 December 2011. [Online]. Available: http://www.nndc.bnl.gov/exfor/servlet/E4sGetTabSect?SectID=340330&req=7037&PenSectID=293126. [Accessed 16 June 2015].

[9] C. E. Sanders and J. C. Wagner, "Study of the Effect of Integral Burnable Absorbers for PWR Burnup Credit," US Nuclear Regulatory Commission, Washington DC, 2002.

[10] W. M. Stacey, Nuclear Reactor Physics, 2nd Edition, Weinheim: Wiley-VCH Verlag GmBH & Co. KGaA, 2007.

[11] F. Franceschini and B. Petrovic, "I2S-LWR Core Design," I2S-LWR Team Meeting, Arlington, VA, 2013.

[12] Westinghouse Electric Company, "AP1000 Design Control Document 4.1: Fuel System Design," 24 November 2008. [Online]. Available: http://pbadupws.nrc.gov/docs/ML0832/ML083230319.pdf. [Accessed 18 July 2015].

[13] Westinghouse Electric Company, "AP1000 Design Control Document 2.1: System Based Design Descriptions and ITAAC," 24 November 2008. [Online]. Available: http://pbadupws.nrc.gov/docs/ML0832/ML083230174.pdf. [Accessed 18 July 2015].

[14] Westinghouse Electric Company, "AP1000 Design Control Document 4.3: Nuclear Design," 24 November 2008. [Online]. Available: http://pbadupws.nrc.gov/docs/ML1117/ML11171A445.pdf. [Accessed 18 July 2015].

[15] N. Tsolfanidis and R. G. Cochran, The Nuclear Fuel Cycle: Analysis and Management, 2nd Edition, La Grange Park, Illinois: American Nuclear Society, 1999.

[16] M. Ragheb, "Decay Heat Generation in Fission Reactors," 2011. [Online]. Available: http://mragheb.com/NPRE%20457%20CSE%20462%20Safety%20Analysis%20of%20Nuclear%20Reactor%20Systems/Decay%20Heat%20generation%20in%20Fission%20Reactors.pdf. [Accessed 16 July 2015].

[17] W. J. Garland and F. Saunders, "Decay Heat Estimates for MNR," McMaster University, Hamilton, Ontario, Canada, 1999.

[18] American Nuclear Society Standards Committee, Working Group ANS-5.1, "ANSI/ANS-5.1-2005: Decay Heat Power in Light Water Reactors," American Nuclear Society, La Grange Park, 2005.

[19] American Nuclear Society Standards Committee, Working Group ANS-5,1, "Decay Heat Power in Light Water Reactors," American Nuclear Society, LaGrange Park, 2014.

[20] F. Storrer, "Review of Decay Heat Predictions and Standards," JEF Working Group on Radioactive Decay and Fission YIeld Data, London, 1994.

[21] US Nuclear Regulatory Commission, "Attachment 1: Appendix K Decay Heat Standards," US Nuclear Regulatory Commission, Rockville, 1994.

[22] D.-K. Cho, D.-H. Kook, J. Choi and J.-H. Park, "Advanced hybrid analysis system for nuclear facility design with best estimate source terms," *Nuclear Engineering and Design,* no. 256, pp. 274-284, 2012.

[23] E. E. Lewis and W. F. Miller Jr., Computational Methods of Neutron Transport, La Grange Park: American Nuclear Society, 1993.

[24] M. D. DeHart, A Discrete Ordinates Approximation to the Neutron Transport Equation Applied to Generalized Geometries, Texas A & M University, 1992.

[25] M. D. DeHart and M. A. Jessee, "NEWT: A New Transport Algorithm for Two-Dimensional Discrete-Ordinates Analysis in Non-Orthogonal Geometries," in *Scale: A Comprehensive Modeling and Simulation Suite for Nuclear Safety Analysis and Design*, Oak Ridge, Oak Ridge National Laboratory, 2011, p. F21.2.6.

[26] B. J. Ade and I. Frankl, SCALE/TRITON Primer: A Primer for Light Water Reactor Lattice Physics Calculations, Oak Ridge: Oak Ridge National Laboratory, 2012, p. 42.

[27] Brookhaven National Laboratory, "Evaluated Nuclear Data File ENDF/B-VII.1," 22 December 2011. [Online]. Available:

http://www.nndc.bnl.gov/exfor/servlet/E4sGetTabSect?SectID=381169&req=11903&PenSectID=333432. [Accessed 8 July 2015].

[28] G. E. Sjoden, Lecture Notes for NRE 6201, v 0.1, Atlanta: Georgia Institute of Technology, 2014.

[29] T. H. Trumbull, RPI Reactor Critical Facility: A Manual of Experiments, MANE4440 Critical Reactor Laboratory, Troy, NY: Rensselaer Polytechnic Institute, 2012.

[30] I2S-LWR Team and B. Petrovic, "Integral Inherently Safe Light Water Reactor (I2S-LWR) Concept: Extending SMR Safety Features to Large Power Output," in *Proceedings of ICAPP 2014*, Charlotte, NC, 2014.

[31] Sandvik AB, "Kanthal APMT (construction materials)," Kanthal, 27 August 2014. [Online]. Available: http://kanthal.com/en/products/material-datasheets/wire/na/kanthal-apmt/. [Accessed 18 Jun 2015].

[32] K. M. Ramey, "WALRUS: Walrus is A Lousy Reaction Utilization Script," Georgia Institute of Technology, Atlanta, 2015.